THERMALLY AWARE PERFORMANCE ANALYSIS OF MIXED CARBON NANOTUBE BASED VLSI INTERCONNECTS

A thesis submitted of the requirement for the Award of the Degree of

DOCTOR OF PHILOSOPHY

Submitted By

Manvi Sharma
Reg. No. 901406014

Under the Supervision of

Dr. Mayank Kumar Rai
(Associate Professor)
ECED

Dr. Rajesh Khanna
(Professor)
ECED

THAPAR INSTITUTE
OF ENGINEERING & TECHNOLOGY
(Deemed to be University)

Department of Electronics and Communication Engineering

THAPAR INSTITUTE OF ENGINEERING AND TECHNOLOGY, PATIALA, PUNJAB

March, 2022

DECLARATION

I, **Manvi Sharma** hereby declare that the work which is being presented in this thesis entitled "***Thermally Aware Performance Analysis of Mixed Carbon Nanotube based VLSI Interconnects***" submitted in partial fulfillment of the requirements for the award of degree of **Doctor of Philosophy** submitted in the **Department of Electronics and Communication Engineering at Thapar Institute of Engineering and Technology, Patiala** is an authentic record of my own work carried out during a period under the supervisions of **Dr. Mayank Kumar Rai , Associate Professor, ECED, TIET and Dr. Rajesh Khanna, Professor , ECED, TIET.** The matter presented in this thesis has not been submitted by me in any other University / Institute for the award of any degree or diploma.

Date: 15-03-2022

(Manvi Sharma)
Signature of candidate

CERTIFICATE

This is certify that the work contained in the thesis titled "***Thermally Aware Performance Analysis of Mixed Carbon Nanotube based VLSI Interconnects***" by Manvi Sharma (Reg. no. 901406014) has been carried out under my/ our supervision and that this work has not been submitted elsewhere for any degree.

Mayank Kumar Rai

Dr. Mayank Kumar Rai
Associate Professor (ECED)
TIET,Patiala
Date:

Dr. Rajesh Khanna
Professor (ECED)
TIET,Patiala
Date:

ACKNOWLEDGEMENT

I would like to offer my heartiest salutation to the Almighty for good health and courage bestowed upon me in all the adversities at every step and at every moment throughout the entire span of my research work and in every aspect of my life.

The completion of any academic work is inconceivable without the expert guidance of a mentor. I acknowledge and extend my deepest gratitude to my respected supervisor Dr. Mayank Kumar Rai, Associate professor, ECED for his patience, guidance and support. I have benefitted greatly from his wealth of knowledge and meticulous editing of my research papers. I am extremely thankful that he took me as his first student and continued to have faith in me over the years. His indispensable tutelage and wise counsel at every step of my work enabled me to complete the work without obstruction. Despite his various academic and official assignments, he always spread his precious time and took great pains in discussing even in minute details of my work. I would also like to thank my second guide Dr. Rajesh Khanna for always being there for any guidance. His dynamism, punctuality and vision have deeply inspired me. It was a privilege and honor to work under his guidance. I would like to thank both of them for their moral support, empathy and motivation.

Sincere thanks to Ministry of Electronics and Information technology (MeitY) for awarding me Vishveswarya Phd scholarship throughout the completion of my research work. Out of deep sense of gratefulness, I express my sincere thanks to Dr. Rafat Siddique, Dean (RSP), Dr. Alpana Agarwal, Head (ECE) and members of doctorate committee for continuous appreciation and support. Special thanks to Dr. Seema Bawa, Professor, (CSED), TIET for always motivating me to strive hard whenever I felt crestfallen. A heartfelt thanks to Dr. Deepak Kumar from Amity Institute of Geoinformatics & Remote Sensing (AIGIRS), Noida for always motivating me, attending my calls at odd hours and for checking plagiarism of my research papers numerous times.

It would be unfair, if I do not mention Mrs. Shreya Rai, wife of Dr. Mayak Kumar Rai. I am highly grateful to her for always being there for me. She was always available to discuss my personal issues. The love and care I have received from her throughout this journey is highly needed to balance the stress and anxiety whenever my research work was not going great. I would defiantly carry forward her ideologies in my personal life.

Big thanks to my lab mates, specially, Hitendra Gupta, Ramneek Sidhu, Dr. Atipriya Sharma, Dr. Naveen Kumar for all the discussions and motivation. Finally a heartfelt thanks to Prabhjot Kaur Chahal, my sisterly friend, she was always there whenever and wherever I needed her. Each midnight draft, each early morning rant, each time I cried, screamed and swore that I would

never write again, she always motivated me to bounce back to work with more enthusiasm. Her name should be on this thesis as much as mine.

Lastly, my family deserves endless gratitude. The most important thanks to my parents Guru Dutt Sharma and Madhu Sharma for their prayers, care and sacrifices throughout this work and in every aspect of my life. A heartiest thanks to my husband for fielding a ridiculous number of phone calls from my side, for calming me down, showering me with all the love and constantly reminding me of the end goal.

My thanks also go to all the people who have supported me to complete my research work directly and indirectly.

Date: 15-03-2022

Manvi Sharma

ABSTRACT

Nowadays, excessive technology scaling in the deep sub-micron (DSM) regime allows the integration of immense functions on a single chip. As a result of excessive scaling, copper-based on-chip interconnect performance degrades, thus necessitating the search for an alternative suitable material for future nano interconnects. For the next generation of interconnects, the potential material should be capable of manifesting minimized propagation delay, power dissipation, and the effects of functional as well as dynamic crosstalk in the coupled interconnects.

The current work aims to find the best material possible for making future generation interconnects which provide better performance by eliminating coupling effects between adjoining interconnects.

The most befitting material has turned out to be carbon-based interconnects such as CNT and GNR. In the present work, a realistic CNT bundle such as mixed CNT (m-CNT) bundle made up of both single wall carbon nanotube (SWCNT) and multi wall carbon nanotubes (MWCNT) with different placements is considered for performance analysis under temperature as an obligatory component.

A temperature-dependent crosstalk model based on ABCD parameter matrix along with decoupling technology, with application of driver interconnect load (DIL) in coupled m-CNT bundle (MCB) interconnects is taken. A study is carried out at 14nm technology node to examine the effects of irradiation-induced defects on MCB interconnects by considering tunneling and inter-shell capacitances in an equivalent capacitance model over a temperature range from 300K to 500K. In addition, the performance of capacitively coupled interconnects of MCB has also been discussed and compared with copper interconnects in terms of propagation delay, power dissipation, crosstalk induced noise voltage, and frequency spectrum. The propagation delay of the four different structures of MCB, e.g. S1, S2, S3 and S4 (aka ST-1, ST-2, ST-3 and ST-4, increases with defects. Propagation delay is appreciably higher when crosstalk effects are taken into consideration. For the entire temperature range, the crosstalk-induced peaks and time durations of victim output pulses in copper are higher than those of all other structures of MCB. A temperature-dependent frequency spectrum of MCB and copper are also analyzed at 14nm technology node. Under this analysis, the time domain signal obtained at the far end of single interconnect and at the far end of victim line in capacitively coupled interconnects are converted into frequency domain to study the band width and crosstalk induced noise voltage, respectively. The effects of temperature variation on noise amplitudes are explore and it showed that the frequency amplitude decreases with increase in temperature which means that the loss in signal power is more at higher temperatures. The structure-4 of MCB interconnect (also known as S4 or ST-4) experiences more loss in signal power when temperature is raised from 300K to 500K. Also, there is decrease in the bandwidth with rise in temperature which is due to increase in resistance. It is also noted that crosstalk induced noise amplitude is becoming larger with rise in temperature. This implies that filtering capability of noise is going to decrease with higher temperatures.
Moreover, dielectric surface roughness scattering induced crosstalk performance of coupled MCB interconnects is also done, where, the most typical and consistent dielectric materials like

silicon dioxide (SiO_2), boron nitride (BN) and silicon carbide (SiC) are taken into account and analyzed w.r.t. mean free path(MFP) created by surface roughness scattering. A complete crosstalk (dynamic & functional) effect in terms of positive peaks, time duration and area of rise glitch is studied. Frequency spectrum and bode stability analysis is also done for all four structures of MCB. Structure-4 (also known as S4 or ST-4) placed on SiC substrate material provides the best results in terms of positive peaks, time duration, and area of rise glitches among all the structures in the MCB. The bode stability of S4 placed on SiC interconnects are more stable and have larger phase margin, gain margin and 3-dB frequency bandwidth in comparison to S4 placed on BN and S4 placed on SiO_2 with the same dimensions. Moreover, MCB interconnects placed on smooth substrate surface have larger 3-dB frequency bandwidth and smaller delay times than those of MCB placed on rough substrate surfaces over a temperature range (300K-500K). Also, for the S4, an increase in surface roughness parameter ($\boldsymbol{\delta}_{SR}$) causes a reduction in frequency bandwidth and a 50% rise time of the transient response at the far end of an aggressor line.

The work presented in this thesis demonstrates that temperature, tunneling effect, inter-shell capacitance, defects, and dielectric surface roughness scattering play an important role in studying the performance and reliability of MCB interconnects in DSM regime.

TABLE OF CONTENTS

Sr. No.	Name of the Chapters	Page No,
	Declaration……	*i*
	Certificate……	*ii*
	Acknowledgement……	*iii*
	Abstract……	*v*
	List of Figures……	*x*
	List of Tables……	*xiv*
	List of Acronyms……	*xvi*
CHAPTER 1	**Introduction and Statement of Problems**	1
1.1	Introduction	1
1.2	Problem of Statements	8
1.3	Organization Of Thesis	8
CHAPTER 2	**Literature Survey**	11
2.1	CNT as an Interconnect	11
2.2	Fabrication of CNT	18
2.3	Performance Analysis of Coupled CNT Interconnects	20
2.3.1	Thermally Aware Crosstalk Induced Noise in Coupled CNT Interconnects	25
2.3.2	Scattering In Coupled CNT Interconnects: Effects on Transport Phenomena	26
2.3.3	Frequency And Stability Analysis in Coupled Interconnects of CNT	28
2.4	Conclusion	30
CHAPTER 3	**Temperature-dependent Irradiation-Induced Defect Oriented Circuit Modeling and Performance Analysis of m-CNT Bundle Interconnects**	31
3.1	Circuit Modeling and Analysis of Thermally Aware MCB Bundle	32
3.1.1	Temperature-Dependent Irradiation-Induced Defect Based Model for SWCNT And MWCNT Bundles	34
3.1.2	Temperature-Dependent Irradiation-Induced Defect Based *RLC* Parameters of MCB	41
3.2	Temperature-Dependent Impedance Analysis	42

3.3	Temperature-Dependent Analyses	43
3.4	Conclusion	50
CHAPTER 4	**Temperature-Dependent Crosstalk Induced Frequency Spectrum Analyses in Adjacent Interconnects of Mixed Carbon Nanotube(M-CNT) Bundle**	51
4.1	Performance Analysis of MCB Structures and Copper	52
4.1.1	Propagation Delay Analysis of MCB Structures and Copper in Single Interconnect	53
4.1.2	Crosstalk analyses of MCB structures and Copper	54
4.2	Frequency Analysis of best MCB Structure (MCB-4) And Copper	62
4.3	Conclusion	66
CHAPTER 5	**Temperature Dependent Crosstalk Model with application Of DIL (Driver-Interconnect-Load) in Coupled M-CNT Bundle Interconnects**	67
5.1	Electrical Model Of M-CNT Bundle Based Interconnects	68
5.2	The Decoupling and ABCD Parameter based Model	69
5.3	Results and Discussions	73
5.4	Conclusion	75
CHAPTER 6	**Dielectric Surface Roughness Scattering Induced Crosstalk Performance of Coupled MCB Interconnects**	76
6.1	Dielectric Surface Roughness Scattering Induced Impedance Analyses of MCB Structures	77
6.2	Results and Discussion	79
6.2.1	Dielectric Surface Roughness (SSR) scattering induced crosstalk analyses	80
6.2.2	Dielectric Surface Roughness (SSR) scattering induced bode stability analysis	85
6.3	Conclusion	90
CHAPTER 7	**Conclusion, Contributions and Future Scope**	92
7.1	Defects Based Irradiation-Induced Performance Analyses Of M-CNT Bundles.	92
7.2	Thermally Aware Crosstalk and Frequency Spectrum Analyses in Adjacent Interconnects Of M-CNT Bundle.	93
7.3	Temperature-Dependent Crosstalk Model with Application of DIL (Driver-Interconnect-Load) in Coupled M-CNT Bundle Interconnects	94
7.4	Dielectric Surface Roughness Scattering Induced Crosstalk Performance of Coupled M-CNT Based Interconnects	95
		95

7.5 Scope for Future Work

References…….. 97

LIST OF FIGURES

Figure No.	Figure Description	Page No.
Figure 1.1	Cross-section view of interconnects (ITRS 2010).	**1**
Figure 1.2	Lattice structure of a single layer graphene sheet (a) Armchair (b) ZigZag GNR.	**4**
Figure 1.3	Schematic diagrams of (a) SWCNT, (b) DWCNT and (c) MWCNT.	**5**
Figure 1.4	Different possible structures of Mixed CNT Bundle (MCB).	**6**
Figure 1.5	A CMOS driven three-line architecture consisting of aggressor and victim lines in the form of (a) L-type and (b) T-type RLC networks [34].	**7**
Figure 2.1	Resistivity and current density of copper as the technology node reduces from 90nm to 22nm.	**12**
Figure 2.2	Normalized time-to-failure of CNT bundle and copper interconnect as the technology node increases.	**12**
Figure 2.3	Non-interacting (a) as well as interacting (b) electron model of a single-walled carbon nanotube.	**14**
Figure 2.4	Signal delay ratios of MWCNT / Cu interconnect at the global level for (a) minimum widths, (b) different widths but the same MWCNT diameter, and (c) identical widths but different MWCNT diameters.	**17**
Figure 2.5	Signal delay ratios of MWCNT interconnect with respect to Cu interconnect at the (a) intermediate level, and (b) local level for 32-, 22-, and 14-nm technology nodes. (c) The impact of R_{mc} per conducting channel on the delay increase in local, intermediate, and global level MWCNT interconnects.	**18**
Figure 2.6	Schematic diagram of Arc Discharge Method.	**19**
Figure 2.7	Schematic diagram of Laser Ablation Method.	**20**
Figure 2.8	Schematic diagram of plasma enhanced chemical vapour deposition (CVD).	**20**
Figure 2.9	Three lines architecture comprising of aggressor-victim-aggressor interconnect lines.	**21**
Figure 2.10	Different configurations of randomly and spatially arranged MCB interconnect.	**23**
Figure 2.11	Worst-case delay of shielded and unshielded RMCB and SMCB interconnect for (a) a resistive driver and (b) CNTFET driver.	**24**
Figure 2.12	Nyquist diagram of CNT bundle interconnect versus (a) length and (b) diameter	**33** **29**

Figure 2.13	Effect of temperature on stability of MLGNR and MWCNT.	**30**
Figure 3.1	Various proposed structures of MCBs: (a) ST-1, (b) ST-2, (c) ST-3 and (d) ST-4.	**33**
Figure 3.2	An equivalent RLC circuit model of MCB.	**34**
Figure 3.3	Geometry and equivalent distributed RLC circuit model of an MWCNT.	**37**
Figure 3.4	(a) MWCNT Resistance, (b), Inductance, and (c) Capacitance networks respectively with different shells.	**40**
Figure 3.5	Equivalent distributed *RLC* circuit model of MCB.	**44**
Figure 3.6	Propagation delay in a single line 'With Defect' (WD) and 'Without Defect' (WoD) for all the proposed structures with rise in temperature (300K to 500K).	**46**
Figure 3.7	CMOS inverter driven ESC model of capacitively coupled aggressor-victim line based MCB interconnect.	**46**
Figure 3.8	Crosstalk induced delay 'With Defect' (WD) and 'Without Defect' (WoD) for all structures of MCB for a temperature range (300K to 500K).	**48**
Figure 3.9	Comparison between coupled and single line delay for ST-4 for a temperature range (300K to 500K).	**48**
Figure 3.10	Positive crosstalk voltage noise peaks of all D-MCB structures & copper for a temperature range (300K to 500K).	**49**
Figure 3.11	Crosstalk induced time duration for all D-MCB structures & copper for a temperature range (300K to 500K).	**49**
Figure 4.1	Propagation delay (ns) (a) with tunnelling and (b) without tunnelling in all MCBs and copper when temperature is varied from 300K to 500 at 14nm technology node.	**54**
Figure 4.2	Crosstalk induced delay (ns) in best structure (MCB-4) taking different transition conditions of aggressor and victim line under even and odd mode of switching for temperature range from 300K to 500K.	**58**
Figure 4.3	Transient response at the far end of the victim line for capacitively coupled (a) MCB -1, (b) MCB-2, (c) MCB -3 and (d) MCB-4 interconnects when the temperature is varied from 300K to 500K.	**60**
Figure 4.4	Transient response at the far end of the victim line for capacitively coupled copper structure interconnects when the temperature is varied from 300K to 500K.	**60**
Figure 4.5	Positive crosstalk voltage noise peak of MCB structures and copper when the	**61**

Table 5.3	Percentage errors from simulated crosstalk induced glitch area values to its analytically calculated values for all structures of m-CNT bundles using ABCD and decoupling method.	**75**
Table 6.1	Impedance parameters for different MCBs on different substrate materials taken at length 1mm for different temperatures (300K-500K) at 14nm technology node.	**78**
Table 6.2	The Crosstalk Induced Glitch Area (CIGA) of various proposed structures of MCB considering smooth (α_1) as well as rough surface (α_2).	**83**
Table 6.3	Crosstalk Induced Noise Area (CIGA) and a relative percentage increase in crosstalk induced delay of S4 by including $\alpha 2$ w. r. t. $\alpha 1$.	**85**
Table 6.4	The Crosstalk Induced Glitch Area (CIGA) and dynamic crosstalk delay of the best structure of MCB (S4) taking various amplitudes of δsr.	**85**
Table 6.5	Bandwidth and 50% rise time for S4 for smooth($\alpha 1$) as well as rough surface ($\alpha 2$).	**89**

clock and signal distraction within a functional block. Local interconnects take control of the lowest layers, which connect the gates and transistors. Vias shown in the Fig.1.1 are metal fillings to enable inter-wire connections. Integrated Circuit (IC) designers initially used to neglect the interconnect modeling. But in Deep Sub-Micron (DSM) regime, the interconnect delay dominates over the gate delay. Consequently, that limits the performance of high-speed ICs. This is due to the fact that as the technology scales down to sub-micron regime, the clock frequency starts increasing and the feature size starts decreasing [5].

Aluminum (Al) was used in the early 1900s as an interconnect material because of its high conductivity and ohmic contact with silicon at higher current densities. As the technology progressed, the lateral and vertical dimensions of on-chip interconnects of Al were reduced. This in turn leads to issues like electro-migration and formation of hillocks [3]-[8]. The use of multiple layers of interconnect materials, such as Al with Ti, Cu, Ni, Cr, Mg, etc. were also used to reduce hillocks to an extent, but it was not sufficient to meet the growing demand for scaling. These issues lead to degrade the overall performance of interconnects. In order to solve this issue, various prospective materials such as gold, silver, and copper were considered. The bulk resistivity and thin film resistivity of these materials are tabulated in Table 1.1 [7]. Among the listed metals, copper (Cu) was preferred due to its more resistant to electro-migration. But, due to decrease in cross–section areas of densely packed copper interconnects at DSM regime, the surface-scattering, diffusive surface scattering and grain boundary scattering are increased. This results in a significant increase in copper's resistivity [7]. Despite such tenacious limitations, other alternatives were also searched for next-generation on-chip interconnects.

Table 1.1 Possible conducting materials [8].

Metal	Bulk resistivity (μΩcm)	Thin- film resistivity (μΩcm)
Ag (Silver)	1.6	3.5
Cu (Copper)	1.7	2.1
Au (Gold)	2.4	4.1
Al (aluminum)	2.65	2.7

Carbon based materials e.g., Carbon Nanotubes (CNTs) and Graphene Nano Ribbons (GNRs) emerged as most optimistic alternative materials for next generation on-chip interconnects [3],[6]-[10],[13]. The origination of CNTs and GNRs is from 2D graphite. A Carbon nanotube (CNT) is a graphene sheet rolled in cylindrical form. The lattice structure of graphene sheets

crosstalk-induced noise due to different signal switching conditions, namely functional crosstalk and dynamic crosstalk.

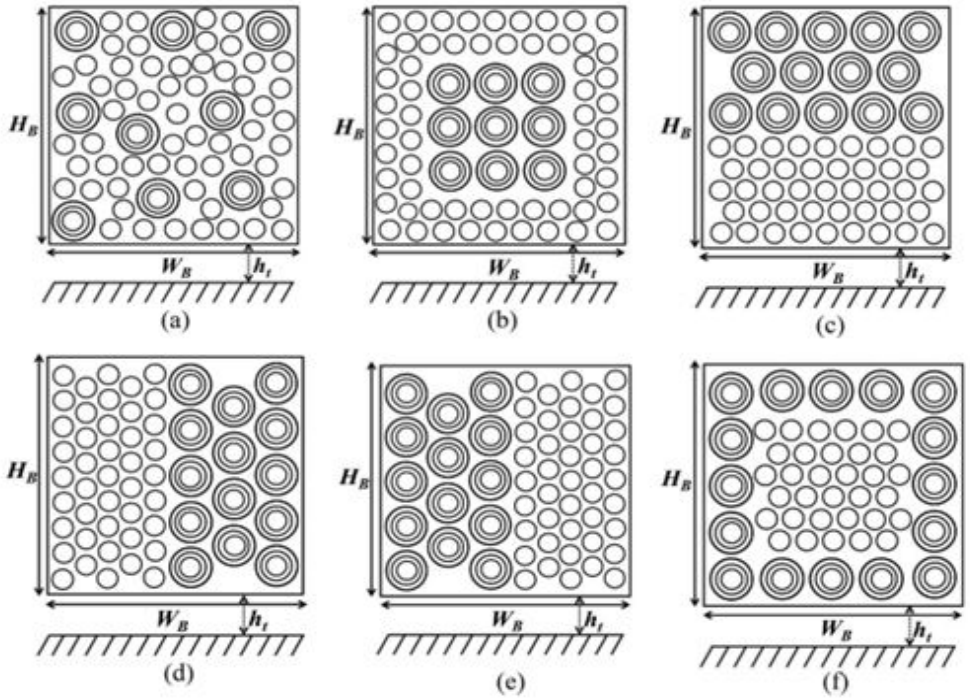


Figure1.4 Different possible structures of Mixed CNT Bundle (MCB) [10],[17]-[19].

A three lines architecture as shown in Figs.1.5 (a) and (b), consisting of aggressor and victim lines in the form of L-type and T-type RLC networks, respectively. An aggressor line is one in which input voltage is implied, causing a spike in voltage at the far end of the adjacent line because of coupling effects. This adjacent line is termed as the victim line. When the transition occurs in the aggressor line and the spikes in voltage are experienced at the far end of the victim line, it is called functional crosstalk. In contrast, when both lines, aggressor as well as victim, are switched simultaneously, then there is dynamic crosstalk [11], [22]-[33]. These both types of crosstalk cause delay, noise and a complete functional failure on the victim line in terms of signal integrity and reliability [11], [22]-[33].

In a m-CNT bundle (MCB) with MWCNT at the periphery and SWCNT at the center, there is the least crosstalk induced delay because current mostly conducts at the center of the tube due to the SWCNT, while MWCNT conducts less and acts as a shield. [11],[17]-[20]. Researchers have published several papers examining the crosstalk effect among coupled interconnects of CNTs kept at room temperature [20]-[32]. Beyond 45 nm technology node, the resistivity of metal

as the substrate for the mixed CNT bundle interconnects. An equivalent single-conductor (ESC) model of the four possible structures of the m-CNT bundle interconnect is applied to examine the crosstalk-induced delay and frequency spectrum in the temperature range from 300 to 500 K. Also, the influence of the substrate surface roughness on the dynamic and functional crosstalk-induced delays for the four possible structures of m-CNT bundle-based interconnects is studied. The frequency responses of the best structures of m-CNT bundle interconnect on all the dielectric materials as well as their frequency spectrums across the studied temperature range are also analyzed at 14nm technology node.

Chapter 7 finally, the thesis concludes with a discussion of future possibilities in the field of VLSI interconnects.

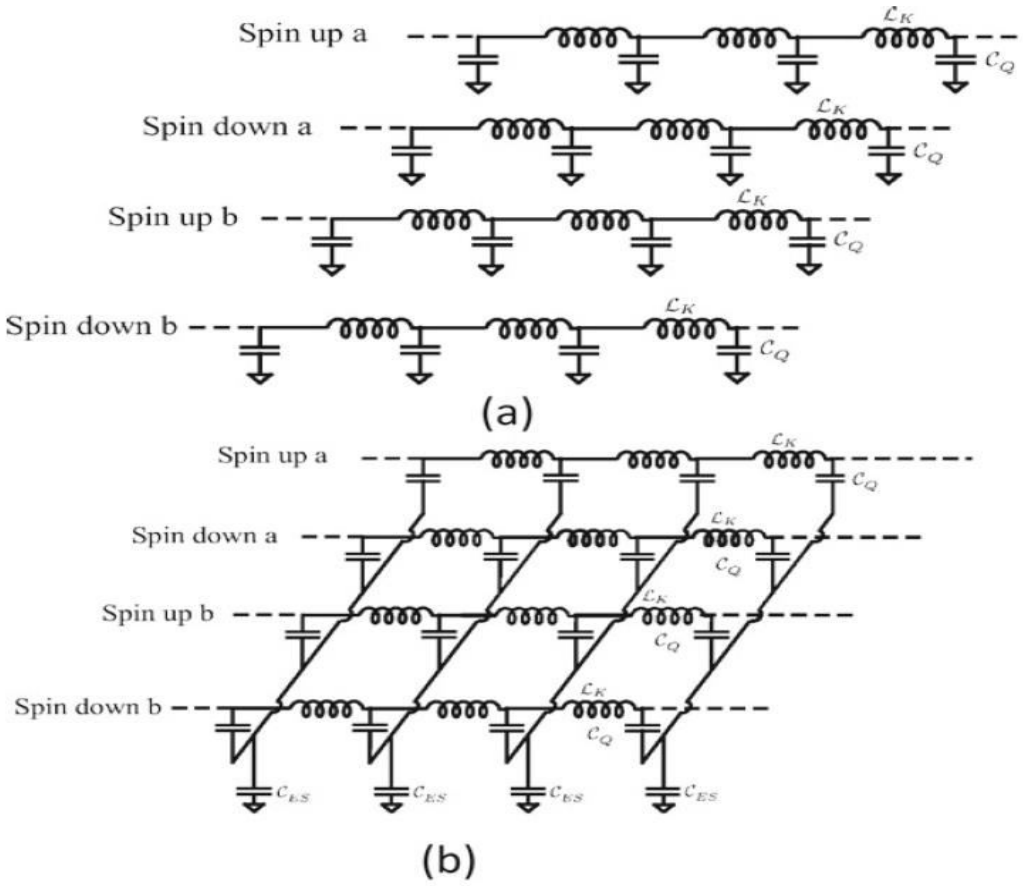


Figure 2.3 Non-interacting (a) as well as interacting (b) electron model of a single-walled carbon nanotube [25].

Here the e-e interaction is taken into consideration and therefore electrostatic capacitance is available in the model. Fig. 2.3 (b) illustrates how all four modes are coupled, and in the case of dc, applying ac voltage will excite all four channels simultaneously, leading to zero voltage at one end of the nanotube, and the voltage associated with all four channels will be equal. This is the normal mode of operation and other three modes do not carry current, hence called as neutral mode. This type of model is known as Interacting Circuit Model for Metallic CNT. Next type of circuit model as stated by burke et al. [52] is the AC SPIN CHARGE SEPARATION CIRCUIT model having 'ac' excitations. Luttinger liquid theory states that in the charge mode, the 'ac' currents flows through spin up and down channels together and hence the corresponding currents are equal in magnitude but flows in opposite direction, leading to no charging of electrostatic capacitance near to the gate. This is spin mode or neutral mode consisting of quantum capacitance whereas on the other hand, charge mode consists of only quantum capacitance.

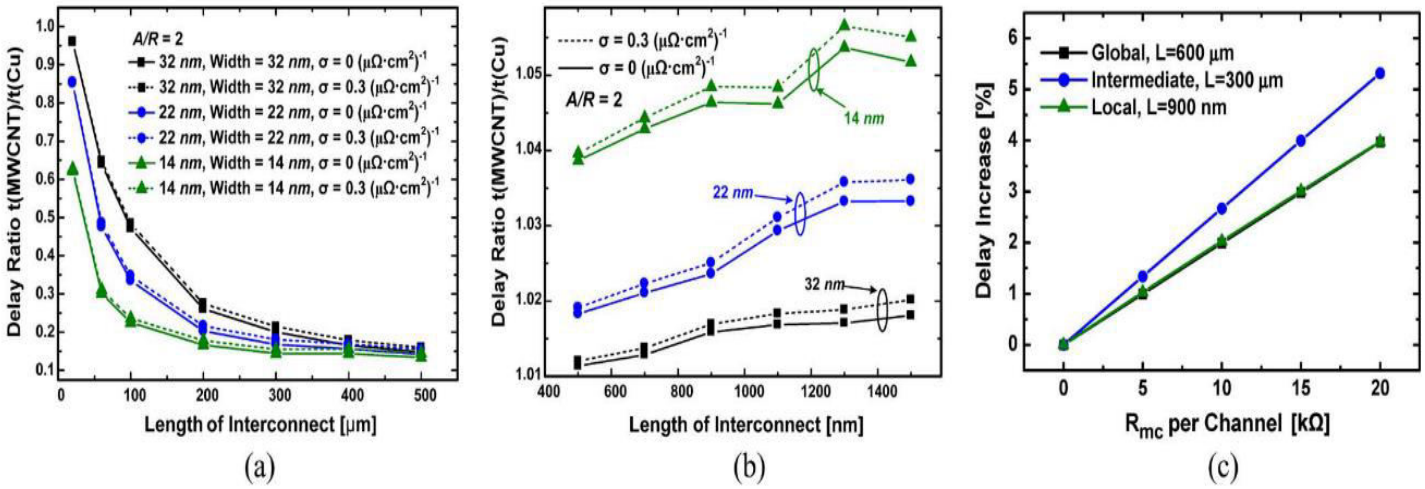


Figure 2.5 Signal delay ratios of MWCNT interconnect with respect to Cu interconnect at the (a) intermediate level, and (b) local level for 32-, 22-, and 14-nm technology nodes. (c) The impact of R_{mc} per conducting channel on the delay increase in local, intermediate, and global level MWCNT interconnects [3].

In the process of fabrication and purification of CNTs, various defects like atom vacancies, doping, impurities etc., get introduced by irradiation with energetic particles which leads to modifications in the properties of CNT as per the requisite of application [68]-[70]. These defects alter the properties of CNTs by bringing a change in the chemical bond. According to scattering theory, due to backscattering of electrons, the MFP of electrons will reduce due to defect causing a considerable increase in the overall resistance of an interconnect. A change in overall resistance will lead to considerable change in the performance of an interconnect [68] [23],[24],[26],[71],[72]. A considerable decay in the MFP of defected CNT is obtained when studied single and double vacancy in a zig-zag CNT is found [70]. Due to the absence of C-C bonds, vacancies in the honeycomb structure of CNTs are created and therefore, short phonon waves diminish leading to a decrease in the MFP [71]. The path of semiconducting tubes is highly responsive to a disorder which makes it a shorter mean free path [40].

2.2 FABRICATION OF CNT

There are various methods of production of carbon nanotubes. The most common and popular one is the Arch Discharge method, shown in Fig.2.6. As pressure is applied to the enclosure, metal catalysts like nickel, cobalt are present, while temperatures are kept at 4000K and a current of 50-100A is passed, all of which causes the carbon to solidify on the cathode tubes, resulting in

work as shield. This study stated that the overall reduction in out-phase and in-phase delays are 79.3%,82.8%, respectively and 80% in MCB structure that has SWCNTs in the center and MWCNTs in the periphery when compared with randomly distributed SWCNTs and MWCNTs in the MCB.

An accurate FDTD (Finite Difference Time Domain) model was developed by Ramesh Kumar et al. [77] which mainly emphasized in analyzing functional and dynamic crosstalk in n- number of coupled interconnect lines. A 1% of error was obtained in propagation delay when the simulation was done on HSPICE software. Aggarwal et al. [78] also used FDTD method to analyze the performance of SWCNT with current signal mode and this proposed model showed a maximum error of 3% when compared with SPICE results for the transient analysis of current mode signaling scheme (CMS) SWCNT bundle-based interconnect. In CNT interconnects, crosstalk effects are computed by using finite difference time domain method at several technology nodes. [79]. Many researchers have analyzed crosstalk effects of multi-walled CNTs or single wall CNTs, by using ABCD parameter based modeling approach at different technology nodes [50] [80]-[85]. In another study, an action shielding of MWCNTs is done for cancelling out the effects of functional crosstalk [86].

While comparing MCBs with MWCNT and Copper, it is showed that mixed CNT bundle structures show less crosstalk induced delay and highest cut off frequency [24]. By using HSPICE simulations, it is also observed that there is a 6.8% reduction in crosstalk induced delay in MCB containing SWCNTs and MWCNTs than, those having SWCNTs and DWCNTs [25]. In another research work, a considerable reduction in crosstalk noise in quaternary integrated circuits using spatially arranged MCBs is obtained, in which 43% and 66% improvement in EDP(Energy Delay Product) is obtained, as compared to copper counterpart using HSPICE simulations at 22nm technology node [26]. Majumder et al. [87] also analyzed crosstalk induced delay of randomly distributed mixed CNT bundle interconnects and showed that the reduction in overall crosstalk induced delay of MCB is 65.03% and 23.54% in comparison with SWCNTs and MWCNTs bundles, respectively. In another work by Kumbhare et al. [88], three different configurations of randomly arranged and spatially arranged MCB interconnects were taken as shown in Fig. 2.10. Now to reduce the miller effect, in case of out of phase switching, a similar material is put as an active shielded line between the two coupled interconnects. The delay obtained when aggressor line switches from low to high and victim line from high to low

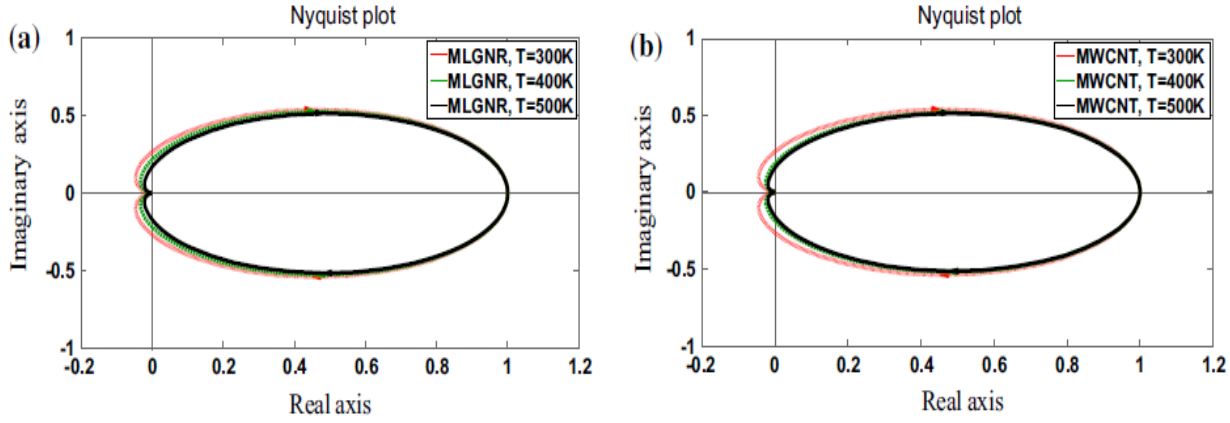
performance due to shielding effect of outer shells. MWCNT, SWCNT, and copper-based interconnects are also examined at the 32, 22nm, and 16nm technology nodes in [93].

MWCNT outperforms SWCNT and copper interconnects in terms of delay, power dissipation, and power delay product over a temperature range of 200K to 450K. Chiariello et al. [28] took graphene nano-ribbons and CNT bundles as a simple *RLC* representation and their case studies reported that w.r.t SWCNT, GNR and MWCNT interconnects are almost insensitive to change in temperature making them better candidate for replacement of copper in a complete chip with an inclusion that they are fabricated very well. Under different process, temperature and voltage variations, the timing delay of CNT and copper interconnect are analyzed at 32nm technology node. The performance varies by 3%, 13.23% and 50% with nominal voltage, room temperature and process variation, respectively. It is found that at long interconnect, CNT outperforms copper [94]. Sandha et al. [95] compared copper and MWCNT bundles at 16, 22 and 32nm technology nodes while taking temperature as a major factor. The MFP of MWCNT bundle decrease when temperature is increased and therefore the resistance increases but due to the number of shells put concentric to each other, the resistance is much lesser than copper interconnects and therefore more suitable for future interconnects. Also as the size of driver and no. of shells of MWCNT bundles increases, the resistance decreases which leads to lesser propagation delay than copper interconnects [96]. Rai, et al. [11] worked on temperature-dependent circuit models of MCB structures by taking consideration of both tunneling and inter-shell coupling effects between adjacent shells. It was discerned by them that the crosstalk induced noise voltage levels in SWCNT bundle interconnects obtained through thermally aware models are higher in comparison to temperature-independent counterpart.

2.3.2 Scattering In Coupled CNT Interconnects: Effects On Transport Phenomena

Surface roughness also plays a vital role, in the transport properties of CNTs or CNT based devices [43], [97]-[99]. The roughness of the surface is a dominant factor that degrades the electronic properties of CNTs. It is observed as a significant contributor for conducting losses, which further aggravates crosstalk induced effects accounting substrate surface roughness (SSR). SSR is an arbitrary phenomenon, which arises as a result of variation in the fabrication process, and is also deliberately added to gain the adherence between layers of dielectric and the surface of the conductor. SSR and assertive scaling to nanometer range causes, extreme signal reliability issues in coupled on-chip interconnect [44]-[46]. An efficient shielding method was used in

and (b). As the temperature rises, resistance rises as well, making the system more stable.



(a) **(b)**

Figure 2.13 Effect of temperature on stability of (a) MLGNR and (b) MWCNT [107].

2.4 CONCLUSION

In reviewing the related literature, it is observed that although temperature-independent crosstalk analysis of various CNT has been done, but temperature-dependent analysis of mixed CNTs as well as of GNRs is yet to be conducted while considering defects caused by vacancies in the lattice structure of a carbon sheet. A comparison of defect free and defect based MCB interconnects has to be drawn. Also, as observed while reviewing performance of CNTs, the dielectric surface based scattering induced performance analysis of MWCNTs and mixed CNTs are also missing in the recent literature. Many researchers have taken various orientations of SWCNT and MWCNT in a MCB and have analyzed their performances but in actual performance analysis of random mixed CNT performance is yet to be analyzed by taking factors like defect and dielectric surface roughness-based scattering. To date, only a few studies have reported an algorithm for describing a randomly distributed SWCNTs and MWCNTs in MCBs. Frequency based stability analysis of a single line and coupled line architecture of MCB interconnects are yet to be studied in the DSM regime.

3.1.1 Temperature-Dependent Irradiation-Induced Defect Based Model For SWCNT And MWCNT Bundles

The model presented in this thesis is based on Laundauer-Buttiker (LB) theory, which deals with transmission function from one contact to another contact. In this model, the internal state of the conducting system never appears in the formalism unlike non-equilibrium green function (NEGF) method, which deals with the special case, when the scattering is non-dissipative in the conducting system [52],[118]. Now assuming that the coordinates of the SWCNTs & MWCNTs are cylindrical, and based on LB theory, the impedance parameters of SWCNT and MWCNT are calculated by using forthcoming expressions.

The contact, quantum and scattering resistances are the three kinds of resistance present in SWCNT bundle [90]. These resistances are expressed as R_C, R_Q and R_S, respectively. The contact resistance occurs because of imperfect contact that exists between metal and semiconductor. When the length of a CNT is less than the MFP (λ), the nanotube travels in a ballistic manner. The resistance, thus produced is the fundamental resistance called as quantum resistance (R_Q). However, scattering resistance (R_S) occurs if the CNT length is greater than λ.

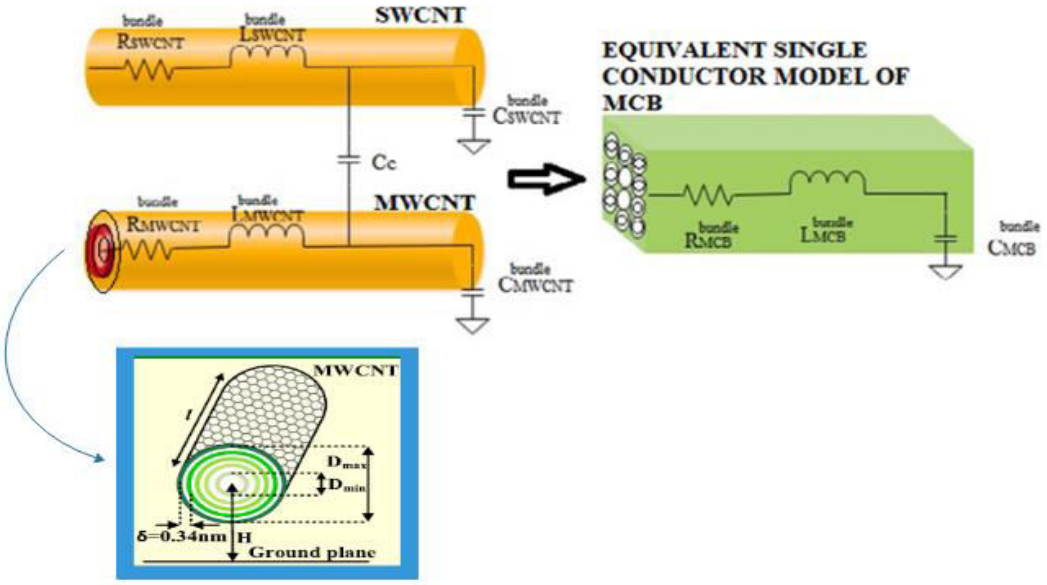


Figure 3.2 An equivalent RLC circuit model of MCB.

Because MWCNTs have variable diameters for different shells, this results in different MFPs and channel counts for each shell, resulting in distinct circuit characteristics. Thus, a recursive scheme is required to calculate circuit parameters of MWCNT bundle. The capacitive coupling between the shells and a tunneling effect is induced due to the potential difference between adjacent shells of an MWCNT. The *p.u.l* inter-shell tunneling conductance is obtained by [3],[33], [54]

$$G_T = \sigma . \pi . D \qquad (3.14),$$

where, 'σ' is 0.3($\mu\Omega cm^2$)$^{-1}$ is the normalized tunneling conductivity at δ=0.34nm, 'D' denotes the shell diameter.

As shown from Fig. 3.4(a), the next shells's scattering resistance R_S is in parallel with a series combination of tunneling resistance R_T and R_S of the prior shell. Rs_p can be obtained by Eqn. (3.2).So, the total *p.u.l* TD resistance of an MWCNT, '$R_{MWCNT}(T)$' is obtained recursively as [3],[33], [54]

$$R_{recursive,p} = R_{Sp}\ , p = 0 \qquad (3.15)$$

here, $R_{recursive,p+1}$is calculated in a recursive manner given as

$$R_{recursive,p+1} = \left[\frac{1}{R_{recursive,p}+R_{T,p}} + \frac{1}{R_{S,p+1}}\right], p = 0,1,2,3 \ldots \ldots n-1 \qquad (3.16),$$

$$R_{MWCNT}(T) = R_{recursive,n-1} \qquad (3.17)$$

In Eq. (3.16), 'p' denotes the shell number which ranges from *0* to *(n-1),* where 'n' represents 'N_{shell}' (total no. of shells). Hence, the total low bias TD resistance of a bundle comprised of MWCNTs is determined by dividing the MWCNT's resistance by number of MWCNTs given as [3],[33], [54]

$$R_{MWCNT}^{bundle}(T) = {R_{MWCNT}(T)}/{n_{MWCNT}} \qquad (3.18)$$

3.2 TEMPERATURE-DEPENDENT IMPEDANCE ANALYSIS

Temperature-dependent impedance study is performed in this part for all four potential architectures of MCB-based interconnects at the 14nm technology node. Table 3.1[120] shows how all of the physical parameters were generated from ITRS-2013. The inter-shell capacitance and tunneling effects are considered in the present analysis because these effects are significant in analyzing the performance of MWCNT bundle as reported in "Ref. [11]". The diameters of SWCNT and MWCNT are presumed as 1nm and 8nm, respectively [119]. Table 3.2 is showing circuit parameters for four different MCB (defected as well defect free) structures and copper of 1mm long interconnect taking complete temperature range (300-500K).The defected and defect free MCBs are represented as D-MCBs and DF-MCBs, respectively.

Table 3.1 ITRS Table (2013) for different structures taken at length 1mm (Global interconnects) at temperature 300K for technology node 14nm[41].

Global Interconnects	**Width, W(nm)**	24
	A/R (wire)	2.34
	Height, T (nm)	56
	A/R (VIA)	1.5
	YILD Thickness, h1 (nm)	36
	ρCu (μΩ-cm)	5.69
	Effective dielectric constant εr	2.48

Table 3.2 Impedance parameters for various structures of MCB and copper taken at length 1mm for temperature (300K-500K) at technology node 14nm.

	RESISTANCE (KΩ) DF-MCBs				**RESISTANCE (KΩ) D-MCBs**				**INDUCTANCE (nH)**				**CAPACITANCE (pF)**			
TEMP (K)	**ST-1**	**ST-2**	**ST-3**	**ST-4**	**ST-1**	**ST-2**	**ST-3**	**ST-4**	**ST-1**	**ST-2**	**ST-3**	**ST-4**	**ST-1**	**ST-2**	**ST-3**	**ST-4**
300	7.75	7.19	7.93	7.44	8.85	8.23	9.23	8.74	58.97	74.24	92.64	69.35	0.4179	0.1784	0.1381	0.1385
350	9.44	9.57	10.7	9.76	10.56	10.65	12.01	11.06	56.59	70.02	87.21	65.45	0.4118	0.1784	0.1381	0.1385
400	10.3	11.7	13.3	11.86	11.43	12.86	14.66	13.16	52.68	63.06	78.27	59.19	0.4118	0.1784	0.1381	0.1385
450	12.5	14.6	16.8	14.59	13.69	15.78	18.18	15.90	51.03	60.14	74.51	56.56	0.4141	0.1792	0.1387	0.1389
500	14.9	18.5	21.53	18.18	16.22	19.64	22.84	19.49	49.57	57.54	71.17	54.22	0.4141	0.1792	0.1387	0.1386

It is noted from Eqs. (3.1), (3.2) and (3.18), that the temperature has a significant effect on the resistance of interconnects because as the temperature increases, scattering of electrons increases which in turn increases the equivalent resistance of interconnect. So, it is justified to say that resistance is a function of TD mean free path of electrons. Also, from Eq. (3.2), a considerable increase in resistance is obtained due to irradiation-induced defect. A D-MCB decays the mean free path of electrons and due to this, a considerable increase in overall resistance occurs. As depicted in Table 3.2, the resistance of all the MCB structures and copper is increasing with the rise in temperature range (300K to 500K). Over the temperature range shown in the table, D-MCB structures have a greater resistance value than DF-MCB structures (300K to 500K). This is because D-MCB structures have a lower value of the mean free path as compared to DF-MCB structures. As seen from Eqs. (3.36) and (3.37), the inductance and capacitance of MCB structures are also dependent upon the TD no. of conducting channels. Table 3.2 is clearly showing the variations of both inductance and capacitance with temperature. The decrease in inductance with the rise in temperature indicates the dominance of conducting channel-dependent kinetic inductance over magnetic inductance. While the capacitance of TD MCB structures is showing inconsiderable effects with the rise in temperature. This is because of the TID electrostatic capacitance dominates over quantum capacitance in the total capacitance of MCB structures. As seen in "Ref. [28],[53]", the equivalent inductance and capacitance of copper are TID quantities.

In the present study, temperature variations (300K to 500K) on the circuit parameters (i.e *R, L&C*) have been taken. Because, it has been observed that with an increase in resistance and inductance, crosstalk induced noise peak increases while in case of increase in capacitance, crosstalk induced noise voltage peaks reduce [28], [32], [53], [87]. On the other hand, the time duration of noise pulse increases with increase in line resistance [11].

3.3 TEMPERATURE-DEPENDENT ANALYSES

From the aforementioned discussion, it is quite clear that temperature plays an essential role in the performance analysis of any interconnect. As the technology is narrowing down, the size of the integrated circuits is decreasing and interconnects are showing significant effect on propagation delay and crosstalk [11], [23], [28], [53], [115]. In the forthcoming subsections, the

propagation delay of DF-MCB and D-MCB bundles are analyzed based on two different distributed *RLC* networks of single interconnect and capacitively coupled interconnects, respectively, shown in Figs. 3.5 and 3.7. Data encapsulated in Table 3.2 are used for the purpose of simulation. Width and thickness of interconnect are taken as 24 nm and 56 nm, respectively [119]. In the repeater, the width of p-MOS transistor is taken as double the n-MOS transistor. The aspect ratio was fixed as 100 and the optimum no. of repeaters were calculated for all the MCB structures and copper**.** The no. of repeaters which give the minimum average delay is selected as the optimum no. of repeaters.

The circuit parameters obtained are obvious to affect the performance of the interconnect w.r.t. propagation delay. It is now quite clear that the temperature affects the effective MFP of SWCNT bundle, MWCNT bundle and MCB bundle. So, it becomes necessary to study the TD propagation delay analysis of these bundles. Now, two cases viz. 'With Defect (WD)'and 'Without Defect (WoD)' are taken into consideration. While considering defected MCB (D-MCB) structures, it is observed from Table 3.2, their resistance is higher than that of defect-free MCB (DF-MCB) structures. A distributed *RLC* circuit of single interconnect is taken to examine the propagation delay as shown in Fig. 3.5. The circuit is driven by a CMOS driver with a clock speed of 0.1 GHz, V_{dd}=0.9V and is terminated by a capacitive load C_L of 0.20fF at 14nm technology node [119].

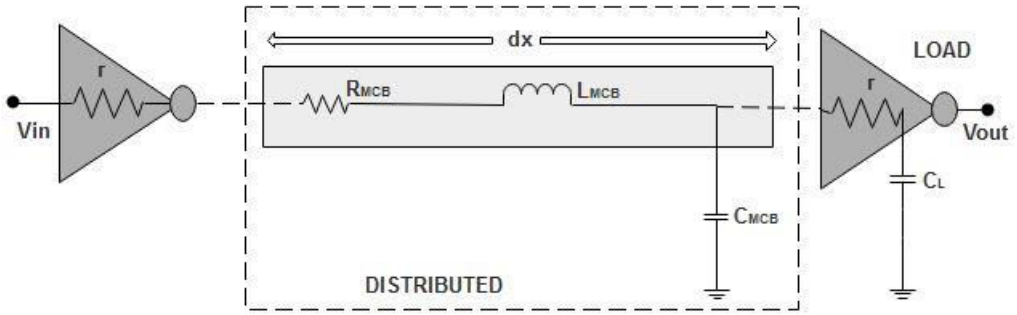


Figure 3.5 Equivalent distributed *RLC* circuit model of MCB.

For all MCB structures (defected as well defect-free), 90% delay is extracted from SPICE simulation results. Fig. 3.6 is clearly showing that with a rise in temperature (300K to 500K), the normalized propagation delay is increasing monotonically for both the cases of 'WD' and

'WoD'. Copper delay is used to normalize the correspondent MCB structures at different temperature from 300K to 500K. Copper has higher resistance, lower inductance and lower capacitance as compared to MCB structures (see Table 3.2). So, copper has a higher delay over a range of temperature (300K to 500K) in comparison to MCBs. Besides, this normalized delay is higher when defects are taken into account for every MCB structure. Also, comparing all the structures, it is observed that ST-4 is showing the least propagation delay in both the cases of WD and WoD. So, from the result shown in Fig. 3.6, it becomes obvious to state that defect in CNT plays an extensive role in analyzing the normalized propagation delay of all the structures of m-CNT bundles.

A major concern for the future generation of CMOS VLSI circuits is the crosstalk noise between two adjoining interconnects [11], [23], [26], [28], [53], [116]. The effect of coupling is mandatory to analyze because the feature size is decreasing in deep submicron dimensions. To investigate crosstalk induced noise voltage, a two-line distributed capacitively coupled RLC interconnect circuit is used, as shown in Fig. 3.7. The circuit is driven by a CMOS driver with a clock speed of 0.1 GHz, V_{dd} =0.9V, and is terminated by a capacitive load of 0.20fF at 14nm technology node. In the two-line architecture, one line is taken as aggressor line and another line is taken as victim line. Various conditions are taken for aggressor and victim in which victim line is kept fixed at logic '0' or '1' and aggressor is switched between '0' to '1' or '1' to '0' under functional crosstalk. While in case of dynamic crosstalk, both lines are switched from '0' to '1' under even mode of switching [23], [87], [115].

Fig. 3.8 shows normalized crosstalk induced delay of capacitively coupled interconnects of MCB w.r.t. copper over a temperature range (300K to 500K). Switching lines; aggressor as well as victim are switched from logic '0' to '1'under even mode of switching for dynamic crosstalk. It was shown in [113] that the performance of coupled interconnects is better under even mode of switching in comparison with odd mode. Copper delay is used to normalize the correspondent MCB structures. The normalised crosstalk generated delay rises with increasing temperature for all configurations, as shown in Fig. 3.8, although this change is more pronounced when defects are considered. The influence of temperature change on circuit characteristics for both MCB structures and copper is reflected in these variations. ST-1 has the longest delay due to the combined effect of greater resistance and capacitance values and

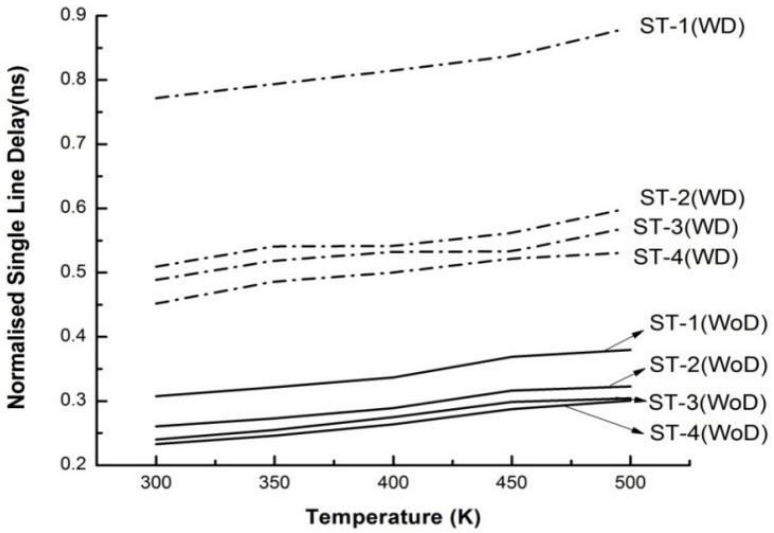


Figure 3.6 Propagation delay in a single line 'With Defect' (WD) and 'Without Defect' (WoD) for all the proposed structures with rise in temperature (300K to 500K).

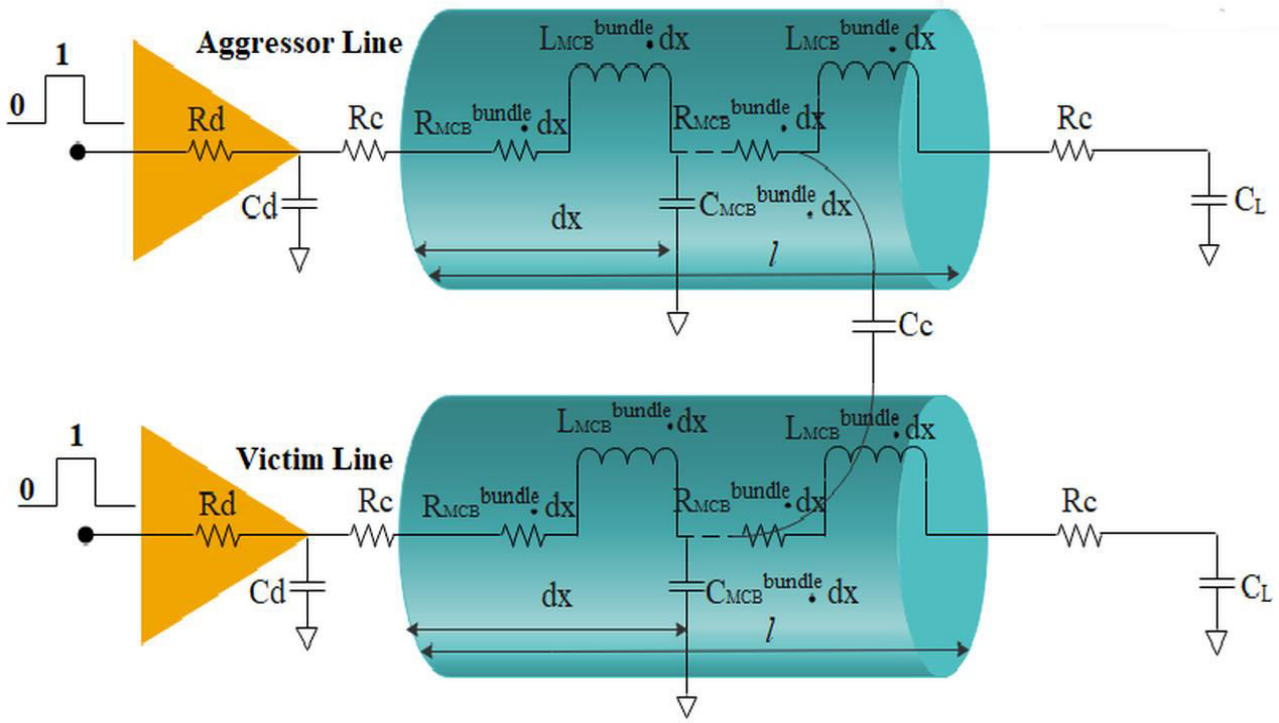


Figure 3.7 CMOS inverter driven ESC model of capacitively coupled aggressor-victim line based MCB interconnect.

lowest inductance values, whereas ST-4 has the shortest delay due to lower resistance and capacitance values and higher inductance values (see Table 3.2)From Figs.6 and 8 it is observed that ST-4 is giving least delay for single and coupled (aggressor-victim) lines architecture in comparison to other structures. Fig. 3.9 depicts the 90% normalized delay w.r.t. copper for ST-4 taking single and coupled lines, respectively, taking entire range of temperature (300K to 500K). In this comparison, irradiation-induced defected ST-4 are taken into consideration. It can be seen that delay is always higher while considering crosstalk induced effects w.r.t. single line delay. It is because of the fact that while considering crosstalk effects, coupling increases which further leads to more delay with increase in temperature. Various conditions are taken for coupled A-V lines of MCB in which victim line is kept fixed at logic '0' or '1' and aggressor line is switched between '0' to '1' or '1' to '0' under functional crosstalk condition. The transient analysis are performed and the crosstalk induced noise peak of the noise pules at the far end of victim line are extracted. The distinct features of the results are illustrated in Fig. 3.10 and 3.11.

From Fig. 3.10, it is noticed that the crosstalk induced noise voltage peaks rises when defect is considered with an increase in temperature (300K to 500K). This is due to the dominating effect of TD circuit parameters like inductance over resistance & capacitance on transient response at the victim line's far end.

In addition, as compared to other topologies including copper, ST-1 exhibits smaller crosstalk induced noise voltage peaks as temperature rises (300K to 500K). This is due to the dominating values of resistance and capacitance over the inductance of ST-1(see Table 3.2). However, Table 3.2 shows that in comparison to other structures (ST- 2, ST-3 and ST-4) of MCBs and copper, ST- 1 has larger resistance and lower inductance and capacitance at every temperature range (300K to 500K). The crosstalk induced noise voltage peaks in capacitively coupled interconnect is observed to be smaller due to larger value of resistance, inductance and a smaller value of capacitance [11],[53].Further, from Fig.11, it has also been seen that the width/duration of crosstalk induced transient responses is increased with a rise in temperature range (300K to 500K). The variations are directly reflections of the consequences of defect generated temperature variations on resistance. As the resistance increases, crosstalk noise peak decreases and time duration of the pulse increases [11], [53]. As compared to all the MCB structures, copper has higher values of resistance and higher inductance, and lower values of capacitance (see Table 3.2). So, the crosstalk induced noise voltage peaks and width of noise pulse obtained

in copper are higher than the crosstalk noise peak obtained by other MCB structures. The width of the crosstalk noise peak is wider when the defect is considered in MCB structures.

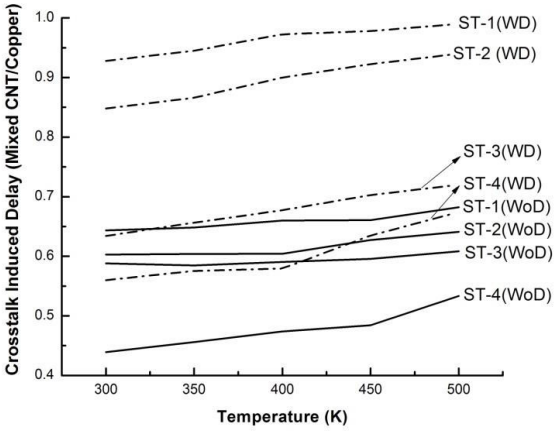


Figure 3.8 Crosstalk induced delay 'With Defect' (WD) and 'Without Defect' (WoD) for all structures of MCB for a temperature range (300K to 500K).

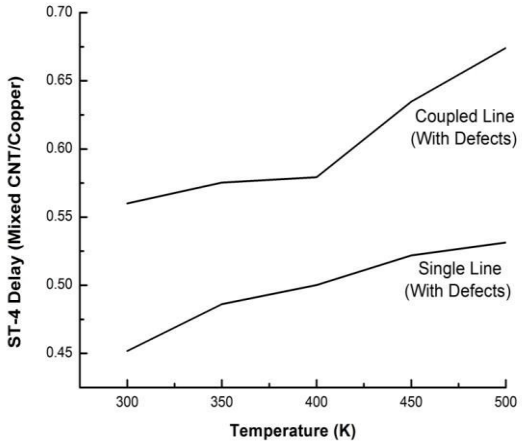


Figure 3.9 Comparison between coupled and single line delay for ST-4 for a temperature range (300K to 500K).

Depending on the relative switching at the near end of aggressor line under functional crosstalk (victim line is kept fixed at logic '0' or '1' and aggressor is switched from '0' to '1'), the crosstalk has distinctive impacts on the circuit performance as depicted in Table 3.3. Thee rise/fall glitches affect the functionality of the circuit whereas undershoot/overshoot affects the reliability of the circuit.

Table 3.3 Various transitions of aggressor and victim lines with their results and impacts under functional crosstalk.

S. No.	Transitions of Aggressor line	Transitions of Victim line	Conclusion	Impacts
1	0 to 1	Logic 0	Overshoot	Reliability
2	0 to 1	Logic 1	Rise Glitch	Functionality
3	1 to 0	Logic 0	Fall Glitch	Functionality
4	1 to 0	Logic 1	Undershoot	Reliability

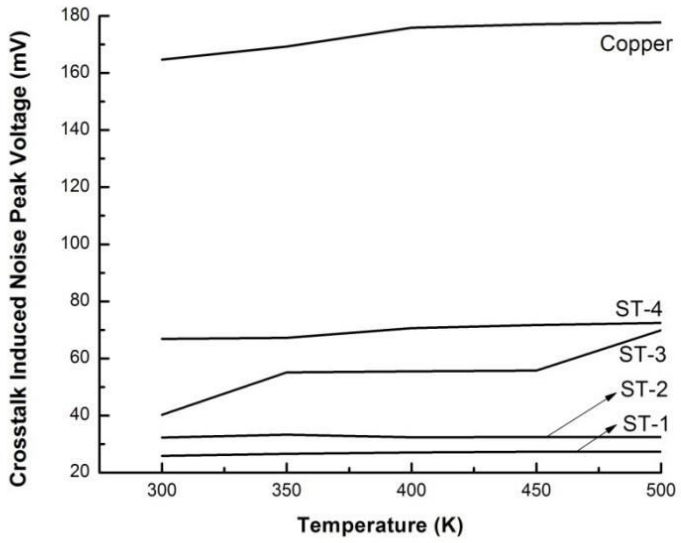


Figure 3.10 Positive crosstalk voltage noise peaks of all D-MCB structures & copper for a temperature range (300K to 500K).

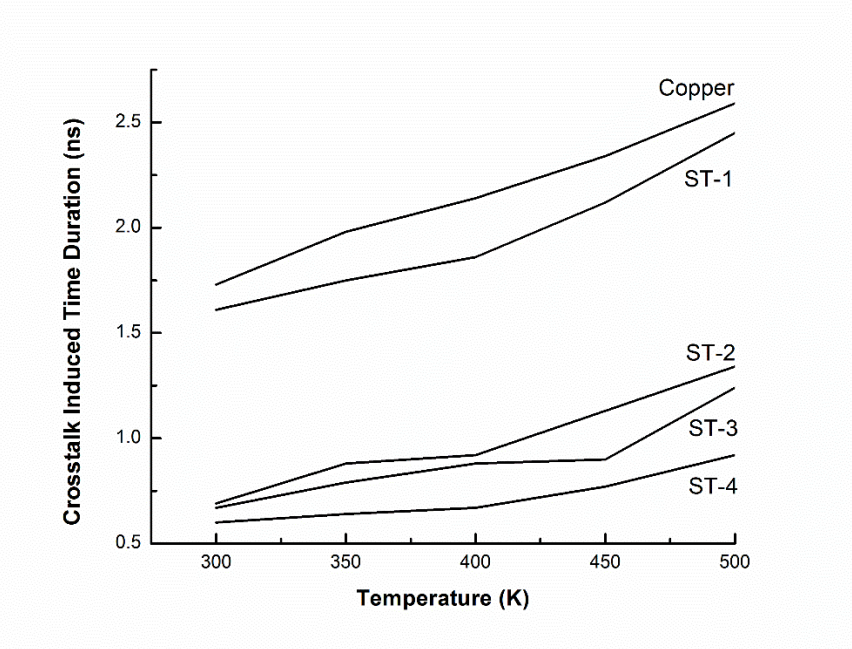


Figure 3.11 Crosstalk induced time duration for all D-MCB structures & copper for a temperature range (300K to 500K).

3.4 CONCLUSION

Temperature-Dependent (TD) irradiation-induced defect-oriented circuit modeling and performances analyses of the capacitively coupled interconnect of MCBs are analyzed for temperature range (300K-500K) for the entire length of interconnect at 14nm technology node. The effect of the irradiation-induced defect in CNT on propagation delay for all four structures of the MCB is observed. The propagation delay of four different structures of MCB increases while the defects are considered. Propagation delay is appreciably higher when crosstalk effects are taken into consideration. Crosstalk induced positive peaks and time durations of victim output pulses in copper are much higher than that of all the structures of MCB for the entire range of temperature. The research work included in this chapter, confirms that rise in temperature and defect considerations in real structures of MCB play a crucial role in the study of the performance and reliability of interconnects in the DSM regime.

CHAPTER-4

TEMPERATURE-DEPENDENT CROSSTALK INDUCED FREQUENCY SPECTRUM ANALYSES IN ADJACENT INTERCONNECTS OF MIXED CARBON NANOTUBE (m-CNT) BUNDLE

Device scaling is decreasing rapidly to nanometer range which leads to the grain boundary, surface-scattering, diffusive surface scattering, and electro-migration effects in existing copper based on-chip interconnect Therefore, a promising new material for on-chip interconnect is required. Nowadays, Carbon Nano Tubes (CNT) is preferred as on-chip interconnect material in place of copper due to its outstanding properties like longer mean free path (MFP), higher tensile strength and high current density [3], [48], [54], [56], [63], [112], [121].

Beyond 45 nm technology node, due to different types of scattering, the resistivity of metal increases which rises the temperature of interconnects and therefore it becomes crucial to study the effects of temperature-dependent aspects in CNTs [11], [33], [28], [53], [90]. Resistance increases with rise in temperature which in turn expands the time duration of noise pulse [56] . It was discovered that the low–bias resistance of CNTs get affected by optical phonon scattering when a variation in temperature is done [48]. It has also been observed that the crosstalk induced noise voltage levels in SWCNT bundle interconnects obtained through thermally aware models are higher in comparison to temperature-independent counterpart [90]. Propagation delay, power dissipation and PDP (Power Delay Product) have already been analyzed taking temperature range from 300K to 500K [28]-[53]. As, the technology is scaling down temperature-dependent crosstalk among interconnects is becoming a major concern. A frequency spectrum analysis of coupled interconnects of SWCNT bundle was performed[11] . It has been observed that for entire range of frequency, SWCNT bundle is showing less noise amplitude as compared to copper. This means SWCNT bundle is filtering more noise frequency components than copper at victim output. In [122], the author has shown that the amplitude of victim's far end output waveform decreases with increase in temperature. Hence, a detail investigation is also required to analyze the temperature-dependent frequency performance in coupled interconnects of MCB.

In this chapter, the temperature-dependent analyses of delay in single line and crosstalk under functional and dynamic signal switching conditions in capacitively coupled interconnects of m-

CNT bundle (MCB) are presented, and their frequency spectrum analyses at the far end of single and coupled lines are also investigated for temperature varying from 300K to 500K at 14nm technology node. In this study, four possible structures of MCB (e.g., ST-1, ST-2, ST-3 and ST-4) are considered. For the sake of simplicity, these four structures are further labeled as MCB-1, MCB-2, MCB-3 and MCB-4. Moreover, the results in terms of delay, crosstalk induced delay and frequency spectrum are compared with copper interconnects at same technology node.

4.1 PERFORMANCE ANALYSIS OF MCB STRUCTURES AND COPPER

In this chapter, different arrangements of SWCNT and MWCNT are taken in four different structures to analyze the performance of MCB bundles. Four different physical structures of MCBs, named as MCB-1, MCB-2, MCB-3 and MCB-4 (also known as ST-1, 2, 3 & 4) are considered as shown in the Fig. 3.1 [11],[17],[28],[53],[122].

This section deals with temperature-dependent (300K-500K) performance analysis of all MCBs and copper based interconnects taking tunneling conductance effects into consideration. Tunneling resistance is a small resistance in series with shell resistance of MWCNTs placed in MCBs which in turn increases the overall resistance of MCB structures.

Many researchers have ignored the effect of tunneling between adjacent shells in MWCNT bundles or have assumed it to be negligible or sparsely small [3], [18], [115]. Also, in [19] conductance between the shells was taken as around $10K\Omega^{-1}$ with shell interval is 0.34nm. In [63] and [121], authors have accepted that at defect free global interconnect, tunneling conductance is negligible but authentically in fabrication process, tunneling conductance is always present and hence should not be ignored as it directly affects the overall resistance and consequently influence the performance of the interconnect. At the far end of victim line, tunneling and inter-shell coupling effects in between adjoining shells are taken into consideration in [56] while calculating crosstalk noise voltage levels.

By considering single line architecture**,** a propagation delay of all the structures of MCB (1-4) and copper is analyzed and percentage increase in delay while considering tunneling effects is obtained for length ranging from 200µm to 1000µm with an increment of 200µm. The influence of temperature variation on bandwidth of the best structure of MCB and copper are also studied. However, the effect of coupling between adjacent lines become significant as device scaling is decreasing rapidly to several nanometer ranges. So, further in this section a capacitively coupled

distributed architecture is taken for four structures of MCB and copper. For coupled lines architecture, functional and dynamic signal switching conditions are considered to perform crosstalk analysis, taking all structures of MCB (1-4) and copper while increasing the temperature from 300K to 500K.

4.1.1 Propagation Delay Analysis of MCB Structures and Copper in Single Interconnect

Temperature-dependent circuit parameters are obvious to affect the propagation delay of interconnects. For temperature extending from 300K to 500K, temperature affects the MFP of the MCB. A distributed *RLC* circuit of MCB structures is taken having a CMOS driver with a clock speed of 0.1GHz, V_{dd}=0.8V and a load capacitance of 0.20fF as shown in Fig. 3.5 [119]. SPICE simulation is done to extract 90% delay. Once the aspect ratio is fixed, optimum number of repeaters are placed in interconnect. For increasing the drive capability and to reduce the delay in signal, optimum number of repeaters are inserted in long interconnects [16]. From Fig. 4.1, it is discerned that the propagation delay increases with rise in temperature. This is simply showing the reflection of temperature-dependent interconnects' resistance variations on delay (see Table 3.1). On the other hand, when temperature is raised from 300K to 500K, highest propagation delay is observed in copper as compared to all structures of MCB for both the cases of tunneling and without tunneling. It is observed from the fig. 4.1 (a) and (b) that propagation delay reduces by taking tunneling effect into consideration.

MCB-4 is showing relative improvement in delay, which is about 22.5%, 9.1%, 4.5% and 33.59% w.r.t other MCBs (1-3) and copper, respectively. Table 4.1 is presenting the average percentage increase in propagation delay by considering 'without tunneling' effect to 'with tunneling' effect in all MCB structures when temperature is raised from 300K to 500K. By observing the table, it becomes quite obvious to state that tunneling effect in MWCNTs of MCB bundles plays an important role in determining the exact propagation delay in MCB structures. Among all structures of MCBs, MCB-4 is showing least average delay increase of 12.08% by considering 'without tunneling' to 'with tunneling' effects with varied length from 200µm to 1000µm.On the basis of these results, it can be concluded that MCB-4 is showing best results w.r.t other MCB structures and copper.

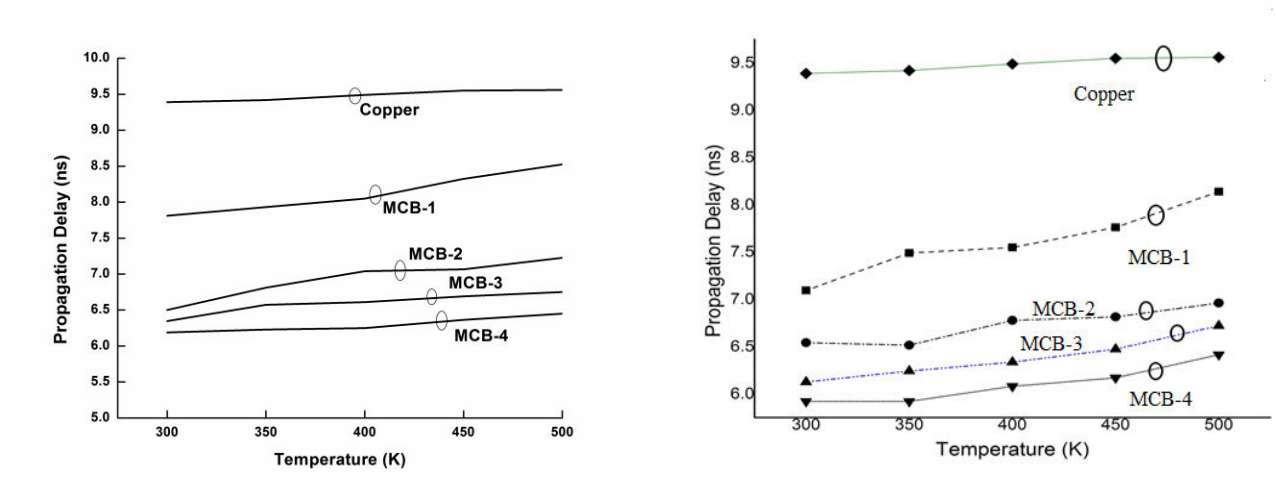


Figure 4.1 Propagation delay (ns) (a) with tunneling and (b) without tunneling in all MCBs and copper when temperature is varied from 300K to 500 at 14nm technology node.

Table 4.1 Average percentage increase in propagation delay from 'without tunneling' to 'with tunneling' for all MCBs with an increase in interconnect length (200µm to 1000µm) at 14nm technology node in single line architecture.

Length (um)	Percentage increase in Propagation Delay			
	MCB1	**MCB2**	**MCB3**	**MCB4**
200	27.48	37.2	21.31	14.63
400	36.4	42.52	24.35	16.73
600	36.55	42.69	24.45	16.8
800	17.51	21.37	12.24	8.05
1000	9.14	11.15	6.3	4.2
Average Percentage Increase (%)	**25.42**	**30.99**	**17.75**	**12.08**

4.1.2 Crosstalk analyses of MCB structures and Copper

In deep sub-micron (DSM) region, researchers are facing a serious challenge in determining the crosstalk induced noise produced between adjacent lines [22], [31], [32], [74], [87]. For examining the crosstalk induced noise voltage, a distributed capacitively coupled interconnects of MCBs are taken which has a CMOS driver having a clock speed of 0.1GHz, V_{dd}= 0.8V and a

load capacitance of 0.20fF as shown in Fig. 3.7. Various switching conditions are taken for aggressor and victim lines. These lines are switched from '0' to '1' or vice versa under different even and odd mode of signal switching conditions as shown in Table 4.2 for dynamic and functional crosstalk analyses [22], [28], [55], [122]. In adjacent lines due to coupling, a voltage glitch (undesirable noise) is experienced at the time of transition. Logic error occurs in the transmitted line when a certain level of threshold amplitude is reached [11], [21], [32], [27], [28]. Table 4.3 shows average dynamic crosstalk induced delay for all MCBs (1-4) and copper within a temperature range from 300k to 500K. From Table 4.3, it is evident that MCB-4 is giving least average dynamic crosstalk induced delay when temperature is varied from 300K to 500K for both even and odd mode of signal switching conditions. Average percentage reduction in dynamic crosstalk induced delay in each MCB and copper w.r.t MCB-4 within a temperature ranging from 300K to 500K under different mode of signal switching is shown in Table 4.4. For case 'DC-1', the obtained average percentage reduction in dynamic crosstalk induced delay in MCB-4 w.r.t MCBs (1-3) and copper is 56.32%, 5.17%, 2.30% and 10.92 %, respectively, and for case 'DC-2', the obtained average percentage reduction in dynamic crosstalk induced delay in MCB-4 w.r.t MCBs (1-3) and copper is 56.89%, 7.47%, 2.30% and 23.56 %, respectively. Similarly, the obtained average percentage reduction in dynamic crosstalk induced delay in MCB-4 w.r.t MCBs (1-3) and copper for case 'DC-3' is 96.36%, 39.09%, 30% and 25.45 %, respectively. For case 'DC-4', the obtained average percentage reduction in dynamic crosstalk induced delay in MCB-4 w.r.t MCBs (1-3) and copper is 90.99%, 37.84%, 27.93% and 24.32%, respectively.

Fig. 4.2 shows crosstalk induced delay of MCB-4 in even and odd mode of signal switching within the temperature range from 300K to 500K. It is clearly evident that in even mode of switching, crosstalk induced delay is less than that of odd mode switching. On an average in even mode of switching, MCB-4 is giving 36.45% lesser crosstalk induced delay in comparison to odd mode of switching when measured for temperature ranging from 300K to 500K. However, even mode time of flight ($t_{fe} = l\sqrt{CL}$) is less than odd mode time of flight ($t_{fo} = l\sqrt{(C + C_c)L}$) and therefore, even mode voltage step arrives earlier than odd mode voltage step and therefore, the delay in even mode switching is lesser than odd mode switching [26].It is also evident from the figure that with increase in temperature, crosstalk induced delay increases mainly due to the reduction of MFP of MCB w.r.t temperature for 1mm long interconnect

[11],[53].Table 4.5 shows the average functional crosstalk induced noise voltage values in each MCB structures for temperature ranging from 300K to 500K under four signal switching conditions "FC-(1-4)" of aggressor and victim lines as shown in Table 4.5 For each signal switching condition, an average crosstalk induced noise glitch at the victim line's output is obtained over a temperature range from 300K to 500K.

From Table 4.5, it is evident that MCB-4 is showing least magnitude of glitches than other MCBs (1-3) and copper. As shown in Table 4.6, for case 'FC-1', the obtained average percentage reduction in functional crosstalk induced positive glitch in MCB-4 w.r.t MCBs (1-3) and copper is 62.66%, 15.54%, 52.30% and 74.44 %, respectively, and for case 'FC-2', the obtained average percentage reduction in functional crosstalk induced overshoot glitch in MCB-4 w.r.t MCBs (1-3) and copper is 4.61%, 0.56%, 3.12% and 8.26 %, respectively. Similarly, the obtained average percentage reduction in functional crosstalk induced undershoot glitch in MCB-4 w.r.t MCBs (1-3) and copper for case 'FC-3' is 61.35%, 15.51%, 51.45% and 73.80 %, respectively. For case 'FC-4', the obtained average percentage reduction in functional crosstalk induced positive glitch in MCB-4 w.r.t MCBs (1-3) and copper is 5.42%, 4.86%, 1.99% and -0.13%, respectively. These rise/fall glitches affect the functionality of the circuit whereas undershoot/overshoot affects the reliability of the circuit.

Table 4.2 Various conditions for Aggressor and Victim line switching in MCB.

Signal switching Conditions	Aggressor Switching	Victim Switching	Switching Case
Dynamic	0 to 1	1 to 0	DC-1
	1 to 0	0 to 1	DC-2
	0 to1	0 to 1	DC-3
	1 to 0	1 to 0	DC-4
Functional	0 to 1	Held at Logic 0	FC-1
	0 to 1	Held at Logic 1	FC-2
	1 to 0	Held at Logic 0	FC-3
	1 to 0	Held at Logic 1	FC-4

Table 4.3 Average dynamic crosstalk induced delay for each MCB structures for temperature ranging from 300K to 500K under even and odd mode of switching.

Switching Case	Delay (ns) MCB-1	Delay (ns) MCB-2	Delay (ns) MCB-3	Delay (ns) MCB-4	Delay (ns) Copper	Results	Impacts
DC-1	2.72	1.83	1.78	1.74	1.93	Increase in fall time	Timing
DC-2	2.73	1.87	1.78	1.74	2.15	Increase in rise time	Timing
DC-3	2.16	1.53	1.43	1.1	1.38	Decrease in rise time	Timing
DC-4	2.12	1.53	1.42	1.11	1.38	Decrease in fall time	Timing

Table 4.4 Average percentage reduction in dynamic crosstalk induced delay in each MCB and copper w.r.t MCB-4 for temperature ranging from 300K to 500K under different mode of switching.

Switching Case	Average percentage reduction in dynamic crosstalk induced delay in MCB-4 with respect to MCB-1, MCB-2,MCB-3 and copper			
	w.r.t MCB-1	w.r.t MCB-2	w.r.t MCB-3	w.r.t Copper
DC-1	56.32	5.17	2.30	10.92
DC-2	56.89	7.47	2.30	23.56
DC-3	96.36	39.09	30.00	25.45
DC-4	90.99	37.84	27.93	24.32

The above discussion on dynamic crosstalk and functional crosstalk analysis of all the MCBs and copper proved that MCB-4 is the best structure for next generation interconnects. Figures 4.3 and 4.4 demonstrate crosstalk-induced noise voltage waveforms at the far end of the victim line for four distinct MCB bundle and copper connector topologies at temperatures ranging from 300K to 500K. The crosstalk induced noise voltage levels increase for all topologies of MCB bundles and copper interconnects as the temperature rises from 300K to 500K, according to the transient data.

Table 4.5 Average functional crosstalk induced glitch results for each MCB structures for temperature ranging from 300K to 500K taking different aggressor and victim conditions.

Switching Case	MCB-1 (mV)	MCB-2 (mV)	MCB-3 (mV)	MCB-4 (mV)	Copper (mV)	Glitch	Impacts
FC-1	70.50	31.18	55.27	26.33	110	Magnitude of rise Glitch	Functionality
FC-2	865.26	829.96	851.95	825.35	900.25	Magnitude of Overshoot	Reliability
FC-3	65.48	18.07	52.02	14.98	101.09	Magnitude of undershoot	Reliability
FC-4	732.67	770.13	747.53	774.67	739.27	Magnitude of rise Glitch	Functionality

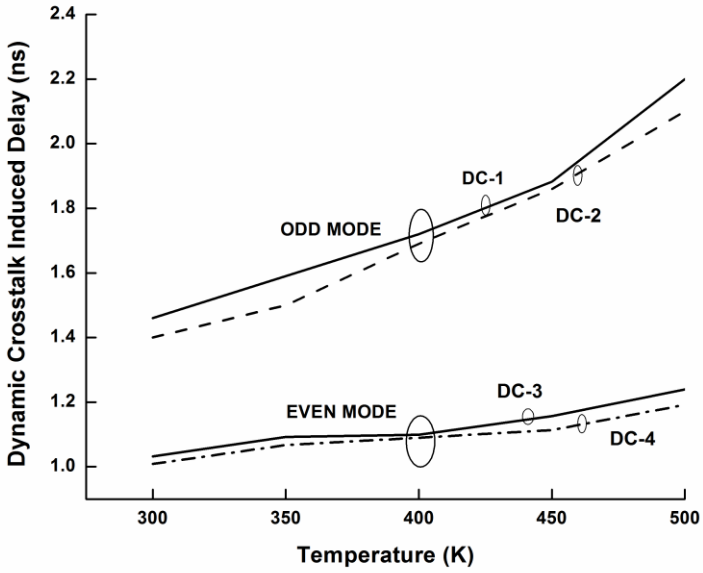


Figure 4.2 Crosstalk induced delay (ns) in best structure (MCB-4) taking different transition conditions of aggressor and victim line under even and odd mode of switching for temperature range from 300K to 500K.

In addition, as temperature rises, the length of transient responses increases. This is due to the combined influence of inductance and capacitance on transient responses at the victim line's far end over a resistance (see Table 3.2). Figs. 3.3 and 4.4 are used to extract distinct aspects of the transient reactions at the far end of the victim line, which are then displayed in Figs. 4.5 and 4.6 throughout a temperature range of 300K to 500K. With a temperature increase from 300K to 500K, the crosstalk induced noise voltage levels (peaks) as well as duration increase in all circumstances.

Table 4.6 Average percentage reduction in functional crosstalk induced noise glitch for each MCB structures for temperature ranging from 300K to 500K under different mode of switching.

Switching Case	Result	Average percentage reduction in functional crosstalk noise in MCB-4 with respect to MCB-1,MCB-2, MCB-3 and copper			
		w.r.t MCB-1	w.r.t MCB-2	w.r.t MCB-3	w.r.t Copper
FC-1	**Rise Glitch**	62.66	15.54	52.3	74.44
FC-2	**Overshoot**	4.61	0.56	3.12	8.26
FC-3	**Fall Glitch**	61.35	15.51	51.45	73.8
FC-4	**Rise Glitch**	5.42	4.86	1.99	-0.13

Also, it is observed that copper is showing largest crosstalk noise peaks and time duration for complete range of temperature from 300K to 500K as compare to all structures of MCB. This is due to the dominating effect of temperature-dependent circuit parameter like inductance over resistance and capacitance on transient response at the far end of victim line.

Fig. 4.7 shows 90% normalized delay considering two cases viz. 'with crosstalk (WX)' and 'without crosstalk (WoX)' noise at the far end of aggressor on temperature in single and capacitively coupled interconnects for all the MCB bundle structures. Copper delay is used to normalize the correspondent MCB structures. In this comparison, it is observed that delay is always higher in case of coupled lines in comparison to single line (without crosstalk) for every structure. It is due to the fact that while considering crosstalk effects, coupling increases which further leads to more delay with rise in temperature.

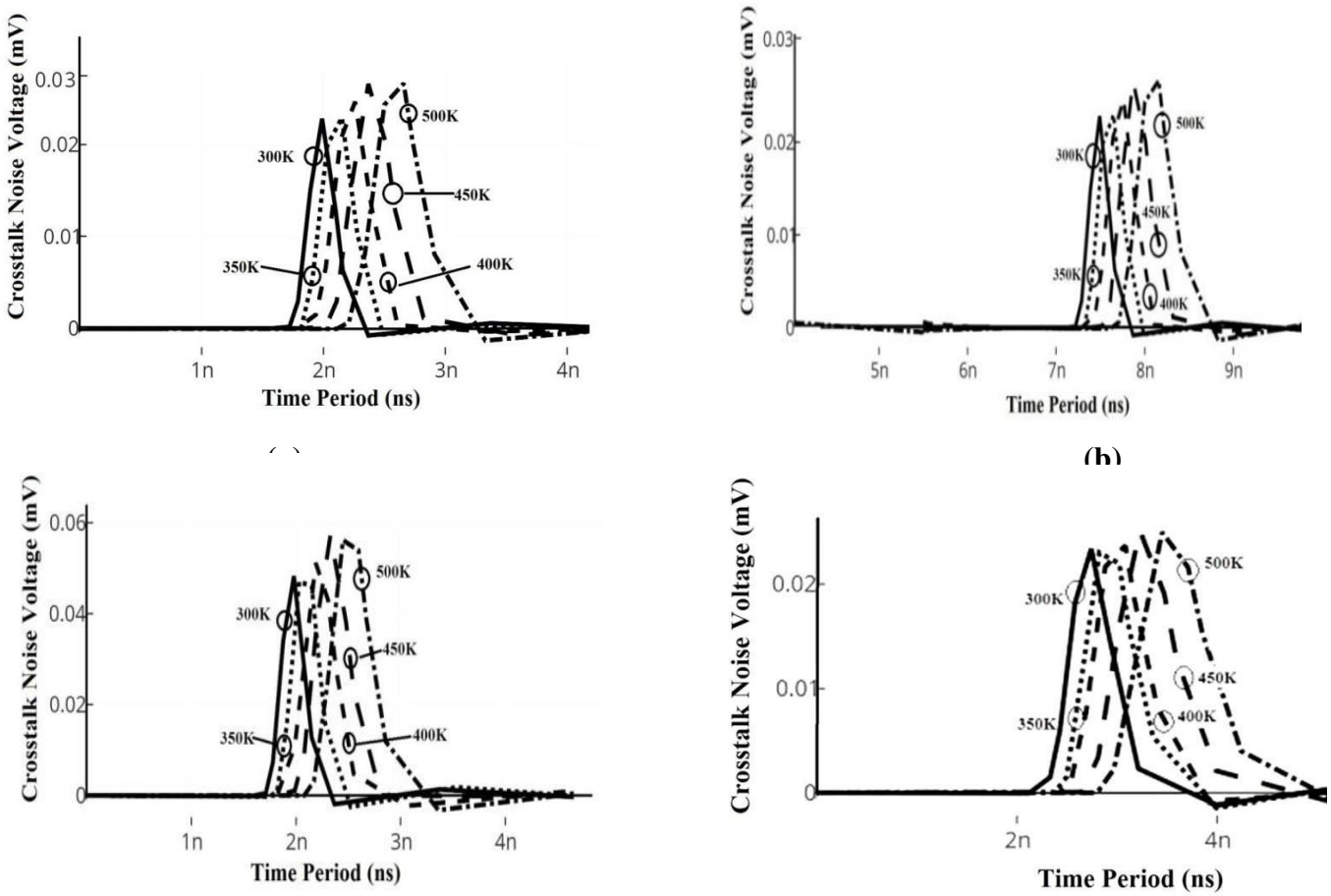


Figure 4.3 Transient response at the far end of the victim line for capacitively coupled **(a)** MCB -1, **(b)** MCB-2, **(c)** MCB -3 and **(d)** MCB-4 interconnects when the temperature is varied from 300K to 500K.

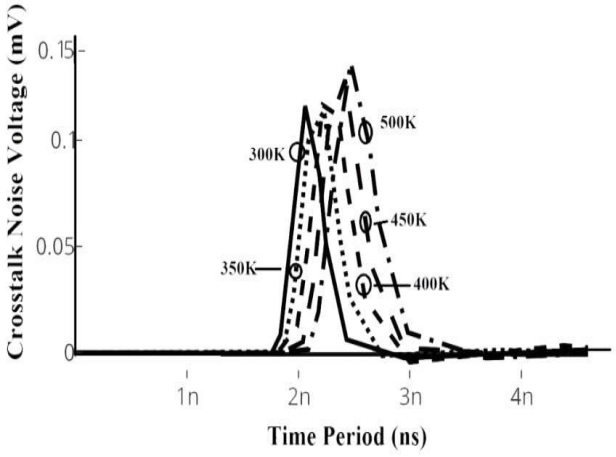


Figure 4.4 Transient response at the far end of the victim line for capacitively coupled copper structure interconnects when the temperature is varied from 300K to 500K.

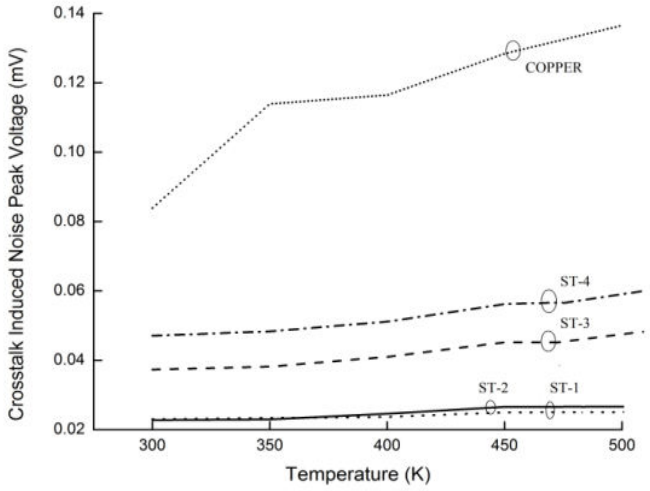


Figure 4.5 Positive crosstalk voltage noise peak of MCB structures and copper when the temperature is varied from 300K to 500K.

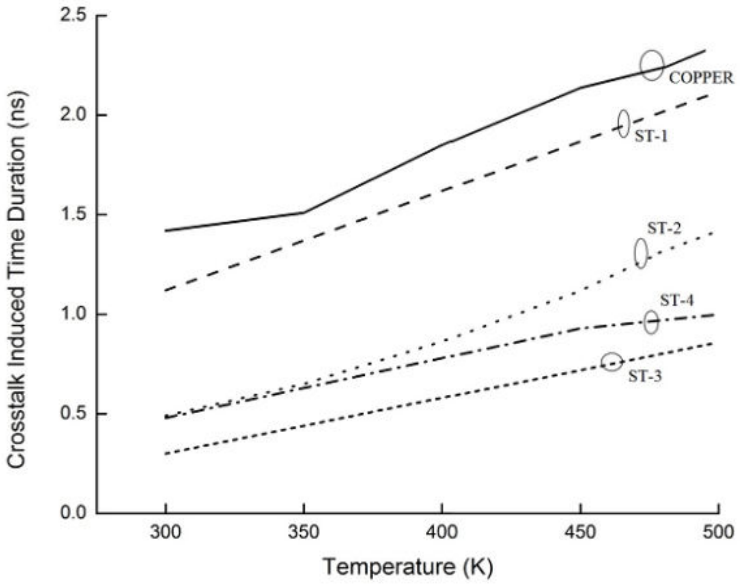


Figure 4.6 Crosstalk induced time duration for all structures and copper at temperature ranging from 300K to 500K.

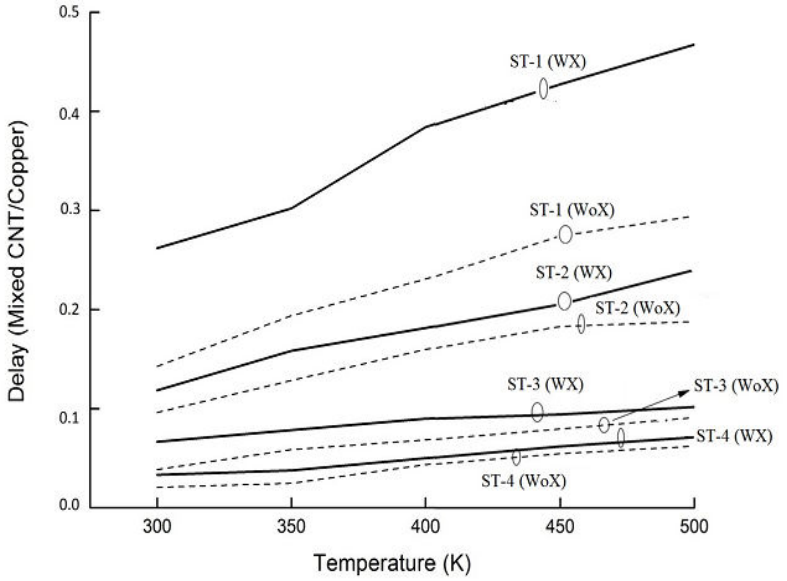


Figure 4.7 Comparison between crosstalk induced delay (WX) and single line delay (WoX) for all structures for temperature range from 300K to 500K.

4.2 FREQUENCY ANALYSIS OF BEST MCB STRUCTURE (MCB-4) AND COPPER

There are several factors and components which are required to be studied in a signal obtained at the output. Here, in this section the temperature-dependent frequency spectrum of best structure (MCB-4) and copper are analyzed at 14nm technology node. Under this analysis, the time domain signal obtained at the far end of single interconnect and at the far end of victim line in capacitively coupled interconnects are converted into frequency domain to study the band width and crosstalk induced noise voltage, respectively. Furthermore, the effects of temperature variation on noise amplitudes are explored.

The time domain signal obtained at the far end of aggressor and victim lines is converted into frequency domain by using FFT transcript written in C language. A 64-point FFT code is used to transform the time domain signal into frequency spectrum with bin spacing of $\Delta f=f_s/N$. Figs. 4.8 and 4.9 present normalized frequency amplitude of output signal w.r.t normalized frequency for single and coupled line architecture, respectively. Here, the Y-axis, frequency spectrum amplitudes are normalized by the input signal frequency amplitudes and X-axis frequency are normalized by input frequency. In Fig. 4.8, the main first lobe contains the maximum signal

power and the amplitude of side lobes keep on decreasing monotonically. This happens when the time domain signal does not have integral number of cycles and the continuous spectrum gets shifted from main lobe to side lobe. This loss of signal power is called as Scalloping loss [122]. It has been observed from Fig. 4.8 that the bandwidth of MCB-4 interconnect is more than copper interconnect for wide range of frequency. The results also revealed that MCB-4 is giving more bandwidth (equivalent to 0.707 times the peaks) of about 17.70% w.r.t copper counter-parts. Copper has higher resistance as compared to MCB-4 and therefore the bandwidth of MCB-4 is higher than that of copper (see Table 3.2). This implies that MCB-4 can retain more signal power for wider range of frequencies in comparison to copper counterpart. Fig. 4.9 shows normalized frequency amplitude with respect to normalized frequency for single interconnects of MCB-4. Figure shows that the frequency amplitude decreases with increase in temperature which means that the loss in signal power is more at higher temperatures. Therefore, MCB-4 experiences more loss in signal power when temperature is raised from 300K to 500K. Also, there is decrease in the bandwidth with rise in temperature which is due to increase in resistance [122].

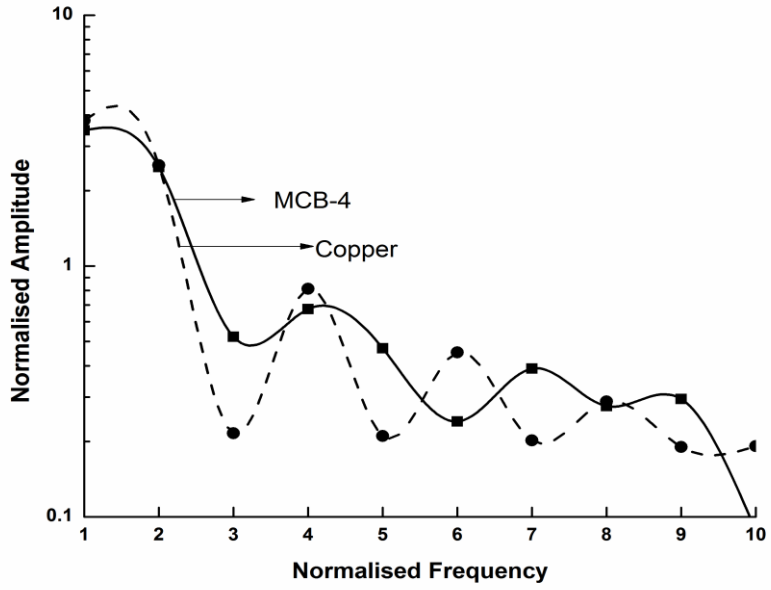


Figure 4.8 Normalized frequency amplitude with respect to normalized frequency of MCB-4 and copper interconnects for single line architecture at 14nm technology node.

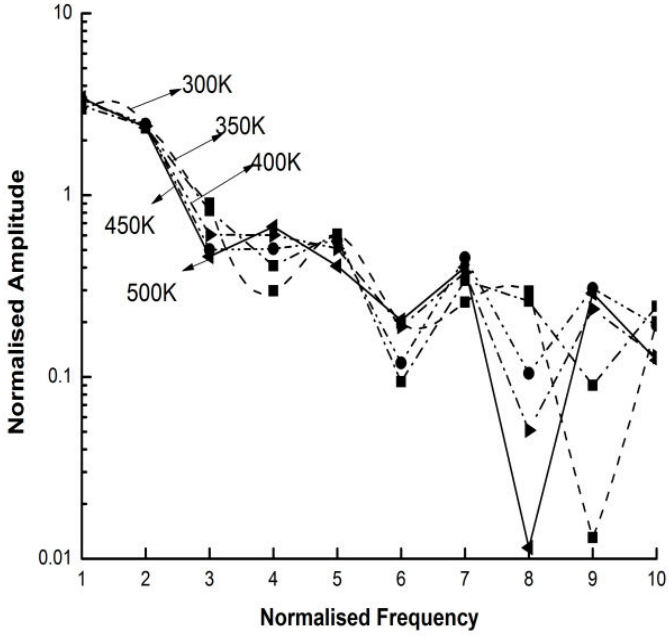


Figure 4.9 Variation in normalized frequency amplitude with respect to normalized frequency for MCB-4 taking different temperature from 300K to 500K for a single line architecture at 14nm technology node.

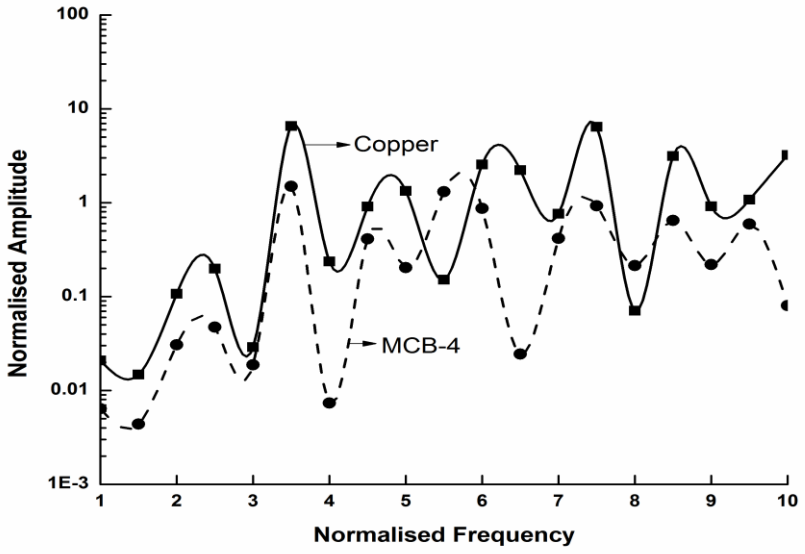


Figure 4.10 Normalized frequency noise amplitude with respect to normalized frequency of MCB -4 and copper interconnects for a coupled line architecture at 14nm technology node.

Fig. 4.10 illustrates the normalized frequency noise amplitudes of victim output w.r.t normalized frequency of the coupled line architecture under functional switching condition. In functional crosstalk switching condition, victim line is kept at logic “0” or “1” and aggressor line is switched from “0” to “1” or “1” to “0” respectively. Here, the noise frequency components are suppressed more in smaller frequency range. From the figure, it is also observed that copper is showing approximately 70.66% larger frequency noise amplitudes as compare to MCB-4. Moreover MCB-4 is filtering more noise frequency components of the victim line output making it best desirable structure for future MCB based interconnects in deep sub-micron (DSM) regime. Fig. 4.11 illustrates normalized frequency noise amplitude with respect to normalized frequency of MCB-4 in coupled line architecture taking temperature extending from 300K to 500K at 14nm technology node. It is noted that crosstalk induced noise amplitude is becoming larger with rise in temperature. This implies that filtering capability of noise is going to decrease with higher temperatures.

.

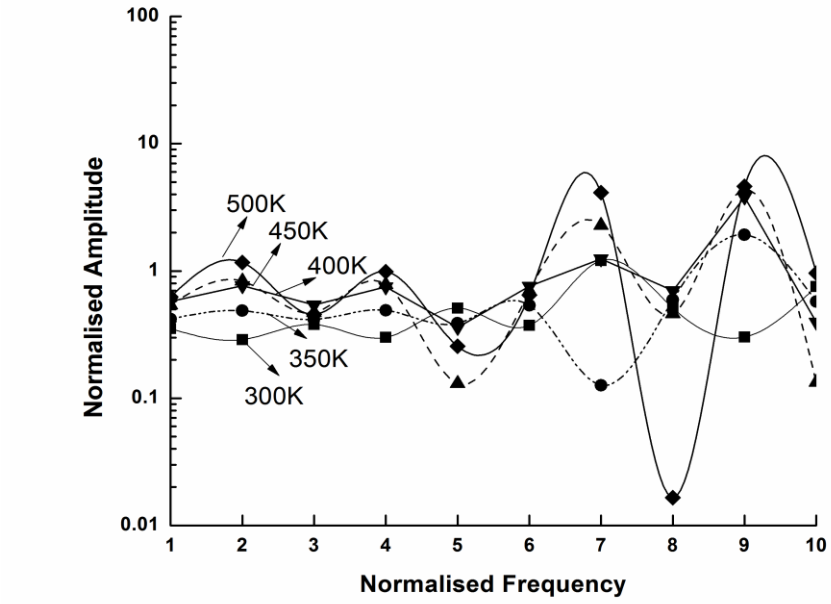


Figure 4.11 Variation in normalized frequency noise amplitude with respect to normalized frequency for MCB-4 taking different temperature from 300K to 500K for a coupled line architecture at 14nm technology node.

4.3 CONCLUSION

This chapter has studied the temperature-dependent (300K to 500K) crosstalk and frequency spectrum analyses of all MCBs (1-4) and copper taking interconnect length from 200µm to 1000µm at 14nm technology node. In single line architecture, MCB-4 is showing least propagation delay among other MCBs (1-3) and copper over temperature from 300K to 500K. While taking tunneling effect into consideration, a percentage increase in propagation delay of MCB-4 by considering "without tunneling" effect to "with tunneling" effect is obtained about 12.08%. Frequency spectrum analysis of MCB-4 with copper has shown an increase of about 17.70% in bandwidth when compared with copper. Also, the bandwidth of MCB-4 has decreased with rise in temperature (300K-500K) which indicates that the loss in signal power is more at higher temperatures. For a capacitively coupled architecture, taking all switching conditions (e.g., DC-(1-4)) of aggressor and victim lines, MCB-4 has shown least average percentage decrease in dynamic crosstalk induced noise voltage w.r.t other MCBs (1-3) and copper. On an average in even mode of signal switching, MCB-4 has shown 36.45% lesser crosstalk induced delay in comparison to odd mode of switching when temperature is raised from 300K to 500K. Also, for various switching signal conditions of aggressor and victim line (e.g., FC-(1-4)) under functional crosstalk, MCB-4 has shown least amplitude of glitches (rise/fall) and overshoot/undershoot w.r.t other MCBs (1-3) and copper. Frequency spectrum analysis of MCB-4 and copper in a capacitively coupled architecture has shown that MCB-4 is having least frequency noise amplitude of about 70.66% w.r.t copper. Also, with rise in temperature (300K-500K), frequency noise amplitude has increased in MCB-4 which means that the noise filtering capability degrades at higher temperatures. This complete work concludes that MCB-4 is the best desirable structure w.r.t. other MCBs (1-3) and copper for next generation interconnects.

CHAPTER-5

TEMPERATURE DEPENDENT CROSSTALK MODEL WITH APPLICATION OF DIL (DRIVER-INTERCONNECT-LOAD) IN COUPLED m-CNT BUNDLE INTERCONNECTS

Interconnects are used to connect the various components that make up an integrated circuit. To analyze the performance of interconnect, characteristics like resistance, inductance, capacitance as well as current carrying capabilities are taken into account [93]. The resistance of any interconnects' material increases and MFP decreases as the dimensions are reduced. MFP reduces because of many factors like surface and grain boundary scattering, continuous increase of current density [123]-[126]. Voids and hillocks are the result of excessive electro-migration. Increasing the transistor count and miniaturizing the feature size leads to a higher power density, thereby increasing the temperature of an integrated circuit. Technological advancements reduce energy efficiency, increase complexity, and promote power leakage. This can be reduced by using a task scheduling algorithm (TSA) able to take into account all the factors and minimize the effects of increasing temperature and energy usage [127]-[128]. Fathi et al. [129] and Zhao et al. [130] used ABCD parameter matrix to solve the proposed model of CNT interconnects. FDTD method which is used by Duksh et al. [96] to discuss the effects of capacitances on crosstalk noise peaks and transistor responses. Lu et al. [131] and Rai et al. [27] used voltage mode signaling scheme (VMS) while using load capacitance for analyzing the performance of SWCNT based bundle interconnects. On the contrary, Aggarwal et al. [132] used current mode signaling scheme (CMS) for presenting the model of SWCNT bundle although crosstalk analysis was missing in the model.

The purpose of this chapter is to investigate the proposed capacitively coupled m-CNT bundle based interconnect model by means of the ABCD parameter matrix along with decoupling technology. Both functional and dynamic crosstalk is taken into consideration at the 14nm technology node. The accuracy of the model is certain by validating it using simulation.

5.1 ELECTRICAL MODEL OF M-CNT BUNDLE BASED INTERCONNECTS

Two isolated interconnects of m-CNT bundle is shown in Fig. 5.1. Width and height are denoted as 'W' and 'H' respectively. The Van der Waal's gap between the shells in MWCNT is denoted by '$\boldsymbol{\delta}$ '.

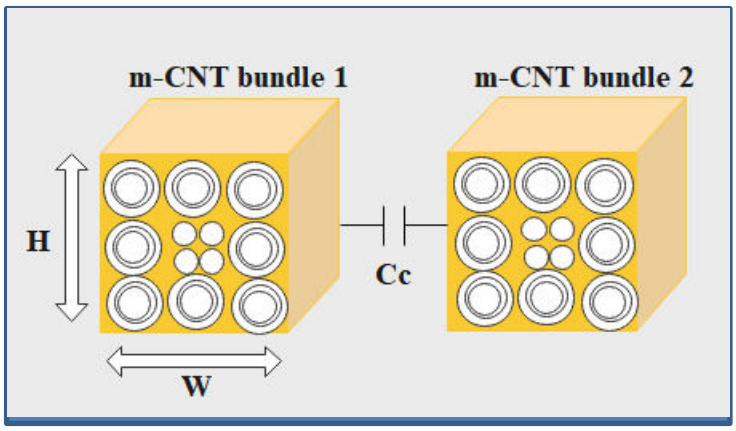


Figure 5.1 Schematic diagram of 2- capacitively coupled m-CNT bundle based interconnects.

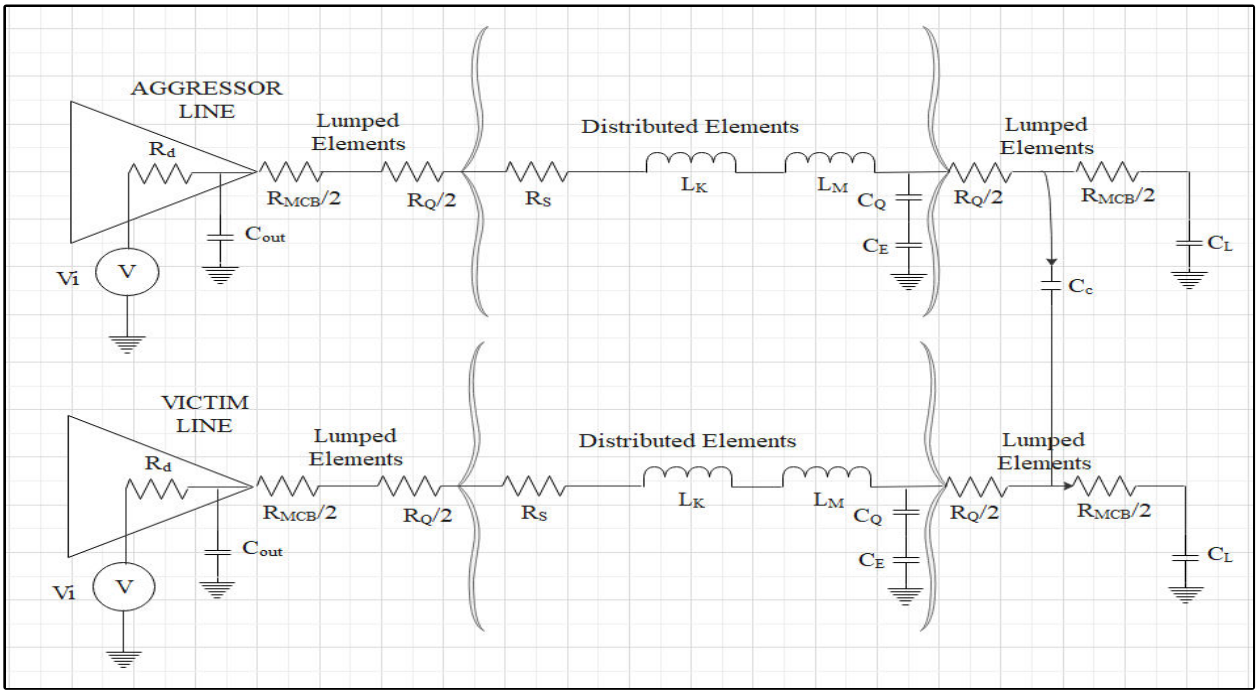


Figure 5.2 Equivalent circuit model of 2-capacitively coupled m-CNT bundle based interconnect.

For MWCNT, the maximum diameter is 8nm, and for SWCNT, 1nm is fixed. Eqns. 3.1 to 3.30 are used for finding the number of CNTs, resistance, inductance and capacitance of m-CNT bundle [74] [133].

5.2 THE DECOUPLING AND ABCD PARAMETER BASED MODEL

Fig. 5.2 shows two capacitively coupled identical m-CNT based interconnects which can be divided into separate independent lines using decoupling technology approach [134], [135]. Functional as well as dynamic crosstalk will be analyzed using this model. Now, to represent in-phase and out-phase signal switching a factor 'k' is taken. If k=1, it denotes in phase signal switching when aggressor and victim line both switches simultaneously in the same direction, if k=-1, it denotes out- phase signal switching, when aggressor and victim lines switch in different directions. Based on above assumptions, a decoupling model of the victim line is shown in Fig. 5.3.

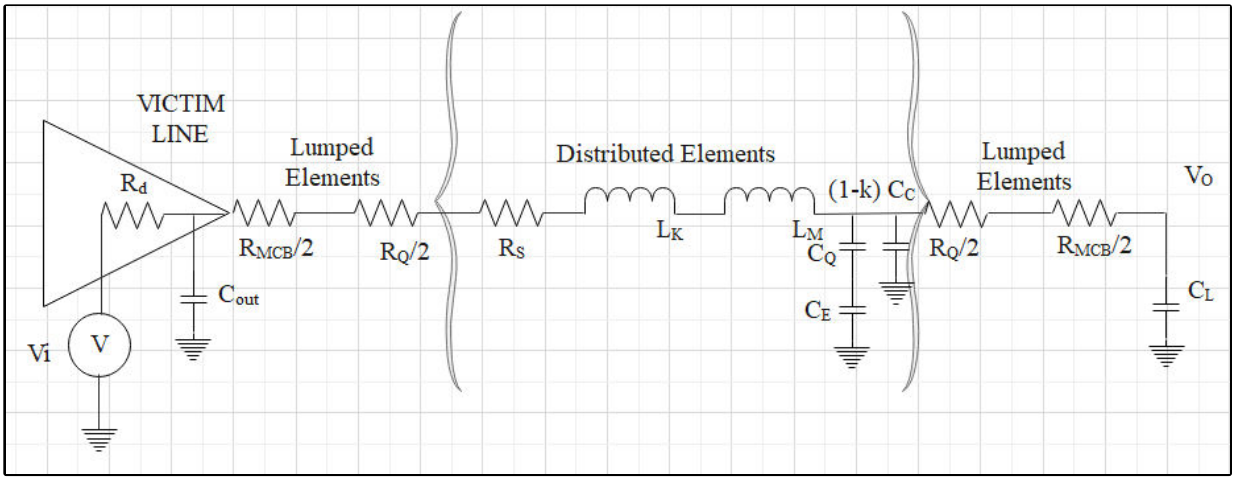


Figure 5.3 Decoupled model of the victim line.

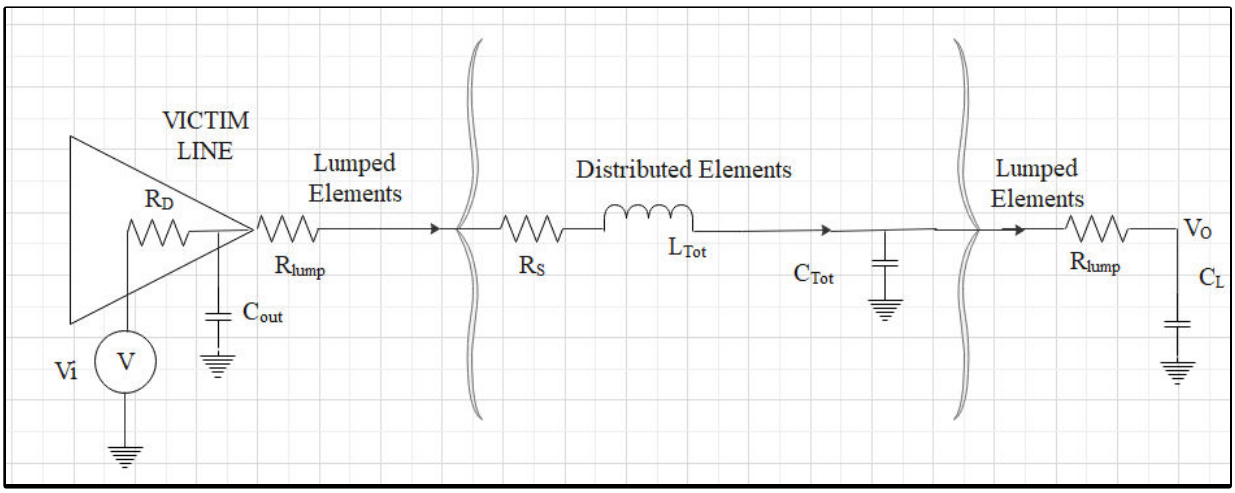


Figure 5.4 The decoupled victim line's equivalent circuit model.

An equivalent model from the decoupled model is shown in Fig. 5.4 where series and parallel combinations of resistances, inductances and capacitances are as [74], [133]:-

$$R_{lump} = \frac{R_{Q+}R_c}{2} \quad (5.1)$$

$$L_{Tot} = L_K + L_M \quad (5.2)$$

$$C_{Tot} = C_Q^{-1} + C_E^{-1} + (1-k)C_c \quad (5.3)$$

As per transmission line theory and ABCD technique the equivalent model shown in Fig. 5.4 is formulated as under [84], [130]:-

$$T_{Tot} = \begin{bmatrix} A & B \\ C & D \end{bmatrix} \quad (5.4)$$

$$T_{Tot} = \begin{bmatrix} 1 & R_D \\ 0 & 1 \end{bmatrix}\begin{bmatrix} 1 & 0 \\ sC_o & 1 \end{bmatrix}\begin{bmatrix} 1 & R_{lump} \\ 0 & 1 \end{bmatrix}\begin{bmatrix} Cosh(\theta l) & Z_0\sinh(\theta l) \\ \frac{1}{Z_0}\sinh(\theta l) & Cosh(\theta l) \end{bmatrix}\begin{bmatrix} 1 & R_{lump} \\ 0 & 1 \end{bmatrix} \quad (5.5)$$

Here, A, B, C and D can be calculated as:-

$$A = (R_D sC_o + 1)\cosh(\theta l) + \frac{\left((R_D sC_o+1)R_{lump}+R_D\right)\sinh(\theta l)\right)}{Z_o} \quad (5.6)$$

$$B = (2(R_D sC_o + 1)R_{lump} + R_D)\cosh(\theta l) + \left(\frac{\left((R_D sC_o+1)R_{lump}+R_D\right)R_{lump}\right)}{Z_0} + (R_D sC_o + 1)Z_0\Big)\sinh(\theta l) \quad (5.7)$$

$$C = sC_o\cosh(\theta l) + \frac{(C_o R_{lump}s+1)\sinh(\theta l)}{Z_o} \quad (5.8)$$

$$D = \left(C_o R_{lump}s + 1\right)\cosh(\theta l) + \left(\frac{(C_o R_{lump}s+1)R_{lump}}{Z_o} + sC_o Z_o\right)\sinh(\theta l) \quad (5.9)$$

Here, $s = j\omega$ is a complex frequency, θ and Z_0 are propagation constant and characteristic impedance given a

$$\theta = \sqrt{(R_s + sL_{Tot})sC_{Tot}} \quad (5.10)$$

$$Z_o = \sqrt{(R_s + sL_{Tot})sC_{Tot}} \quad (5.11)$$

The voltage given at the input of victim line can be expressed as a function of voltage and current received at the output of the victim line given as

$$I_{o\,(s)} = sC_l V_{o(s)} \quad (5.12$$

$$V_o = \frac{V_i(s)}{A+sC_lB} \quad (5.13$$

Now, by using eq. (5.1) and (5.2) & (5.13) , the transfer function of the victim line can be computed as

$$H = \frac{V_o(s)}{V_i(s)} = \frac{1}{x_1 \cosh(\theta l)+x_2 \sinh(\theta l)} \quad (5.14)$$

Where,

$$x_1 = 2s^2 C_l C_o R_{lump} R_D + \left(R_D C_o + 2(C_o R_{lump} R_D\right) + 2C_l R_{lump} + C_l R_D)s + 1 + 2R_{lump} + R_D \quad (5.15)$$

$$x_2 = \left(\frac{C_l R_{lump}^2 C_o R_D}{Z_0} + C_l C_o R_D Z_0\right) \times s^2 + \left(\frac{R_{lump}^2 C_o R_D}{Z_0} + \frac{R_D C_o Z_0}{1} + \frac{R_{lump}\left(C_l R_{lump}+C_l R_D+R_D C_o\right)}{Z_0} + C_l Z_0\right) \times s + \frac{R_{lump}+R_D}{Z_0} + \frac{R_{lump}\left(R_{lump}+R_D\right)}{Z_0} + \frac{Z_0}{1} \quad (5.16)$$

The transfer function can be recomputed after substituting the values of propagation constant and characteristic impedance along with sixth-order Padè [84], [130] approximation method a

$$H = \frac{1}{b_0+b_1 s+b_2 s^2+b_3 s^3+b_4 s^4+b_5 s^5+b_6 s^6} \quad (5.17)$$

Where,

$$\boldsymbol{b_0} = \frac{R_S l}{1} + 1 + \frac{2lump+R_D}{1} \quad (5.18)$$

$$\boldsymbol{b_1} = C_{Tot} l\left(1 + R_{lump} + R_D\right) + \frac{\frac{1}{6}C_{Tot} R_S^2 l^3 + L_{Tot} l}{R_L} + \left(C_l + \frac{R_D C_o}{1}\right) R_S l + R_D C_o + 2\frac{C_o R_{lump} R_D}{1} + 2C_l R_{lump} + C_l R_D + \frac{1}{2} C_{Tot} R_S l^2 \left(1 + \frac{2R_{lump}+R_D}{1}\right) \quad (5.19)$$

$$\boldsymbol{b_2} = C_{Tot} l \left(R_{lump}\left(C_l R_{lump} + C_l R_D + R_D C_o\right) + \frac{R_{lump}^2 C_o R_D}{1}\right) + \frac{1}{6} C_{Tot}^2 R_s l^3 \left(\frac{R_{lump}\left(R_{lump}+R_D\right)}{1} + R_{lump} + R_D\right) + \left(\frac{C_{Tot}^2 R_S^3 l^5}{120} + \frac{1}{3} C_{Tot} L_{Tot} R_s l^3\right) + \left(C_L + \frac{R_D C_o}{1}\right)\left(\frac{1}{6} C_{Tot} R_s^2 l^3 + L_{Tot} l\right) + 2C_l C_o R_{lump} R_D + \frac{1}{2} C_{Tot} L_{Tot} l^2 \left(R_D C_o + 2\frac{C_o R_{lump} R_D}{1} + 2C_l R_{lump} + C_l R_D\right) + \left(\frac{1}{2} C_{Tot} L_{tot} l^2 + \frac{1}{24} C_{Tot}^2 R_S^2 l^4\right)\left(1 + \frac{2R_{lump}+R_D}{1}\right) + C_l C_o R_D R_s l \quad (5.20)$$

$$\boldsymbol{b_3} = C_{Tot}lC_lR_{lump}^2C_oR_D + \frac{1}{6}C_{Tot}^2R_sl^3\left(R_{lump}\left(C_lR_{lump} + C_lR_D + R_DC_o\right) + \frac{R_{lump}^2C_oR_D}{1}\right)$$
$$+ \left(\frac{C_{Tot}^3R_s^2l^5}{120} + \frac{1}{6}C_{Tot}^2L_{Tot}l^3\right)\left(\frac{R_{lump}\left(R_{lump} + R_D\right)}{1}\right) + R_{lump} + R_D$$
$$+ C_{Tot}R_sl^2C_lC_oR_{lump}R_D + \left(\frac{C_{Tot}^3R_s^4l^7}{5040} + \frac{1}{40}C_{Tot}^2R_s^2l^4 + \frac{1}{6}C_{Tot}L_{Tot}^2l^3\right)$$
$$+ \left(\frac{1}{2}C_{Tot}L_{Tot}R_sl^2 + \frac{1}{24}C_{Tot}^2R_s^2l^4\right)\left(R_DC_o + 2\frac{C_oR_{lump}R_D}{1} + 2C_lR_{lump} + C_lR_D\right)$$
$$+ \left(\frac{1}{12}C_{Tot}^2L_{Tot}R_sl^4 + \frac{C_{Tot}^2R_s^3l^6}{720}\right)\left(1 + \frac{2R_{lump} + R_D}{1}\right)$$
$$+ \left(C_l + \frac{R_DC_o}{1}\right)\left(\frac{C_{Tot}^3R_s^3l^5}{120} + \frac{1}{3}C_{Tot}L_{Tot}R_sl^3\right) + C_lC_oR_D\left(\frac{1}{6}C_{Tot}^2R_sl^3 + L_{Tot}l\right) \quad (5.21)$$

$$\boldsymbol{b_4} = \tfrac{1}{6}C_{Tot}^2R_sl^3C_lR_{lump}^2C_oR_D + C_lC_oR_D + \left(\tfrac{C_{Tot}^2R_s^3l^5}{120} + \tfrac{1}{6}C_{Tot}^2L_{Tot}l^3\right)\Big(R_{lump}\big(C_lR_{lump} + C_lR_D +$$
$$R_DC_o\big) + \tfrac{R_{lump}^2C_oR_D}{1}\Big) + \left(\tfrac{C_{Tot}^4R_s^3l^7}{5040} + \tfrac{1}{40}C_{Tot}^2L_{Tot}R_s^2l^5\right)\left(\tfrac{R_{lump}\left(R_{lump}+R_D\right)}{1} + R_{lump} + R_D\right) +$$
$$\left(C_l + \tfrac{R_DC_o}{1}\right)\left(\tfrac{C_{Tot}^3R_s^4l^7}{5040} + \tfrac{1}{40}C_{Tot}^2L_{Tot}R_s^2l^5 + \tfrac{1}{6}C_{Tot}^2{L_{Tot}}^2l^3\right) +$$
$$2\left(\tfrac{1}{2}C_{Tot}L_{Tot}l^2 + \tfrac{1}{24}C_{Tot}^2R_s^2l^4\right)C_lC_oR_{lump}R_D + \left(\tfrac{C_{Tot}^3R_s^3l^7}{5040} + \tfrac{1}{40}C_{Tot}^2L_{Tot}^2R_s^2l^5\right) +$$
$$\left(\tfrac{1}{12}C_{Tot}^2L_{Tot}R_sl^4 + \tfrac{C_{Tot}^3R_s^3l^6}{720}\right) \times \left(R_DC_o + 2\tfrac{C_oR_{lump}R_D}{1} + 2C_lR_{lump} + C_lR_D\right) + \left(\tfrac{C_{Tot}^3L_{Tot}R_s^2l^6}{240} +\right.$$
$$\left.\tfrac{1}{40320}C_{Tot}^4R_s^4l^8 + \tfrac{1}{24}C_{Tot}^2{L_{Tot}}^2l^4\right)\left(1 + \tfrac{2R_{lump}+R_D}{1}\right) \quad (5.22)$$

$$\boldsymbol{b_5} =$$
$$\left(\tfrac{C_{Tot}^3R_s^2l^5}{120} + \tfrac{1}{6}C_{Tot}^2L_{Tot}l^3\right)C_lR_{lump}^2C_oR_D + 2\left(\tfrac{C_{Tot}^3R_s^3l^6}{720} + \tfrac{1}{12}C_{Tot}^2L_{Tot}R_sl^4\right) \times C_lC_o\,R_{lump}R_D +$$
$$\left(\tfrac{C_{Tot}^4R_s^3l^7}{5040} + \tfrac{1}{40}C_{Tot}^2L_{Tot}R_s^2l^5\right) \times \left(R_{lump}\left(C_lR_{lump} + C_lR_D + R_DC_o\right) + \tfrac{R_{lump}^2C_oR_D}{1}\right) + \left(C_l +\right.$$
$$\left.\tfrac{R_DC_o}{1}\right)\left(\tfrac{C_{Tot}^3L_{Tot}R_s^3l^7}{1260} + \tfrac{1}{40}C_{Tot}^2L_{Tot}R_s^2l^5\right) +$$
$$C_lC_oR_D\left(\tfrac{C_{Tot}^3R_s^4l^7}{5040} + \tfrac{1}{40}C_{Tot}^2L_{Tot}R_s^2l^5 + \tfrac{1}{6}C_{Tot}^2{L_{Tot}}^2l^3\right) + \left(\tfrac{C_{Tot}^3L_{Tot}R_s^2l^6}{240} + \tfrac{1}{40320}C_{Tot}^4R_s^4l^8 +\right.$$
$$\left.\tfrac{1}{24}C_{Tot}^2{L_{Tot}}^2l^4\right) \times \left(R_DC_o + 2\tfrac{C_oR_{lump}R_D}{1} + + C_l\left(2R_{lump} + R_D\right)\right) \quad (5.23)$$

$$\boldsymbol{b_6} = \left(\frac{C_{Tot}^4 R_s^3 l^7}{5040} + \frac{1}{60} C_{Tot}^2 L_{Tot} R_s^2 l^5\right) C_l R_{lump}^2 C_o R_D + C_l C_o R_D \left(\frac{C_{Tot}^3 L_{Tot} R_s^3 l^7}{1260} + \frac{1}{40} C_{Tot}^2 L_{Tot} R_s^2 l^5\right) +$$
$$2\left(\frac{C_{Tot}^3 L_{Tot} R_s^2 l^6}{240} + \frac{1}{40320} C_{Tot}^4 R_s^4 l^8 + \frac{1}{24} C_{Tot}^2 {L_{Tot}}^2 l^4\right) C_l C_o R_{lump} R_D \quad (5.24)$$

The output at the victim line in laplace domain can be obtained as

$$V_o(s) = V_i(s) \frac{1}{b_0 + b_1 s + b_2 s^2 + b_3 s^3 + b_4 s^4 + b_5 s^5 + b_6 s^6} \quad (5.25)$$

Transient response can be calculated in time domain, using inverse laplace transformation as

$$V_o(t) = L^{-1}\left[V_i(s) \frac{1}{b_0 + b_1 s + b_2 s^2 + b_3 s^3 + b_4 s^4 + b_5 s^5 + b_6 s^6}\right] \quad (5.26)$$

The output voltage can be calculated for in-phase and out-phase crosstalk using Eq. (5.26). The noise voltage induced at the victim line under functional crosstalk can be calculated using

$$V_{noise}(s) = \frac{1}{2}\{H_{in}(s) - H_o(s)\} \times V_{agg}(s) \quad (5.27)$$

Here, $H_{in}(s)$ and $H_o(s)$ are taken as transfer function under in-phase and out-phase domain, $V_{noise}(s)$ is the noise voltage of the victim line n Laplace domain and $V_{agg}(s)$ is the input of the aggressor line.

5.3 RESULTS AND DISCUSSIONS

As a part of this section, the analysis results in terms of dynamic and functional crosstalk are compared with the simulation results for four different m-CNT bundle structures (S1, S2, S3, and S4). All the physical parameters are taken from Table 3.1. Table 5.1 to 5.3 shows the simulated as well as analytically calculated crosstalk induced delay, crosstalk induced peaks and crosstalk induced noise glitch area (CIGA), respectively. It has been noted from Table 5.1 that the proposed model is found to have high accuracy based on simulated results; the errors are within the range of 0.99-1.8% when crosstalk induced delay is taken into consideration for all structures of m-CNT bundles. Similarly from Table 5.2, it is discerned that the proposed model has high accuracy w.r.t simulated results, the errors are within the range of -5.41 to 15.47% when crosstalk induced peaks are taken into consideration for all structures of m-CNT bundles.

Table 5.1 Percentage errors from simulated crosstalk induced delay values to its analytically calculated values for all structures of m-CNT bundles using ABCD and decoupling method.

Simulated as well as analytically calculated crosstalk induced delay values for all structures of m-CNT bundles									**Percentage error from simulated values to analytically calculated values**			
Temp	**S1S**	**S1A**	**S2S**	**S2A**	**S3S**	**S3A**	**S4S**	**S4A**	**S1S V/s S1A**	**S2S V/s S2A**	**S3S V/s S3A**	**S4S V/s S4A**
K	**mV**	**mV**	**mV**	**mV**	**mV**	**mV**	**mV**	**mV**	**%**	**%**	**%**	**%**
300	0.858	0.859	1.388	1.389	1.344	1.345	0.588	0.590	0.107	0.065	0.074	0.340
350	0.903	0.908	1.515	1.515	1.425	1.427	0.584	0.585	0.523	0.007	0.140	0.164
400	0.933	0.935	1.486	1.486	1.433	1.443	0.590	0.591	0.214	0.007	0.698	0.017
450	0.983	0.993	1.661	1.680	1.573	1.593	0.596	0.597	1.018	1.145	1.271	0.168
500	0.999	1.000	1.738	1.768	1.640	1.660	0.648	0.650	-0.060	1.697	1.220	0.308

*S stands for simulated and A stands for analytical, e.g. 'S1S' stands for Structure 1 simulated and 'S1A' stands for Structure 2 analytical.

Table 5.2 Percentage errors from simulated crosstalk induced peak values to its analytically calculated values for all structures of m-CNT bundles using ABCD and decoupling method.

Simulated as well as analytically calculated crosstalk voltage peaks values for all structures of m-CNT bundles									**Percentage error from simulated values to analytically calculated values**			
Temp	**S1S***	**S1A***	**S2S**	**S2A**	**S3S**	**S3A**	**S4S**	**S4A**	**S1S V/s S1A**	**S2S V/s S2A**	**S3S V/s S3A**	**S4S V/s S4A**
K	**mV**	**mV**	**mV**	**mV**	**mV**	**mV**	**mV**	**mV**	**%**	**%**	**%**	**%**
300	27.30	26.84	32.23	30.72	55.72	54.25	66.88	66.61	1.68	4.69	2.64	0.40
350	27.87	26.54	32.30	31.54	55.96	55.09	67.19	70.85	4.77	2.35	1.55	5.45
400	28.72	27.05	32.37	32.03	56.84	56.44	70.57	71.16	5.81	1.05	0.70	0.84
450	28.75	28.36	32.42	32.44	57.79	57.68	71.68	71.58	1.36	0.06	0.19	0.14
500	29.38	28.84	32.49	32.75	57.91	56.65	72.41	72.17	1.84	0.80	2.18	0.33

*S stands for simulated and A stands for analytical, e.g. 'S1S' stands for Structure 1 simulated and 'S1A' stands for Structure 2 analytical .

Table 5.3 Percentage errors from simulated crosstalk induced glitch area values to its analytically calculated values for all structures of m-CNT bundles using ABCD and decoupling method.

Simulated as well as analytically calculated crosstalk voltage peaks values for all structures of m-CNT bundles									**Percentage error from simulated values to analytically calculated values**			
Temp	**S1S***	**S1A***	**S2S**	**S2A**	**S3S**	**S3A**	**S4S**	**S4A**	**S1S V/s S1A**	**S2S V/s S2A**	**S3S V/s S3A**	**S4S V/s S4A**
K	**mV**	**mV**	**mV**	**mV**	**mV**	**mV**	**mV**	**mV**	**%**	**%**	**%**	**%**
300	79	78.20	75	74.70	212	211.00	67	66.30	1.01	0.40	0.47	1.04
350	113	112.40	113	112.60	106	105.60	95	94.90	0.53	0.35	0.38	0.11
400	108	107.50	123	122.30	126	125.70	103	102.60	0.46	0.57	0.24	0.39
450	161	160.00	161	159.80	173	172.70	111	110.90	0.62	0.75	0.17	0.09
500	170	168.40	164	163.70	205	204.60	154	153.70	0.94	0.18	0.20	0.19

*S stands for simulated and A stands for analytical. e.g. 'S1S' stands for Structure 1 simulated and 'S1A' stands for Structure 2 analytical

In case of crosstalk induced glitch area (CIGA) the error range is 0.29-0.71%. For best structure, i.e S4 , the average percentage error from simulated values to analytical values calculated using ABCD and decoupling method in case of crosstalk delay is 0.998%, and in case of crosstalk peaks is -5.41% and, for CIGA is 0.7% respectively.

5.4 CONCLUSION

An ABCD parameter-based matrix approach is presented in this chapter for solving transmission lines based on decoupling technology. An equivalent circuit model with application of DIL (Driver-Interconnect Load) having two capacitively coupled m-CNT bundle-based interconnects were taken and their performance was analyzed w.r.t dynamic crosstalk and functional crosstalk. The values, thus obtained analytically were compared with simulated values. It was observed that for best structure, i.e S4 , the average errors between simulated values and the analytically calculated values calculated using ABCD and decoupling method in case of crosstalk delay is 0.998%, in case of crosstalk peaks is -5.41%, and in case of CIGA is 0.7%, respectively. The accuracy of the model lies below 1% and therefore it can be considered for superior performance and greater potential in futuristic IC designs.

CHAPTER-6
DIELECTRIC SURFACE ROUGHNESS SCATTERING INDUCED CROSSTALK PERFORMANCE OF COUPLED MCB INTERCONNECTS

As part of this chapter, some of the most common and consistent dielectric materials are taken into consideration and analyzed in relation to the mean free path (MFP) caused by surface roughness scattering. This study analyzes the crosstalk effect in terms of positive peaks, time duration and the area of rise glitch under dynamic and functional signal switching conditions. In addition, frequency spectrum and bode stability analyses are made for four different structures of m-CNT bundles (MCB) at 14nm node for a temperature range of 300-500K.

From previous chapters, it is been certain that m-CNTs are giving satisfactory results in optimizing crosstalk induced delay as the technology is scaling to nanometer scale [3], [17]-[20], [33], [48], [56], [63], [90], [112], [115]. Over scaling reduces the pitch (thickness/width) of interconnects, resulting in reduced dimensions. This further increases coupling effects, towards the end of the technology roadmap. Crosstalk between the two adjacent VLSI interconnects has been a major contributor in facing signal integrity, logic failures and a severe uncertainty in delay [19, 20]. Scaling down to 22nm technology node or below, the effect of roughness of substrate on which a VLSI interconnects are placed, play a critical role in the functionality and reliability of the circuits. The effect of surface roughness becomes more dominant due to scattering caused by surface and grain boundary. Sometimes, during the process of fabrication of VLSI interconnects, roughness in the substrate material is deliberately added to bring better adhesion between the layers of dielectric substrate and the surface of conductor. When the interconnect dimension reduces to nanometer scale, the effect of grain size, is also responsible for increasing the crosstalk, apart from the coupling effects between interconnects [43], [44]. Therefore, it is quite imperative to analyze and discuss these effects as the technology scales down to nanometer meter range. Chemical mechanical planarization (CMP) process during the fabrication of interconnects can govern the effect of roughness caused by upper as well as lower surfaces of VLSI interconnects, whereas, the side wall roughness majorly leads to coupling effects in the aggressor-victim-aggressor (AVA) line bus architecture [136].

In the range of many giga-hertz, the effect of surface roughness becomes more prominent and induces more delay and power losses in integrated circuit designs [41], [42], [46], [100]-[105]. It is observed in the chapter-2 that while analyzing the performance of CNTs, most researchers assumed that the substrate surface on which the CNT interconnects are placed is smooth. But in real, the impact of substrate surface roughness (SSR) is more pronounced at ultra-scaled technology nodes due to size effects and grain boundary scattering in nanometer dimensions. Therefore, the objective of this chapter is to investigate the effects of dielectric SSR impact on the performance of coupled interconnects of MCB for a range of temperature (300-500K) at 14nm technology node. Commonly used, dielectrics like silicon carbide (SiC), boron nitride (BN) and silicon dioxide (SiO_2) are taken for performance analyses of four different structures of MCBs w.r.t. crosstalk induced glitch area (CIGA), crosstalk induced delay, stability and 3-dB frequency bandwidth analyses.

6.1 DIELECTRIC SURFACE ROUGHNESS SCATTERING INDUCED IMPEDANCE ANALYSES OF MCB STRUCTURES

Four physical structures of MCB, namely S1, S2, S3 and S4 (also named as MCB-1, MCB-2, MCB-3 and MCB-4) are taken as shown in the Fig.3.1 having various arrangements of MWCNTs and SWCNTs used to study the performance of m-CNT bundle (MCB) interconnects [25-27]. Fig. 3.2 shows an equivalent RLC circuit of MCB, the temperature-dependent (TD) per unit length (*p.u.l)* resistance, inductance and capacitance of a SWCNT bundle can be obtained using Eqs. (3.1) and (3.2).

Using Matthiessen's rule, the effective mean free path '$\lambda_{eff}(T)$' formulated as shown in Eq. 3.6 can be altered [42] after considering surface roughness and is given as:-

$$\lambda_{eff}(T) = \left[\lambda_{AC}^{-1} + \lambda_{OZ}^{-1} + \lambda_{D}^{-1} + \lambda_{sr}^{-1}\right]^{-1} \quad (6.1),$$

where 'λ_{AC}' is the acoustic MFP and 'λ_{OZ}' is the effective optical and zone boundary MFP and a new factor affecting the mean free path, 'λ_{sr}', which is the mean free path due to surface roughness. 'λ_{sr}' is denoted as [42]:

$$\lambda_{sr} = \frac{m}{\delta_{sr}^2}\{nm\} \quad (6.2),$$

Here, '*m'* is a fitting parameter with a value equal to 2.07×10^9 and '$\boldsymbol{\delta}_{sr}$', which is the amplitude of surface roughness of the substrate material, is taken in pico-meters. The amplitude of surface

roughness for SiO_2, BN and SiC substrate materials are taken as 70pm, 170pm and 10pm, respectively [42].

All the ITRS 2013 physical parameters involved during the simulation are encapsulated in Table 3.1 [120]. Table 6.1 is showing the impedance parameters of four different structure of MCB (e.g. S1, S2, S3 and S4) placed on different substrates viz. SiO_2, BN, SiC for a temperature range (300-500K). It is noticed that the equivalent resistance of every structure is reduced when SiC is

Table 6.1 Impedance parameters for different MCBs on different substrate materials taken at length 1mm for different temperatures (300K-500K) at 14nm technology node.

		RESISTANCE (K-Ohms)				**INDUCTANCE (nH)**				**CAPACITANCE (fF)**			
TEMP (K)	**SUBSTRATE MATERIAL**	**S1**	**S2**	**S3**	**S4**	**S1**	**S2**	**S3**	**S4**	**S1**	**S2**	**S3**	**S4**
300	**SILICON DIOXIDE (SiO2)**	24.27	24.36	24.24	24.32	58.97	74.24	92.64	69.35	0.4179	0.1784	0.13805	0.1385
350		29.89	29.87	29.68	29.83	56.59	70.02	87.21	65.45	0.4118	0.1784	0.13806	0.1385
400		32.29	32.05	31.78	32.03	52.68	63.06	78.27	59.19	0.4118	0.1784	0.13806	0.1385
450		38.11	37.76	37.39	37.78	51.03	60.14	74.51	56.56	0.4141	0.1792	0.13865	0.1389
500		45.2	44.61	44.11	44.67	49.57	57.54	71.17	54.22	0.4141	0.1792	0.13865	0.1386
300	**SILICON DIOXIDE (SiO2)**	25.21	25.36	25.24	25.32	58.97	74.24	92.64	69.35	0.4117	0.1784	0.13805	0.13854
350		30.8	30.87	30.68	30.83	56.59	70.02	87.21	65.45	0.4118	0.1784	0.13806	0.13854
400		33.16	33.05	32.78	33.03	52.68	63.06	78.27	59.19	0.4118	0.1784	0.13806	0.13854
450		38.79	38.76	38.39	38.77	51.03	60.14	74.51	56.56	0.4141	0.1792	0.13865	0.13895
500		45.72	45.61	45.11	45.67	49.57	57.54	71.17	54.22	0.4141	0.1792	0.13865	0.1386
300	**SILICON CARBIDE (SiC)**	22.01	22.18	22.06	22.15	58.97	74.24	92.64	69.35	0.4117	0.1784	0.13805	0.13854
350		27.6	27.7	27.51	27.68	56.59	70.02	87.21	65.45	0.4118	0.1784	0.13806	0.13854
400		29.96	29.9	29.64	29.91	52.68	63.06	78.27	59.19	0.4118	0.1784	0.13806	0.13854
450		35.59	35.68	35.32	35.75	51.03	60.14	74.51	56.56	0.4141	0.1792	0.13865	0.13895
500		42.52	42.6	42.1	42.73	49.57	57.54	71.17	54.22	0.4141	0.1792	0.13865	0.1386
300	**SMOOTH SURFACE MATERIAL**	7.751	7.195	7.931	7.449	58.96	74.23	92.64	69.35	0.4117	0.1784	0.13804	0.13853
350		9.442	9.572	10.70	9.762	56.59	70.01	87.21	65.45	0.4118	0.1784	0.13805	0.13854
400		10.31	11.78	13.35	11.86	52.67	63.06	78.27	59.19	0.4118	0.1784	0.13805	0.13854
450		12.57	14.69	16.87	14.59	51.03	60.13	74.51	56.56	0.4141	0.1792	0.13864	0.13895
500		14.98	18.52	21.53	18.18	49.57	57.53	71.17	54.22	0.4141	0.1792	0.13864	0.13859

used as the substrate. It is due to the fact that the MFP increases since the amplitude of surface roughness ('δ_{sr}') is lowest in SiC substrate material in comparison with other substrate materials.

Although the inductances and the capacitances of MCB based interconnect depict a variation w.r.t. temperature dependent no. of conducting channel. The inductance and the capacitance have no influence of substrate surface roughness. Since the conducting channel-dependent kinetic inductance dominates the magnetic inductance over a range of temperatures (300K-500K), an increase in equivalent inductance is observed. However, a minimal effect in the capacitance of TD-MCBs is seen with the increase in temperature. The quantum capacitance dominates over electrostatic capacitance, in the capacitance of MCBs.

6.2 RESULTS AND DISCUSSION

In the following sections, based on the temperature-dependent MFP model described in Section 6.1, which accounts for substrate surface roughness, crosstalk and stability analyses of MCB interconnects are discussed at 14 nm technology, and the results are compared with those for MCB interconnects placed on smooth surfaces. Here, '$\boldsymbol{\alpha}_1$' notation is used for smooth surface case in which MCB is placed on smooth substrate, while, '$\boldsymbol{\alpha}_2$' notation is used for rough surface case where MCB is placed on different rough substrate materials such as silicon carbide (SiC), boron nitride (BN) and silicon dioxide (SiO_2).

An equivalent single conductor (ESC) *RLC* circuit model of capacitively coupled aggressor-victim (A-V) lines, shown in Fig.3.7, is considered to perform the crosstalk analyses. The circuit is driven by a CMOS driver with a clock speed of 0.1 GHz, V_{dd}=0.8V and is terminated by a capacitive load C_L of 0.020fF at 14nm technology node. The width ratio (w_p/w_n) of PMOS and NMOS transistors is kept as 2:1 and the NMOS transistor size is 100 times the minimum size of the transistor. All the simulations are carried out at 14nm technology node [119]. Due to global/long interconnects, CMOS repeaters are optimized in order to reduce pulse duration and increase drive capability. Various conditions are taken for coupled A-V lines of MCB in which victim line is kept fixed at logic '0' or '1' and aggressor line is switched between '0' to '1' or '1' to '0' under functional crosstalk condition. While in case of dynamic crosstalk, both lines (e.g. aggressor and victim) are switched from '0' to '1' under even mode of signal switching [23], [26], [32], [114]. Even-mode signal switching is considered for dynamic crosstalk analysis since the time of flight(t_f) is observed to be less in even mode signal switching compared to odd mode [26]. In an even mode of signal switching, the time of flight is defined as ($t_{fe} = l\sqrt{CL}$) , while in an odd mode, it is defined as ($t_{fo} = l\sqrt{(C + C_c)L}$). Hence, the crosstalk induced delay is

obtained to be less, under even mode of signal switching as compared to odd mode of signal switching.

6.2.1 Dielectric Surface Roughness (SSR) scattering induced crosstalk analyses

The detail study of positive peaks and time duration of the output noise pulse on the victim side in a capacitively coupled MCB interconnects, considering temperature-dependent *RLC* parameters estimated for (a)smooth ('α_1'case) and (b)rough ('α_2'case), is presented in Figs. 6.1 and 6.2 at 14 nm technology node. These are two salient features (positive peak and time duration) of the transient responses of the victim output, depending on scattering induced by substrate surface roughness, for coupled interconnects of MCB. These salient features are extracted from transient responses of the victim output, plotted in Fig.6.1 and Fig.6.2, over a range of temperatures from 300K to 500K. In these analyses the optimum diameter of MWCNTs and SWCNTs in each MCB of four different structures are considered to be 8nm and 1nm, respectively. The results shown in Figs.6.1 and 6.2 are under functional crosstalk 'rise glitch' case, where the transitions of aggressor line are taken from logic '0' to '1' and victim line transitions are fixed at logic '1'.

Fig. 6.1 shows the positive peaks of rise glitch as a function of temperature (300-500K) of four different structures of MCB (S1, S2, S3 &S4), taking both the cases 'α_1' and 'α_2'. It can be apparently seen that the positive peaks of rise glitch are falling with increase in temperature from 300K to 500K. The positive peaks of rise glitch are obtained to be higher in case of 'α_1' w.r.t. 'α_2'. The noise peaks fall as the temperature rises [26]. As seen from Eq. (3.1), the resistance is directly proportional to the temperature and therefore, it is justified to state that as the resistance increases, the positive peaks of rise glitch falls. The structure 'S4' is showing the lowest positive peaks of rise glitch among other structures due to the combined effect of impedance parameters associated with it. As stated by [11], if the voltage level is exceeded, a positive peak of the rise glitch will cause a dielectric breakdown.

Fig. 6.2 shows the time duration of rise glitch of four different structures of MCB for a temperature range (300-500K). The computed results, as shown in Fig. 6.2, are extracted from the transient responses obtained at the far end of victim line, under functional signal switching condition at different temperature (300-500K). It can be noted that the time duration of rise glitch increases with rise in temperature. This is due to the dominance of line resistance over

capacitance and inductance. The resistance of interconnect increases with increase in temperature (see Table 3.1). When the resistance increases, noise peaks falls and time duration broadens [11]. In case of 'α_2' the time duration is higher than 'α_1'. It has been observed from Figs. 6.1 & 6.2 that the structure-4 of MCB (i.e. S4) placed on 'SiC' substrate gives the best results in terms of positive peak and time duration of rise glitch in comparison to other dielectric materials (BN & SiO_2).

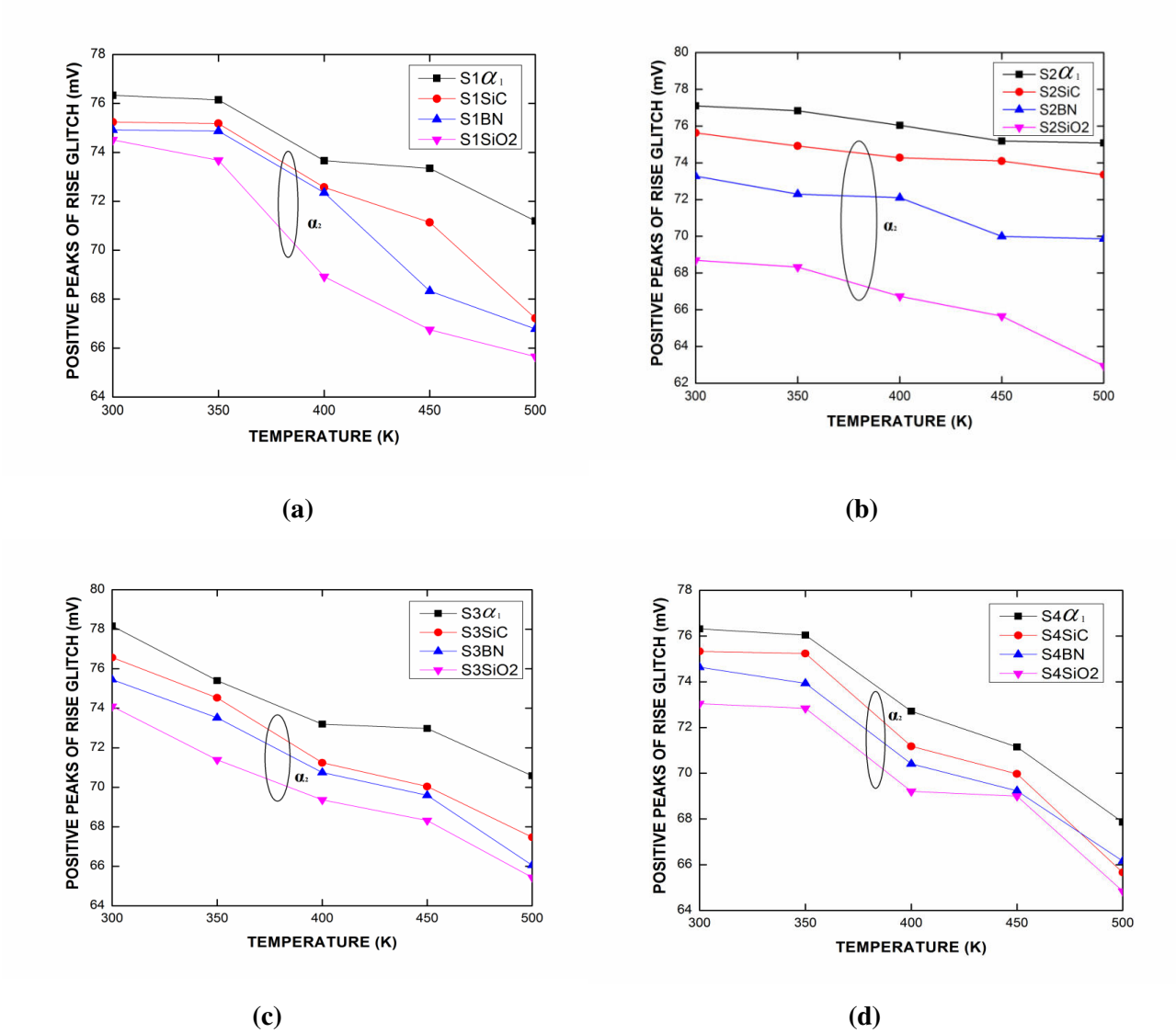


Figure 6.1 Positive peaks of rise glitch of four different structures of MCB (a) S1, (b) S2, (c) S3, (d) S4 for a temperature range (300-500K).

The crosstalk induced glitch area (CIGA) of the victim line's output under functional crosstalk comprises of positive peak of rise glitch and its time duration. It is formulated as

$$(CIGA) = \frac{1}{2} \times Positive\ Peak\ of\ Rise\ Glitch \times Time\ Duration\ of\ Rise\ Glitch \qquad (6.3)$$

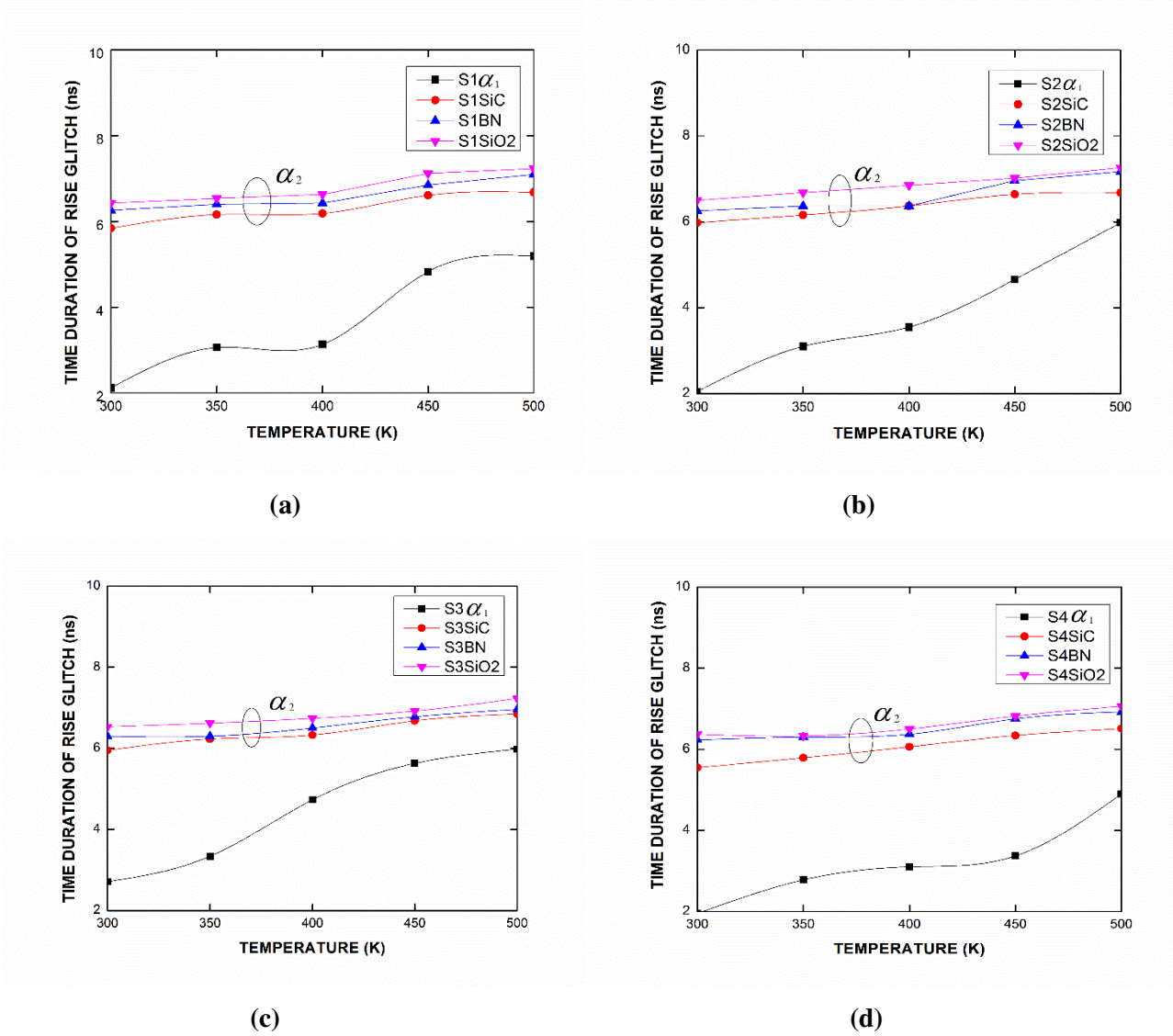


Figure 6.2 Time duration of rise glitch of four different structures of MCB (a) S1, (b) S2, (c) S3, (d) S4 for a temperature range (300-500K).

The computed values of CIGA of various structures (i.e. S1,S2,S3 and S4) of MCB, considering both cases viz. smooth surface ('$\boldsymbol{\alpha}_1$') as well as rough surface ('$\boldsymbol{\alpha}_2$'), is listed in Table 6.1. In '$\boldsymbol{\alpha}_2$' case, as seen from Table 6.2, the S4 on SiC substrate is giving the lowest CIGA of victim line's noise pulse as compared to other substrate materials, for the complete range of temperature (300K-500K). Apparently, CIGA increases by increasing temperature from

300K to 500K, which is due to the combined effect of positive peak and time duration of rise glitch.

Table 6.2 The Crosstalk Induced Glitch Area (CIGA) of four different structures of MCB considering smooth ($\boldsymbol{\alpha}_1$) as well as rough surface ($\boldsymbol{\alpha}_2$).

TEMP	S1				S2				S3				S4			
(K)	α1	SiC	BN	SiO2	α1	SiC	BN	SiO2	α1	SiC	BN	SiO2	α1	SiC	BN	SiO2
300	149	439	466	486	158	457	476	488	212	456	475	484	146	418	465	465
350	229	463	464	482	234	463	477	483	252	464	463	473	211	436	466	461
400	224	447	439	479	263	461	445	461	346	451	460	467	225	431	449	450
450	230	470	451	500	341	465	464	447	411	468	472	473	240	444	467	471
500	327	444	466	515	431	439	430	421	422	462	460	473	333	427	458	458

Also, over the entire range of temperature, the S4 with smooth surface (i.e. '$\boldsymbol{\alpha}_1$' case) has always the lowest CIGA in comparison to other structures of MCB. This implies that with rise in temperature, the performance of MCB based interconnects deteriorates.

Fig. 6.3 shows the normalised dynamic crosstalk induced delay of four different structures of MCB on various substrate materials for temperature range (300-500K). The crosstalk induced delay obtained for all structures of MCB placed on different substrate materials(e.g. '$\boldsymbol{\alpha}_2$') are normalised w.r.t. crosstalk induced delay obtained in the case of '$\boldsymbol{\alpha}_1$'. As depicted in the figure, the S4 of MCB is showing the lowest normalized crosstalk induced delay w.r.t. other structures of MCB (i.e. S1, S2 and S3), placed on all three rough surfaces. Particularly, it has also been observed from the figure that the S4, placed on a rough surface of silicon carbide (S4SiC) in case of '$\boldsymbol{\alpha}_2$' , is always showing the lowest crosstalk induced delay w.r.t. other substrate materials (e.g. BN & SiO_2), which is due to the proportionally lower values of the resistance (see Table 3.1).

However, the line resistance decreases by decreasing the amplitude of the surface roughness parameter ('$\boldsymbol{\delta}_{sr}$'). As seen from Eq. (6.1), the '$\boldsymbol{\delta}_{sr}$' is inversely proportional to the MFP, i.e., a decrease in the '$\boldsymbol{\delta}_{sr}$' results in a higher MFP and lower resistance. In '$\boldsymbol{\alpha}2$' case, as stated in Table 6.2, S4 on SiC substrate is giving the lowest CIGA of victim line's noise pulse as compared to other substrate materials, for the complete range of temperature (300K-500K). This increase of CIGA obtained at the far end of the victim line of 'S4SiC' is, due to the increase of its resistance

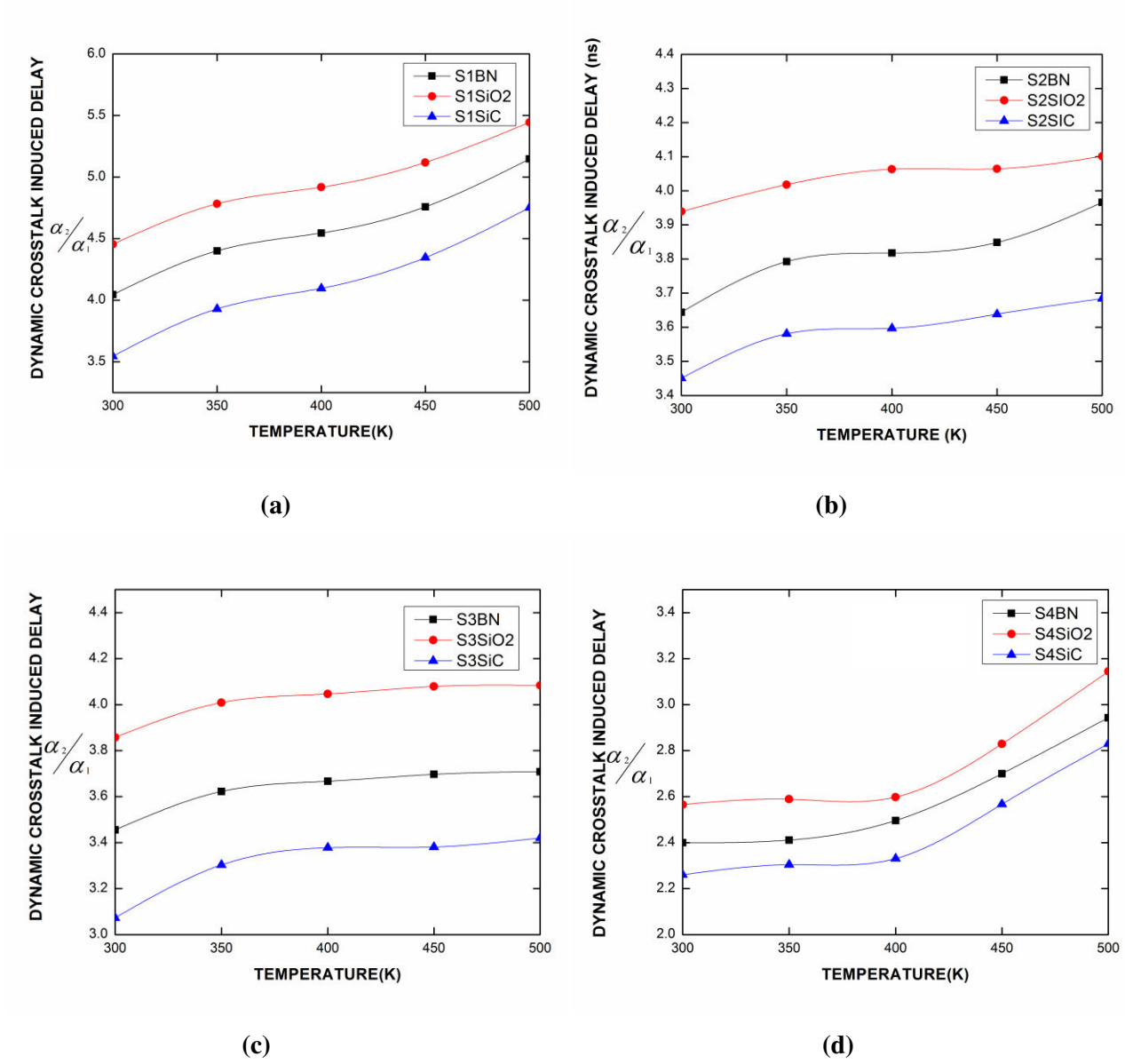


Figure. 6.3 Normalised dynamic crosstalk delay of four different structures of MCB on various substrate materials for temperature range (300-500K).

with rise in temperature (300K-500K). This implies that with rise in temperature, the mechanism of mixed CNT interconnect deteriorates, as the duration decreases and peak of crosstalk induced noise increases. Table 6.4 illustrates the effect of '$\boldsymbol{\delta}_{sr}$' on the CIGA and dynamic crosstalk induced delay of the best structure of MCB(S4) over a range from 40*pm* to 200*pm*. From Eqs. (3.1),(3.2),(6.2) and (6.3), it is justified to state that the amplitude of rough surface ('δ_{sr}') is directly proportional to the resistance of MCB interconnect and therefore, as seen from Table

6.3, the CIGA and dynamic crosstalk induced delay of the S4 is increasing with an increase in 'δ_{sr}'.

Table 6.3 Crosstalk Induced Noise Area (CIGA) and a relative percentage increase in crosstalk induced delay of S4 by including $\alpha 2$ w. r. t. $\alpha 1$.

CIGA of S4 considering μ1 as well as $\alpha 2$					**A relative percentage increase in crosstalk induced delay of S4 by including $\alpha 2$ w. r. t $\alpha 1$.**		
Surface Type	**($\alpha 1$)**	**($\alpha 2$)**			**BN (%)**	**Sio2 (%)**	**SiC (%)**
Temperature (K)	**S4**	**S4 (BN)**	**S4 (SiO2)**	**S4 (SiC)**			
300	44.81	235.81	231.01	232.97	304.50	345.50	254.50
350	53.08	213.38	213.74	211.8	340.09	378.30	292.92
400	62.1	215.78	215.78	216.94	354.59	391.74	309.63
450	64.51	242.02	243.1	245.42	414.71	411.84	334.65
500	89.79	260.18	259.41	262.01	357.95	444.54	375.21

$\alpha 1$= Crosstalk induced delay of S4 assuming Smooth surface,$\alpha 2$= Crosstalk induced delay of S4 assuming Rough surface.

Table 6.4 The Crosstalk Induced Glitch Area (CIGA) and dynamic crosstalk delay of the best structure of MCB (S4) taking various amplitudes of δsr.

Amplitude of Rough Surface (δ_{sr}) (*pm*)	**Crosstalk Induced Glitch Area (CIGA)**	**Dynamic Crosstalk Induced Delay (*ns*)**
40	443.18	5.95
80	452.71	5.98
120	454.52	6.02
160	467.3	6.06
200	480.99	6.09

6.2.2 Dielectric Surface Roughness scattering (SRS) induced bode stability analysis

To analyze the stability of the best structure of MCB (S4), a CMOS inverter driven, equivalent single conductor (ESC) *RLC* model of capacitively coupled aggressor-victim (A-V) lines is taken as shown in Fig.3.2. In this architecture, for dynamic signal switching condition both lines (i.e. aggressor and victim) are switched from '0' to '1' simultaneously under even mode of signal

switching. In order to determine the stability of the system, a step signal is passed through it, and the output received is categorized primarily into three categories [137]:-

1. Over-damped
2. Critically-damped
3. Under-damped

These conditions are categorized according to the damping ratio. If the damping ratio is greater than '1', the system is over-damped, if it is equal to '1', the system is critically-damped and if it is between '0' and '1', the system is under-damped. It is reported that the under-damped condition is more stable and faster than other conditions [138]. As the switching delay increases, the step response tends to damp more rapidly, and the system becomes more stable [139]. Using standardized mathematical approach, the ESC model circuit shown in Fig.3.2 represents a second order *RLC* circuit and its transfer function can be computed as [140]

$$H(j\omega) = \frac{V_{out}(j\omega)}{V_{in}(j\omega)} = \frac{1}{[L_{MCB}C_{MCB}j\omega^2 + R_{MCB}C_{MCB}j\omega + 1]} \quad (6.4),$$

Using MATLAB tool (version 10), bode stability of MCB structure 'S4', placed on smooth surface (e.g. $\boldsymbol{\alpha}_1$ case) and different rough substrate materials (e.g. '$\boldsymbol{\alpha}_2$' case) such as silicon carbide (SiC), boron nitride (BN) and silicon dioxide (SiO2) over a temperature range (300-500K), are analyzed taking 1mm long interconnect at 14nm technology node. Along the Y-axis, magnitude in decibel and phase in degrees are plotted w.r.t. frequency (Hz) on X- axis. Fig.6.4 shows the magnitude and phase response w.r.t. frequency of 'S4' under '$\boldsymbol{\alpha}_1$' case and '$\boldsymbol{\alpha}_2$' case at 300K. Using these bode plots, gain margin (GM) and phase margin (PM) are obtained. The gain added to move 0dB line at phase crossover frequency is termed as GM and the difference between 0dB cross-point of the curve of gain line and -180° is termed as PM. If the PM and GM increases the system becomes stable [138]. From Fig.6.4, it is seen that S4SiC is having higher GM and PM than S4 in '$\boldsymbol{\alpha}_1$'case (S4 $\boldsymbol{\alpha}_1$). It has also been noted that S4SiC is having higher GM and PM in comparison to S4BN and S4SiO_2. Therefore it is justified to conclude that S4SiC is better than other cases taken. Fig. 6.5 shows amplitude frequency response (AFR) at 1mm long interconnect of 'S4SiC' taking temperature range (300-500K). It is observed from Fig.6.5, that as the temperature is rising from 300K to 500K with an increment of 50K, the 3-dB frequency (0.707) of transfer function $H(j\omega)$ is decreasing. It is justified by the impedance values tabulated in Table 6.1 that rise in temperature increases the resistance, which further leads to reduction in

bandwidth. Table 6.5 is showing the bandwidth and 50% rise time of S4 for '$\boldsymbol{\alpha}_1$' and '$\boldsymbol{\alpha}_2$' cases. It can be observed that for S4 with smooth surface (S4 $\boldsymbol{\alpha}_1$) has wider bandwidth than S4 placed on different rough substrate materials with the same dimensions. It can also be noted from the table that in case of '$\boldsymbol{\alpha}_2$', S4SiO_2 has the lowest 3-dB bandwidth, which is due to higher value of '$\boldsymbol{\delta}$sr'. Simulataneously, an increase in 50% rise time at the far end of aggressor line is also observed.

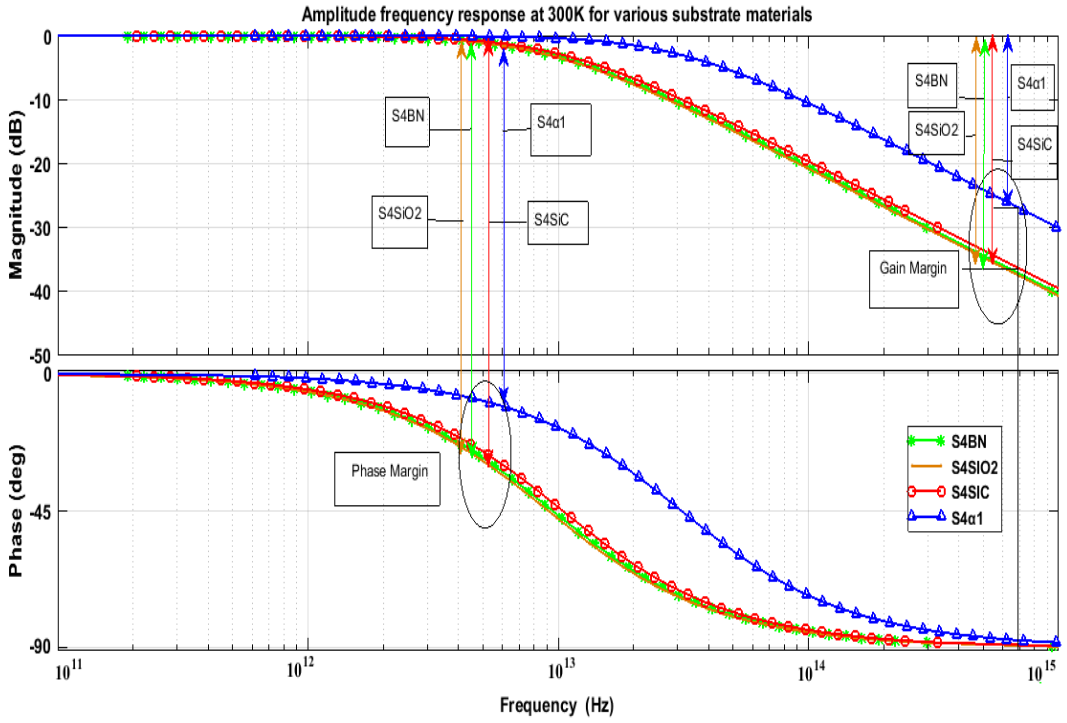


Figure 6.4 Amplitude frequency response (AFR) at 300K for 1mm long interconnect of structure-4 on various substrate materials.

To perform the frequency spectrum analysis of the victim' output under function signal switching, the time domain values of transient response are converted into frequency domain using a Fast Fourier Transform (FFT) algorithm written in C script. A bin spacing of $\Delta f = f_s/N$ is taken in the calculation using the 64-point FFT code.

Figure 6.6 shows the dynamic crosstalk based frequency responses of S4 at far end of the aggressor line, taking different substrate materials. Here, the X-axis frequency is normalized by input frequency. It has been noticed from Fig. 6.6, that the bandwidth of S4 when SiC is taken as a substrate material, is higher than the bandwidth of S4 placed on other substrate materials (SiO_2 & BN). This is due to the reason that the resistance due to surface roughness in SiC, is least

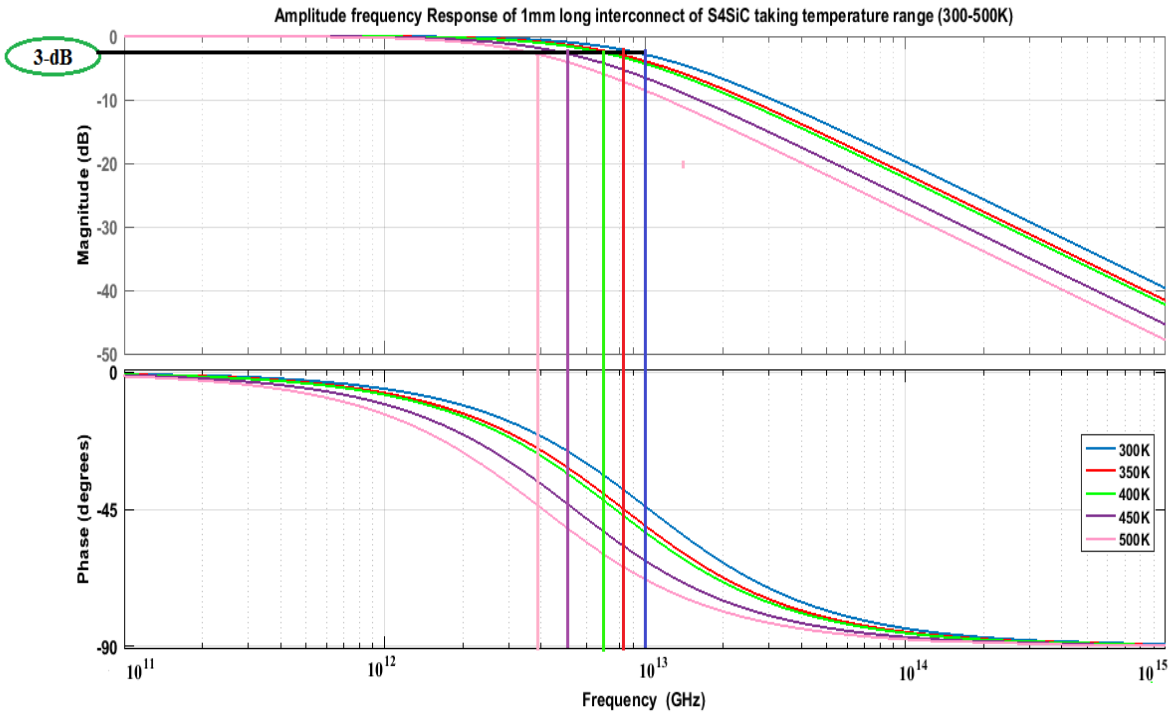


Figure 6.5 Amplitude frequency response (AFR) of transfer function at 1mm long interconnect of S4SiC taking temperature range (300-500K).

among other substrate materials. It is also observed that there is an abrupt decrease in amplitude w.r.t frequency in Fig.6.7.It is due to the fact that the first lobe contains the maximum signal power and the amplitude of side lobes keep on decreasing monotonically. This happens when the time domain signal does not have integral number of cycles and the continuous spectrum gets shifted from first lobe to side lobes. The first lobe is important, as it determines the bandwidth as well as, it carries the maximum signal power of the respective MCB structure [139].

Fig.6.7 shows the normalised functional crosstalk induced amplitude versus normalised frequency at the far end of the victim line for the best structure of MCB (S4) taking '$\boldsymbol{\alpha}_1$' and '$\boldsymbol{\alpha}_2$' cases. In this figure x-axis frequency is normalised w.r.t. the frequency of input signal,while y-axis amplitude of noise is normalised w.r.t. the amplitude of input signal. Here, the noise frequency components are suppressed more in the low frequency range. This figure also reveals that $S4SiO_2$ is showing larger frequency noise amplitudes as compared to S4 placed on SiC and BN. It is worth noting that, the S4 with smooth surface (i.e. '$\boldsymbol{\alpha}_1$' case) has the lowest noise frequency components with respect to rough surface (i.e. '$\boldsymbol{\alpha}_1$' case). Moreover, the S4 placed on SiC (S4SiC),

filters more noise frequency components of the victim line output, making it the most desirable structure (S4SiC) for future MCB-based interconnects in the deep-submicron (DSM) regime.

TABLE 6.5 Bandwidth and 50% rise time for S4 for smooth(α1) as well as rough surface (α2).

Type of Interconnect	**Bandwidth at 3-dB Frequency (Hz)**	**50% Rise time of Aggressor Line**
S4 (α1)	$1.07X10^{12}$	1.16ns
S4SiC	$3.06X10^{11}$	1.65ns
S4BN	$9.44X10^{10}$	1.68ns
S4SiO2	$9.02X10^{10}$	1.72ns

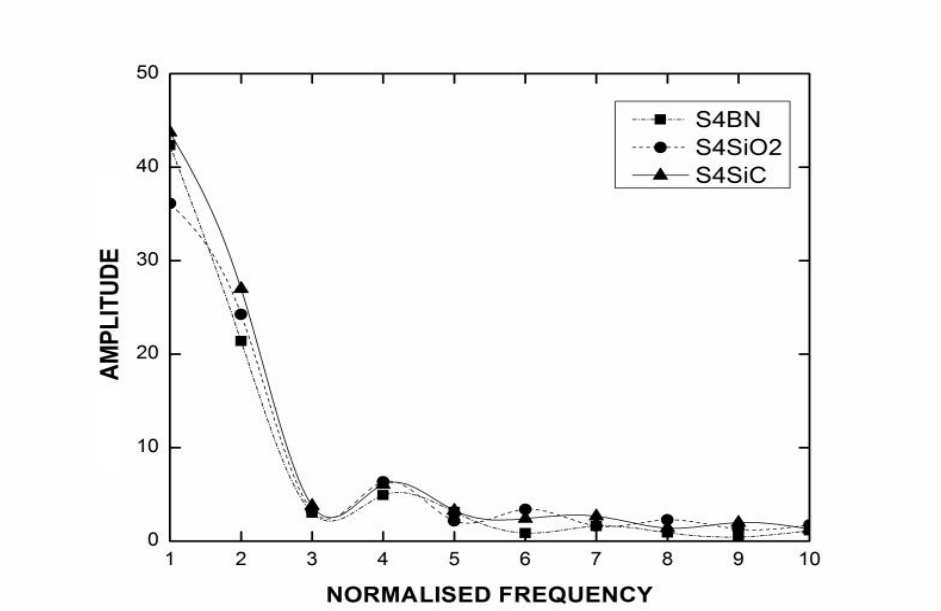


Figure 6.6 Frequency responses of S4 on different substrate materials while considering dynamic crosstalk at 14nm technology node.

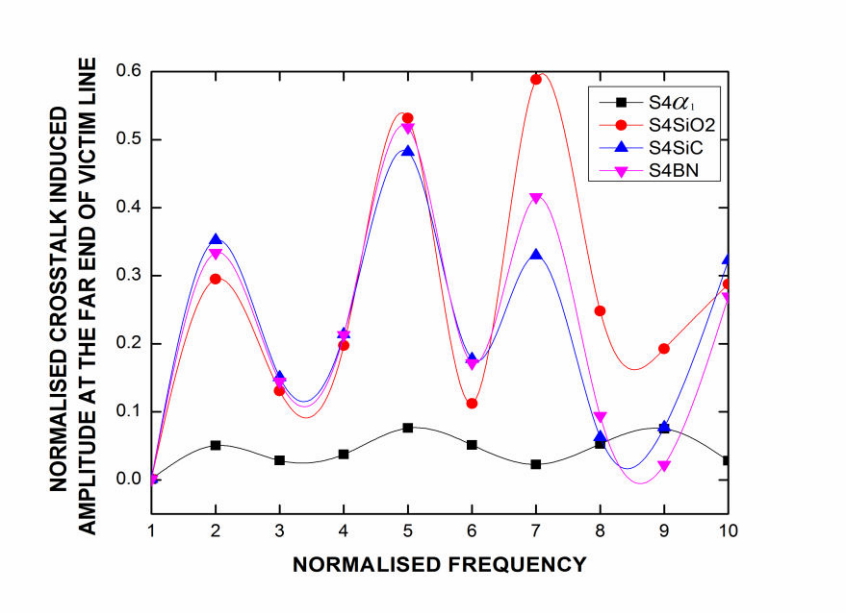


Figure 6.7 Normalised functional crossstalk induced amplitude at the far end of the victim line for the best structure (S4) taking $\boldsymbol{\alpha}_1$ and $\boldsymbol{\alpha}_2$ cases.

6.3 CONCLUSION

The performance of coupled MCB interconnects, placed on different rough substrate materials (e.g. '$\boldsymbol{\alpha}_2$' case) such as silicon carbide (SiC), boron nitride (BN) and silicon dioxide (SiO2), has been compared to that of MCB interconnects placed on smooth substrate surfaces (e.g. '$\boldsymbol{\alpha}_1$' case) in terms of crosstalk induced glitch area (CIGA), crosstalk induced delay, stability and 3-dB frequency bandwidth analysis. In comparison with smooth surface results, the relative crosstalk induced delay in S4 increases, on average, by 357.95%, 394.38%, and 313.38%, respectively, when placed on substrate materials such as BN, SiO_2 and SiC. When S4 is placed on substrate materials (e.g. BN, SiO2, and SiC), the crosstalk induced glitch area (CIGA) is approximately 5 times greater than on smooth surfaces. In addition, the bandwidth of S4SiC is greater than that of S4 placed on other substrate materials (e.g. SiO2 and BN). Among all the structures, S4 placed on SiC substrate material is showing admirable results for positive peaks, time duration, area of rise glitch. Amplitude frequency response of S4SiC came out to be least among other structures of MCB placed on other substrate materials. It has been confirmed from the bode stability diagrams that S4SiC interconnects are more stable and have larger phase margin, gain margin and 3-dB frequency bandwidth in comparison to S4BN and $S4SiO_2$ with the same dimensions. Moreover, MCB interconnects placed on smooth substrate surface have larger 3-dB frequency

bandwidth and smaller delay times than those of MCB placed on rough substrate surfaces over a temperature range (300K-500K). Furthermore, when the surface roughness parameter ($\boldsymbol{\delta}_{sr}$) is increased, it reduces the frequency bandwidth and 50% rise time of the aggressor line at its far end. On the basis of the results, we conclude that for on-chip MCB interconnects at current and future technology nodes, it is imperative to account for substrate surface roughness in crosstalk analysis.

CHAPTER-7

CONCLUSION, CONTRIBUTIONS AND FUTURE SCOPE

This chapter summarizes the entire research work presented in this thesis along with the scope of future work. Section 7.1 to 7.4 deals with every objective of this thesis, its findings and conclusion. Section 7.5 discusses the scope of the future work of the research work furnished in this thesis.

7.1 DEFECTS BASED IRRADIATION-INDUCED PERFORMANCE ANALYSES OF m-CNT BUNDLES

In the process of fabrication and purification of CNTs, various defects like atom vacancies, doping, impurities etc., get introduced by irradiation with energetic particles which leads to modifications in the properties of CNT, as per the requisite of application. These defects alter the properties of CNTs by bringing a change in the chemical bond. The scattering theory states that due to backscattering, the average MFP of electrons gets reduced due to defects, causing an overall resistance increase for interconnects. An increase in overall resistance will also have a significant impact on the performance of interconnection. The MFP decays considerably in defected zig-zag CNT in which single and double vacancy are found. Due to the absence of C-C bonds, vacancies in the honeycomb structure of CNTs are created and therefore, short phonon wave diminishes leading to a decrease in the MFP. The path of semiconducting tubes is highly responsive to a disorder which makes it a MFP. While considering defects in the research work stated in chapter-3, the propagation delay of four different structures of m-CNT bundle increases. The propagation delay increases significantly when crosstalk is considered. Crosstalk induced positive peaks and time durations of victim output pulses in copper are much higher than that of all the structures of m-CNT bundle for the entire range of temperature (300-500K).

7.2 THERMALLY AWARE CROSSTALK AND FREQUENCY SPECTRUM ANALYSES IN ADJACENT INTERCONNECTS OF M-CNT BUNDLE

The research work stated in chapter-3 and 4, addresses a thermally aware performance analyses in single as well as capacitively coupled interconnects of mixed CNT bundles (MCBs) while taking tunneling effect into consideration, for temperature varying from 300K to 500K at 14nm technology node. Four possible structures of MCBs are considered and their results in terms of crosstalk and frequency spectrum are compared with copper-based interconnect taking interconnect length from 200µm to 1000µm at 14nm technology node**.** In single line architecture, MCB-4 (aka S4) is showing least propagation delay among other MCBs (S1-S3) and copper over temperature from 300K to 500K. While taking tunneling effect into consideration, a percentage increase in propagation delay of MCB-4 (aka S4) by considering "without tunneling" effect to "with tunneling" effect is obtained about 12.08%. Frequency spectrum analysis of MCB-4 has shown an increase of about 17.70% in bandwidth when compared with copper. Also, the bandwidth of MCB-4 (aka S4) has decreased with rise in temperature (300K-500K) which indicates that the loss in signal power is more at higher temperatures. For a capacitively coupled architecture, taking all switching conditions (DC-(1-4)) of aggressor and victim lines, MCB-4 (aka S4) has shown least average percentage decrease in dynamic crosstalk induced noise w.r.t other MCBs (1-3) and copper. On an average in even mode of switching, MCB-4 (aka S4) has shown 36.45% lesser crosstalk induced delay in comparison to odd mode of switching when temperature is raised from 300K to 500K. Also, for various switching conditions of aggressor and victim line (FC-(1-4)) under functional crosstalk, MCB-4 (aka S4) has shown least amplitude of glitches (rise/fall/overshoot/undershoot) w.r.t other MCBs (1-3) and copper. Frequency spectrum analysis of MCB-4 (aka S4) and copper in a capacitively coupled architecture has shown that MCB-4 (aka S4) is having least frequency noise amplitude of about 70.66% w.r.t copper. Also, with rise in temperature (300K-500K), frequency noise amplitude has increased in MCB-4 (aka S4) which means that the noise filtering capability of MCB-4 (aka S4) degrades at higher temperatures.

7.3 TEMPERATURE-DEPENDENT CROSSTALK MODEL WITH APPLICATION OF DIL (DRIVER-INTERCONNECT-LOAD) IN COUPLED m-CNT BUNDLE INTERCONNECTS

By using an ABCD parameter matrix-based approach combined with a decoupling technique, the research work stated in chapter-5 aims to solve the model of capacitively coupled interconnects of m-CNT bundle. Functional as well as dynamic crosstalk is studied at 14nm technology node taking global lengths. The accuracy of the model is certain by validating it using simulation results. An equivalent circuit model of two capacitively coupled m-CNT bundle-based interconnects were taken and their performance was analyzed w.r.t dynamic crosstalk and functional crosstalk. The values, thus obtained analytically were compared with simulated results. It was observed that for best structure, i.e 'S4' , the average percentage error from simulated values to analytical values calculated using ABCD and decoupling method in case of crosstalk delay is 0.998%, and in case of crosstalk peaks is -5.41% and in case of CIGA is 0.7% , respectively. The accuracy of the model lies below 1% and therefore it can be considered for superior performance and greater potential in futuristic IC designs.

7.4 DIELECTRIC SURFACE ROUGHNESS SCATTERING INDUCED CROSSTALK PERFORMANCE OF COUPLED m-CNT BASED INTERCONNECTS

In the research work stated in chapter-6, the most typical and consistent dielectric materials such as silicon dioxide (SiO_2), boron nitride (BN) and silicon carbide (SiC) are taken into account and analyzed w.r.t. MFP created by surface roughness scattering. A complete crosstalk (dynamic & functional) effect in terms of positive peaks, time duration and area of rise glitch is studied. Frequency spectrum and bode stability analyses are also done for all four structures of m-CNT bundles (MCB) at 14nm technology node for a temperature range (300-500K). The performance of capacitively coupled MCB interconnects, placed on different rough substrate materials (i.e. $\boldsymbol{\alpha}_2$ case) such as silicon carbide (SiC), boron nitride (BN) and silicon dioxide (SiO2), has been compared with that of MCB interconnects placed on smooth substrate surface (i.e.'$\boldsymbol{\alpha}_1$' case) in terms of crosstalk induced glitch area (CIGA), crosstalk induced delay, stability and 3-dB frequency bandwidth analysis. The relative crosstalk induced delay in S4 increases, on average of 357.95%, 394.38% and 313.38%, when placed on substrate materials viz. BN, SiO_2 and SiC, respectively, as compared to smooth surface results. CIGA of S4 is observed almost 5 times

higher when placed on substrate materials (BN, SiO_2 and SiC), than on the smooth surface. It is also observed that the bandwidth of S4SiC is greater than the bandwidth of S4 placed on other substrate materials (SiO_2 & BN). Among all the structures, S4 placed on SiC substrate material is showing admirable results w.r.t. positive peaks, time duration, area of rise glitch. Amplitude frequency response of S4SiC came out to be least among other structures of MCB placed on other substrate materials. It has also been confirmed from the bode stability diagrams that S4SiC interconnects are more stable and have larger phase margin, gain margin and 3-dB frequency bandwidth in comparison to S4BN and S4SiO_2 with the same dimensions. Moreover, MCB interconnects placed on smooth substrate surface have larger 3-dB frequency bandwidth and smaller delay than those of MCB placed on rough substrate surfaces over a temperature range (300K-500K). Furthermore, an increase in amplitude of surface roughness parameter ($\boldsymbol{\delta}_{sr}$) reduces the frequency bandwidth and 50% rise time of 'S4' at its far end of the aggressor line. Based on results, it is concluded that for on-chip MCB interconnects at current and future technology nodes, it is imperative to analyze crosstalk effects considering substrate surface roughness.

7.5 SCOPE FOR FUTURE WORK

1. The model presented in this thesis, has not taken mutual inductance into account. The results will be more precise if mutual inductance is also taken in the calculations.
2. The structures considered in this thesis were having fixed orientation of SWCNTs and MWCNTs. The random arrangement of these CNTs is yet to be analyzed by making a suitable algorithm to calculate its impedance parameters.
3. The performance of hybrid CNTs consisting of copper and any CNT (SWCNT/DWCNT/MWCNT) while taking temperature as a factor, is yet to be analyzed.
4. The fabrication of GNR (Graphene Nano Ribbons) is easier and less cumbersome than CNTs, as GNRs have more number of fan outs as compare to only one fan out in CNTs. Researchers are considering GNRs for FET applications in place of CNTs.
5. This thesis has taken 14nm technology node, although it could be extended to 10nm.
6. There is a need to focus on low power IC design and therefore temperature-dependent sub-threshold needs to be addressed.

7. The high frequency analysis of m-CNT based interconnects is also left for future scope of this research work.

References

[1] Das, P.K., Majumder, M.K., Kaushik, B.K. and Dasgupta, S., 2012, December. Analysis of propagation delay in mixed carbon nanotube bundle as global VLSI interconnects. In *2012 Asia Pacific Conference on Postgraduate Research in Microelectronics and Electronics* (pp. 118-121). IEEE.

[2] Bethune, D.S., Kiang, C.H., De Vries, M.S., Gorman, G., Savoy, R., Vazquez, J. and Beyers, R., 1993. Cobalt-catalysed growth of carbon nanotubes with single-atomic-layer walls. *Nature*, *363*(6430), pp.605-607.

[3] Li, H., Yin, W.Y., Banerjee, K. and Mao, J.F., 2008. Circuit modeling and performance analysis of multi-walled carbon nanotube interconnects. *IEEE Transactions on electron devices*, *55*(6), pp.1328-1337.

[4] Fujita, M., Wakabayashi, K., Nakada, K. and Kusakabe, K., 1996. Peculiar localized state at zigzag graphite edge. *Journal of the Physical Society of Japan*, *65*(7), pp.1920-1923.

[5] Elgamel, M.A. and Bayoumi, M.A., 2003. Interconnect noise analysis and optimization in deep submicron technology. *IEEE Circuits and Systems Magazine*, *3*(4), pp.6-17.

[6] Kaushik, B.K. and Majumder, M.K., 2015. *Carbon nanotube based VLSI interconnects: Analysis and design* (pp. 1-14). New Delhi: Springer India.

[7] Kaushik, B.K. and Sarkar, S., 2008. Crosstalk analysis for a CMOS-gate-driven coupled interconnects. *IEEE Transactions on Computer-Aided Design of Integrated Circuits and Systems*, *27*(6), pp.1150-1154.

[8] Cao, Q. and Rogers, J.A., 2009. Ultrathin films of single-walled carbon nanotubes for electronics and sensors: a review of fundamental and applied aspects. *Advanced Materials*, *21*(1), pp.29-53.

[9] Li, F., Cheng, H.M., Bai, S., Su, G. and Dresselhaus, M.S., 2000. Tensile strength of single-walled carbon nanotubes directly measured from their macroscopic ropes. *Applied physics letters*, *77*(20), pp.3161-3163.

[10] Hone, J., Whitney, M., Piskoti, C. and Zettl, A., 1999. Thermal conductivity of single-walled carbon nanotubes. *Physical Review B*, *59*(4), p.R2514.

[11] Rai, M.K., Garg, H. and Kaushik, B.K., 2017. Temperature-dependent modeling and crosstalk analysis in mixed carbon nanotube bundle interconnects. *Journal of Electronic Materials*, *46*(8), pp.5324-5337.

[12] Yu, M.F., Lourie, O., Dyer, M.J., Moloni, K., Kelly, T.F. and Ruoff, R.S., 2000. Strength and breaking mechanism of multiwalled carbon nanotubes under tensile load. *Science*, *287*(5453), pp.637-640.

[13] Wei, B.Q., Vajtai, R. and Ajayan, P.M., 2001. Reliability and current carrying capacity of carbon nanotubes. *Applied physics letters*, *79*(8), pp.1172-1174.

[14] Javey, A. and Kong, J. eds., 2009. *Carbon nanotube electronics*. Springer Science & Business Media.

[15] Li, H. and Banerjee, K., 2009. High-frequency analysis of carbon nanotube interconnects and implications for on-chip inductor design. *IEEE Transactions on Electron Devices*, *56*(10), pp.2202-2214.

[16] Kaushik,B.K.,Agarwal,P.Sarkar,S.: Repeater insertion in crosstalk-aware inductively and capacitively coupled interconnects. Int. J. Circuit Theory Appl.(2011).https://doi.org/10.1002/cta.666

[17] Pandya, N.D., Majumder, M.K., Kaushik, B.K. and Manhas, S.K., 2012, May. Performance Comparision of Mixed CNT Bundle in Global VLSI Interconnect. In *2012 International Conference on Communication Systems and Network Technologies* (pp. 790-793). IEEE.

[18] Iijima, S., 1991. Helical microtubules of graphitic carbon. *nature*, *354*(6348), pp.56-58.

[19] Majumder, M.K., Kumari, A., Alam, A., Kumar, V.R. and Kaushik, B.K., 2015, June. Signal integrity improvement with peripherally placed MWCNTs in mixed CNT bundle based TSVs. In *2015 IEEE International Conference on Electron Devices and Solid-State Circuits (EDSSC)* (pp. 649-652). IEEE.

[20] Majumder, M.K., Das, P.K. and Kaushik, B.K., 2014. Delay and crosstalk reliability issues in mixed MWCNT bundle interconnects. *Microelectronics Reliability*, *54*(11), pp.2570-2577.

[21] Subash, S., Kolar, J. and Chowdhury, M.H., 2011. A new spatially rearranged bundle of mixed carbon nanotubes as VLSI interconnection. *IEEE Transactions on Nanotechnology*, *12*(1), pp.3-12.

[22] Rai, M.K., Garg, H. and Kaushik, B.K., 2017. Temperature-dependent modeling and crosstalk analysis in mixed carbon nanotube bundle interconnects. *Journal of Electronic Materials*, *46*(8), pp.5324-5337.

[23] Kumar, A., Kumar, V.R. and Kaushik, B.K., 2018. Transient analysis of crosstalk induced effects in mixed CNT bundle interconnects using FDTD technique. *IEEE Transactions on Electromagnetic Compatibility*, *61*(5), pp.1621-1629.

[24] Singh, A. and Dhiman, R., 2019. Proposal and analysis of mixed CNT bundle for sub-threshold interconnects. *IEEE Transactions on Nanotechnology*, *18*, pp.584-588.

[25] Kumbhare, V.R., Paltani, P.P. and Majumder, M.K., 2020. Signal Integrity Analysis for Diameter-Dependent Mixed Carbon Nanotube Bundle Interconnects. In *Information and Communication Technology for Sustainable Development* (pp. 481-489). Springer, Singapore.

[26] Moaiyeri, M.H., Hajmohammadi, Z., Khezeli, M.R. and Jalali, A., 2018. Effective reduction in crosstalk effects in quaternary integrated circuits using mixed carbon nanotube bundle interconnects. *ECS Journal of Solid State Science and Technology*, *7*(5), p.M69.

[27] Agarwal, K., Sylvester, D. and Blaauw, D., 2006. Modeling and analysis of crosstalk noise in coupled RLC interconnects. *IEEE Transactions on Computer-Aided Design of Integrated Circuits and Systems*, *25*(5), pp.892-901.

[28] Rai, M.K., Kaushik, B.K. and Sarkar, S., 2016. Thermally aware performance analysis of single-walled carbon nanotube bundle as VLSI interconnects. *Journal of Computational Electronics*, *15*(2), pp.407-419.

[29] Rossi, D., Cazeaux, J.M., Metra, C. and Lombardi, F., 2007. Modeling crosstalk effects in CNT bus architectures. *IEEE Transactions on Nanotechnology*, *6*(2), pp.133-145.

[30] Sheikhassadi, H., Masoumi, N. and Hakimi, A., 2011, May. Crosstalk modeling in multiwalled carbon nanotubes as interconnects using the compact RC model. In *2011 IEEE 15th Workshop on Signal Propagation on Interconnects (SPI)* (pp. 133-136). IEEE.

[31] Pu, S.N., Yin, W.Y., Mao, J.F. and Liu, Q.H., 2009. Crosstalk prediction of single-and double-walled carbon-nanotube (SWCNT/DWCNT) bundle interconnects. *IEEE Transactions on Electron Devices*, *56*(4), pp.560-568.

[32] Majumder, M.K., Pandya, N.D., Kaushik, B.K. and Manhas, S.K., 2012. Analysis of MWCNT and bundled SWCNT interconnects: Impact on crosstalk and area. *IEEE Electron Device Letters*, *33*(8), pp.1180-1182.

[33] Liang, F., Wang, G. and Lin, H., 2011. Modeling of crosstalk effects in multiwall carbon nanotube interconnects. *IEEE transactions on electromagnetic compatibility*, *54*(1), pp.133-139.

[34] Pop, E., Mann, D.A., Goodson, K.E. and Dai, H., 2007. Electrical and thermal transport in metallic single-wall carbon nanotubes on insulating substrates. *Journal of Applied Physics*, *101*(9), p.093710.

[35] Das, D. and Rahaman, H., 2017. *Carbon nanotube and graphene nanoribbon interconnects*. CRC press.

[36] Islam, M.Z., Mahboob, M. and Lowe, R.L., 2016. Mechanical properties of defective carbon nanotube/polyethylene nanocomposites: A molecular dynamics simulation study. *Polymer Composites*, *37*(1), pp.305-314.

[37] Sevik, C., Sevinçli, H., Cuniberti, G. and Cagın, T., 2011. Phonon engineering in carbon nanotubes by controlling defect concentration. *Nano Letters*, *11*(11), pp.4971-4977.

[38] Ohnishi, M., Shiga, T. and Shiomi, J., 2017. Effects of defects on thermoelectric properties of carbon nanotubes. *Physical Review B*, *95*(15), p.155405.

[39] McKelvey, J.P., Longini, R.L. and Brody, T.P., 1961. Alternative approach to the solution of added carrier transport problems in semiconductors. *Physical Review*, *123*(1), p.51.

[40] Lundstrom, M. and Ren, Z., 2002. Essential physics of carrier transport in nanoscale MOSFETs. *IEEE Transactions on Electron Devices*, *49*(1), pp.133-141.

[41] Meunier, V., 2016. Filho, AGS; Barros, EB; Dresselhaus, MS Physical properties of low-dimensional sp2-based carbon nanostructures. *Rev. Mod. Phys*, *88*(025005.10), p.1103.

[42] Pathania, S., Kumar, S. and Sharma, R., 2018, December. Crosstalk analysis for rough copper interconnects considering ternary logic. In *2018 IEEE Electrical Design of Advanced Packaging and Systems Symposium (EDAPS)* (pp. 1-3). IEEE.

[43] Sanaeepur, M., 2018. Dielectric surface roughness scattering limited performance of MLGNR interconnects. *IEEE Transactions on Electromagnetic Compatibility*, *61*(2), pp.532-537.

[44] Kumar, S. and Sharma, R., 2016. Analytical model for resistivity and mean free path in on-chip interconnects with rough surfaces. *IEEE Transactions on Emerging Topics in Computing*, *6*(2), pp.233-243.

[45] Kumar, S. and Sharma, R., 2017. Analytical modeling and performance benchmarking of on-chip interconnects with rough surfaces. *IEEE Transactions on Multi-Scale Computing Systems*, *4*(3), pp.272-284.

[46] Pathania, S., Kumar, S. and Sharma, R., 2019. Analyzing crosstalk-induced effects in rough on-chip copper interconnects. *IEEE Transactions on Components, Packaging and Manufacturing Technology*, *9*(10), pp.1984-1992.

[47] Li, J., Ye, Q., Cassell, A., Ng, H.T., Stevens, R., Han, J. and Meyyappan, M., 2003. Bottom-up approach for carbon nanotube interconnects. *Applied Physics Letters*, *82*(15), pp.2491-2493.

[48] Banerjee, K. and Srivastava, N., 2006, July. Are carbon nanotubes the future of VLSI interconnections?. In *Proceedings of the 43rd annual Design Automation Conference* (pp. 809-814).

[49] Akinwande, D., Huyghebaert, C., Wang, CH. *, 2019.* Graphene and two-dimensional materials for silicon technology. *Nature* 573, (pp 507–518) .

[50] Srivastava, N., Joshi, R.V. and Banerjee, K., 2005, December. Carbon nanotube interconnects: implications for performance, power dissipation and thermal management. In *IEEE InternationalElectron Devices Meeting, 2005. IEDM Technical Digest.* (pp. 249-252). IEEE.

[51] Bockrath, M., Cobden, D.H., Lu, J., Rinzler, A.G., Smalley, R.E., Balents, L. and McEuen, P.L., 1999. Luttinger-liquid behaviour in carbon nanotubes. *Nature*, *397*(6720), pp.598-601..

[52] Burke, P. J. (2002). Luttinger liquid theory as a model of the gigahertz electrical properties of carbon nanotubes. IEEE Transactions on Nanotechnology, 99(3), 129–144.

[53] Rai, M.K. and Sarkar, S., 2015. Temperature dependant crosstalk analysis in coupled single-walled carbon nanotube (SWCNT) bundle interconnects. International journal of circuit theory and applications, 43(10), pp.1367-1378.

[54] Rai, M.K., Khanna, R. and Sarkar, S., 2014. Control of tube parameters on SWCNT bundle interconnect delay and power dissipation. *Microelectronics International*.

[55] Zhang, K., Tian, B., Zhu, X., Wang, F. and Wei, J., 2011, June. Crosstalk analysis of carbon nanotube bundle interconnects. In The 4th IEEE International NanoElectronics Conference (pp. 1-2). IEEE.

[56] Naeemi, A., Sarvari, R. and Meindl, J.D., 2004, December. Performance comparison between carbon nanotube and copper interconnects for GSI. In *IEDM Technical Digest. IEEE International Electron Devices Meeting, 2004.* (pp. 699-702). IEEE.

[57] Sheikhassadi, H. and Masoumi, N., 2011, April. A RC model for multiwalled carbon nanotubes as interconnects. In *2011 IEEE EUROCON-International Conference on Computer as a Tool* (pp. 1-4). IEEE.

[58] Majumder, M.K., Das, P.K., Kaushik, B.K. and Manhas, S.K., 2012, December. Optimized delay and power performances for multi-walled CNT in global VLSI interconnects. In *2012 5th International Conference on Computers and Devices for Communication (CODEC)* (pp. 1-4). IEEE.

[59] Tang, M., Lu, J. and Mao, J., 2012, December. Study on equivalent single conductor model of multi-walled carbon nanotube interconnects. In *2012 Asia Pacific Microwave Conference Proceedings* (pp. 1247-1249). IEEE.

[60] Gholipour, M. and Masoumi, N., 2011, December. Efficient model for delay estimation of MWCNT interconnects. In *ICM 2011 Proceeding* (pp. 1-4). IEEE.

[61] Tang, M. and Mao, J., 2014. Modeling and fast simulation of multiwalled carbon nanotube interconnects. *IEEE Transactions on Electromagnetic Compatibility*, *57*(2), pp.232-240.

[62] Ferranti, F., Antonini, G., Dhaene, T., Knockaert, L. and Orlandi, A., 2011. Compact and accurate models of large single-wall carbon-nanotube interconnects. *IEEE transactions on electromagnetic compatibility*, *53*(4), pp.1025-1033.

[63] Naeemi, A., Sarvari, R. and Meindl, J.D., 2005. Performance comparison between carbon nanotube and copper interconnects for gigascale integration (GSI). *IEEE Electron Device Letters*, *26*(2), pp.84-86.

[64] Srivastava, N., Li, H., Kreupl, F. and Banerjee, K., 2009. On the applicability of single-walled carbon nanotubes as VLSI interconnects. *IEEE Transactions on Nanotechnology*, *8*(4), pp.542-559.

[65] Rahman, M. and Chowdhury, A.A., 2010, December. Analyzing Carbon Nanotube interconnects in VLSI application. In *2010 13th International Conference on Computer and Information Technology (ICCIT)* (pp. 237-240). IEEE.

[66] Chiariello, A.G., Maffucci, A. and Miano, G., 2012, August. A temperature-dependent circuit model for carbon-based on-chip global interconnects. In 2012 12th IEEE International Conference on Nanotechnology (IEEE-NANO) (pp. 1-6). IEEE.

[67] Majumder, M.K., Kaushik, B.K., Manhas, S.K. and Kumar, J., 2012, December. Analysis of crosstalk delay and power dissipation in mixed CNT bundle interconnects. In 2012 International Conference on

Communications, Devices and Intelligent Systems (CODIS) (pp. 361-364). IEEE.

[68] Esqueda, I.S., Cress, C.D., Cao, Y., Che, Y., Fritze, M. and Zhou, C., 2015. The impact of defect scattering on the quasi-ballistic transport of nanoscale conductors. *Journal of Applied Physics*, *117*(8), p.084319.

[69] Islam, M.Z., Mahboob, M. and Lowe, R.L., 2016. Mechanical properties of defective carbon nanotube/polyethylene nanocomposites: A molecular dynamics simulation study. *Polymer Composites*, *37*(1), pp.305-314.

[70] Sevik, C., Sevinçli, H., Cuniberti, G. and Cagın, T., 2011. Phonon engineering in carbon nanotubes by controlling defect concentration. *Nano Letters*, *11*(11), pp.4971-4977.

[71] Ohnishi, M., Shiga, T. and Shiomi, J., 2017. Effects of defects on thermoelectric properties of carbon nanotubes. *Physical Review B*, *95*(15), p.155405.

[72] McKelvey, J.P., Longini, R.L. and Brody, T.P., 1961. Alternative approach to the solution of added carrier transport problems in semiconductors. *Physical Review*, *123*(1), p.51.

[73] Che, G., Lakshmi, B.B., Martin, C.R., Fisher, E.R. and Ruoff, R.S., 1998. Chemical vapor deposition based synthesis of carbon nanotubes and nanofibers using a template method. *Chemistry of Materials*, *10*(1), pp.260-267.

[74] Pu, S.N., Yin, W.Y., Mao, J.F. and Liu, Q.H., 2009. Crosstalk prediction of single-and double walled carbon-nanotube (SWCNT/DWCNT) bundle interconnects. IEEE Transactions on Electron Devices, 56(4), pp.560-568.

[75] Libo, Q., Zhangming, Z., Ruixue, D. and Yintang, Y., 2013. Circuit modeling and performance analysis of SWCNT bundle 3D interconnects. Journal of Semiconductors, 34(9), p.095014.

[76] Das, P.K., Majumder, M.K. and Kaushik, B.K., 2014. Dynamic crosstalk analysis of mixed multi-walled carbon nanotube bundle interconnects. The Journal of Engineering, 2014(5), pp.227-233.

[77] Kumar, V.R., Kaushik, B.K. and Patnaik, A., 2015. Crosstalk noise modeling of multiwall carbon nanotube (MWCNT) interconnects using finite-difference time-domain (FDTD) technique. Microelectronics Reliability, 55(1), pp.155-163.

[78] Agrawal, Y., Girish, M. and Chandel, R., 2018. An efficient and novel FDTD method based performance investigation in high-speed current-mode signaling SWCNT bundle interconnect. Sādhanā, 43(11), pp.1-12.

[79] Kumar, V.R., Kaushik, B.K. and Patnaik, A., 2014. An accurate FDTD model for crosstalk analysis of CMOS-gate-driven coupled RLC interconnects. *IEEE Transactions on Electromagnetic Compatibility*, *56*(5), pp.1185-1193.

[80] Sahoo, M., Ghosal, P. and Rahaman, H., 2014, January. An ABCD parameter based modeling and analysis of crosstalk induced effects in multiwalled carbon nanotube bundle interconnects. In *2014 27th International Conference on VLSI Design and 2014 13th International Conference on Embedded Systems* (pp. 433-438). IEEE.

[81] Fathi, D., Forouzandeh, B., Mohajerzadeh, S. and Sarvari, R., 2009. Accurate analysis of carbon nanotube interconnects using transmission line model. *Micro & Nano Letters*, *4*(2), pp.116-121.

[82] Xu, Q. and Mazumder, P., 2002, January. Rational ABCD modeling of high-speed interconnects. In *Proceedings of ASP-DAC/VLSI Design 2002. 7th Asia and South Pacific Design Automation Conference and 15h International Conference on VLSI Design* (pp. 147-152). IEEE.

[83] Sahoo, M., Ghosal, P. and Rahaman, H., 2013, August. An ABCD parameter-based modeling and analysis of crosstalk induced effects in single-walled carbon nanotube bundle interconnects. In *Fifth Asia Symposium on Quality Electronic Design (ASQED 2013)* (pp. 264-273). IEEE.

[84] Sahoo, M. and Rahaman, H., 2015. Modeling of crosstalk induced effects in copper-based nanointerconnects: an ABCD parameter matrix-based approach. *Journal of Circuits, Systems and Computers*, *24*(02), p.1540007.

[85] Zhao, S. and Pan, Z., 2018. Performance comparison between current-mode signaling and voltage-mode signaling for single-walled carbon nanotube bundle interconnects. *Journal of Circuits, Systems and Computers*, *27*(11), p.1850173.

[86] Khezeli, M.R., Moaiyeri, M.H. and Jalali, A., 2018. Active shielding of MWCNT bundle interconnects: An efficient approach to cancellation of crosstalk-induced functional failures in ternary logic. *IEEE Transactions on Electromagnetic Compatibility*, *61*(1), pp.100-110.

[87] Majumder, M.K., Das, P.K., Kumar, V.R. and Kaushik, B.K., 2015. Crosstalk induced delay analysis of randomly distributed mixed CNT bundle interconnect. *Journal of Circuits, Systems and Computers*, *24*(10), p.1550145.

[88] Kumbhare, V.R., Paltani, P.P. and Majumder, M.K., 2020. Performance analysis of mixed CNT bundle interconnects at 10 nm technology. *IET Circuits, Devices & Systems*, *14*(7), pp.1049-1057.

[89] Majumder, M.K., Kumar, J., Kumar, V.R. and Kaushik, B.K., 2014. Performance analysis for randomly distributed mixed carbon nanotube bundle interconnects. *Micro & Nano Letters*, *9*(11), pp.792-796.

[90] Hosseini, A. and Shabro, V., 2010. Thermally-aware modeling and performance evaluation for single-walled carbon nanotube-based interconnects for future high performance integrated circuits. *Microelectronic Engineering*, *87*(10), pp.1955-1962.

[91] Jia, L. and Yin, W.Y., 2008, December. Temperature effects on crosstalk in carbon nanotube interconnects. In *2008 Asia-Pacific Microwave Conference* (pp. 1-4). IEEE.

[92] Singh, K. and Raj, B., 2015. Temperature-dependent modeling and performance evaluation of multi-walled CNT and single-walled CNT as global interconnects. *Journal of Electronic Materials*, *44*(12), pp.4825-4835.

[93] Singh, K. and Raj, B., 2015. Influence of temperature on MWCNT bundle, SWCNT bundle and copper interconnects for nanoscaled technology nodes. *Journal of Materials Science: Materials in Electronics*, *26*(8), pp.6134-6142.

[94] Das, D. and Rahaman, H., 2010, December. Timing analysis in carbon nanotube interconnects with process, temperature, and voltage variations. In *2010 International Symposium on Electronic System Design* (pp. 27-32). IEEE.

[95] Sandha, K.S. and Raj, B., 2015, October. Thermally aware modeling and performance for MWCNT bundle as VLSI interconnects for high performance integrated circuits. In *2015 IEEE 4th Global Conference on Consumer Electronics (GCCE)* (pp. 560-564). IEEE.

[96] Duksh, Y.S., Kaushik, B.K., Sarkar, S. and Singh, R., 2011, February. Effect of Driver Size and Number of Shells on Propagation Delay in MWCNT Interconnects. In *2011 International Conference on Devices and Communications (ICDeCom)* (pp. 1-5). IEEE.

[97] Achar, R. and Nakhla, M.S., 2001. Simulation of high-speed interconnects. *Proceedings of the IEEE*, *89*(5), pp.693-728.

[98] Das, D. and Rahaman, H., 2011, December. Crosstalk and gate oxide reliability analysis in graphene nanoribbon interconnects. In *2011 International Symposium on Electronic System Design* (pp. 182-187). IEEE.

[99] Rakheja, S., Kumar, V. and Naeemi, A., 2013. Evaluation of the potential performance of graphene nanoribbons as on-chip interconnects. *Proceedings of the IEEE*, *101*(7), pp.1740-1765.

[100] Cho, H., Kapur, P. and Saraswat, K.C., 2004. Power comparison between high-speed electrical and optical interconnects for interchip communication. *Journal of lightwave technology*, *22*(9), p.2021.

[101] Tsang, L., Gu, X. and Braunisch, H., 2006. Effects of random rough surface on absorption by conductors at microwave frequencies. *IEEE microwave and wireless components letters*, *16*(4), pp.221-223.

[102] Hammerstad, E. and Jensen, O., 1980, May. Accurate models for microstrip computer-aided design. In *1980 IEEE MTT-S International Microwave Symposium Digest* (pp. 407-409). IEEE..

[103] Lai, L. and Irene, E.A., 1999. Area evaluation of microscopically rough surfaces. *Journal of Vacuum Science & Technology B: Microelectronics and Nanometer Structures Processing, Measurement, and Phenomena*, *17*(1), pp.33-39.

[104] Namba, Y., 1968. Electrical conduction of thin metallic films with rough surface. *Journal of Applied Physics*, *39*(13), pp.6117-6118.

[105] Kumar, S. and Sharma, R., 2017. Chip-to-chip copper interconnects with rough surfaces: analytical models for parameter extraction and performance evaluation. *IEEE Transactions on Components, Packaging and Manufacturing Technology*, *8*(2), pp.286-299.

[106] Fathi, D. and Forouzandeh, B., 2009. A novel approach for stability analysis in carbon nanotube interconnects. *IEEE electron device letters*, *30*(5), pp.475-477.

[107] Kaur, T., Kumar Rai, M. and Khanna, R., 2021. Analytical Frequency-Domain Model for Coupled Interconnects of Doped Multilayer Graphene Nanoribbons and Mixed Carbon Nanotube Bundles. *physica status solidi (a)*, *218*(4), p.2000588.

[108] Kumar, V.R., Majumder, M.K., Alam, A., Kukkam, N.R. and Kaushik, B.K., 2015. Stability and delay analysis of multi-layered GNR and multi-walled CNT interconnects. *Journal of Computational Electronics*, *14*(2), pp.611-618.

[109] Steinhögl, W., Schindler, G., Steinlesberger, G., Traving, M. and Engelhardt, M., 2005. Comprehensive study of the resistivity of copper wires with lateral dimensions of 100 nm and smaller. *Journal of Applied Physics*, *97*(2), p.023706.

[110] B. Meyer, U. Gottlieb, O.Laborde, H. Yang, J.C. Lasjaunia, A. Sulpice, R.Madar,. 1997 J. Alloys Compd. *262*, pp. 235-237.

[111] Pable, S.D. and Hasan, M., 2012. Interconnect design for subthreshold circuits. *IEEE transactions on nanotechnology*, *11*(3), pp.633-639.

[112] P. Uma Sathyakam & P.S. Mallick, 2012 .Inter-CNT capacitance in mixed CNT bundle interconnects for VLSI circuits, *International Journal of Electronics*, 99(10), pp.1439-1447.

[113] Meunier, V., Souza Filho, A.G., Barros, E.B. and Dresselhaus, M.S., 2016. Physical properties of low-dimensional s p 2-based carbon nanostructures. *Reviews of Modern Physics*, *88*(2), p.025005.

[114] Subash, S., Kolar, J. and Chowdhury, M.H., 2011. A new spatially rearranged bundle of mixed carbon nanotubes as VLSI interconnection. *IEEE Transactions on Nanotechnology*, *12*(1), pp.3-12.

[115] Majumder, M.K., Kaushik, B.K. and Manhas, S.K., 2014. Analysis of delay and dynamic crosstalk in bundled carbon nanotube interconnects. *IEEE transactions on electromagnetic compatibility*, *56*(6), pp.1666-1673

[116] Kaushik, B.K. and Sarkar, S., 2008. Crosstalk analysis for a CMOS gate driven inductively and capacitively coupled interconnects. *Microelectronics Journal*, *39*(12), pp.1834-1842.

[117] Mohsin, K.M., Srivastava, A., Sharma, A.K. and Mayberry, C., 2013. A thermal model for carbon nanotube interconnects. *Nanomaterials*, *3*(2), pp.229-241.

[118] Pourfath, M., 2014. *The non-equilibrium Green's function method for nanoscale device simulation* (Vol. 3). Vienna: Springer.

[119] Predictive Technology Model (PTM), www.eas.edu/~ptm/, (2016), Accessed 26May 2016.

[120] Semiconductor Industry Association, International Technology Roadmap for Semiconductors (ITRS),http://www.itrs.net/,(2013 update), Accessed 26 May 2016.

[121] Rai, M. and Sarkar, S., 2011. Carbon nanotube as a VLSI interconnect. *Electronic Properties of Carbon Nanotubes*, pp.475-494.

[122]Das, D. and Rahaman, H., 2011. Analysis of crosstalk in single-and multiwall carbon nanotube interconnects

and its impact on gate oxide reliability. *IEEE transactions on nanotechnology*, *10*(6), pp.1362-1370.

[123] Sahoo, M., Ghosal, P. and Rahaman, H., 2015. Modeling and analysis of crosstalk induced effects in multiwalled carbon nanotube bundle interconnects: An ABCD parameter-based approach. *IEEE Transactions on Nanotechnology*, *14*(2), pp.259-274.

[124] Lu, Q.J., Zhu, Z.M., Yang, Y.T. and Ding, R.X., 2015. Influence of temperature on the conductivity of multi-walled carbon nanotube interconnects. *Chinese Physics Letters*, *32*(4), p.047305.

[125] Sahoo, M. and Rahaman, H., 2017. Analysis of crosstalk-induced effects in multilayer graphene nanoribbon interconnects. *Journal of Circuits, Systems and Computers*, *26*(06), p.1750102.

[126] Kumar, M.G., Agrawal, Y. and Chandel, R., 2016. Carbon nanotube interconnects− a promising solution for VLSI circuits. *IETE Journal of Education*, *57*(2), pp.46-64.

[127] Wei, T., Mishra, P., Wu, K. and Zhou, J., 2012. Quasi-static fault-tolerant scheduling schemes for energy-efficient hard real-time systems. *Journal of Systems and Software*, *85*(6), pp.1386-1399.

[128] Zhou, J., Cao, K., Cong, P., Wei, T., Chen, M., Zhang, G., Yan, J. and Ma, Y., 2017. Reliability and temperature constrained task scheduling for makespan minimization on heterogeneous multi-core platforms. *Journal of Systems and Software*, *133*, pp.1-16.

[129] Fathi, D., Forouzandeh, B., Mohajerzadeh, S. and Sarvari, R., 2009. Accurate analysis of carbon nanotube interconnects using transmission line model. *Micro & Nano Letters*, *4*(2), pp.116-121.

[130] Zhao, W.S., Wang, G., Hu, J., Sun, L. and Hong, H., 2015. Performance and stability analysis of monolayer single-walled carbon nanotube interconnects. *International Journal of Numerical Modelling: Electronic Networks, Devices and Fields*, *28*(4), pp.456-464.

[131] Lu, Q., Zhu, Z., Yang, Y. and Ding, R., 2016. Analysis of propagation delay and repeater insertion in single-walled carbon nanotube bundle interconnects. *Microelectronics Journal*, *54*, pp.85-92.

[132] Zhao, S. and Pan, Z., 2018. Performance comparison between current-mode signaling and voltage-mode signaling for single-walled carbon nanotube bundle interconnects. *Journal of Circuits, Systems and Computers*, *27*(11), p.1850173.

[133] Das, P.K., Majumder, M.K. and Kaushik, B.K., 2014. Dynamic crosstalk analysis of mixed multi-walled carbon nanotube bundle interconnects. *The Journal of Engineering*, *2014*(5), pp.227-233.

[134] Zhang, J. and Friedman, E.G., 2004, May. Decoupling technique and crosstalk analysis for coupled RLC interconnects. In *2004 IEEE International Symposium on Circuits and Systems (IEEE Cat. No. 04CH37512)* (Vol. 2, pp. II-521). IEEE.

[135] Palit, A.K., Hasan, S. and Anheier, W., 2009, December. Decoupled victim model for the analysis of crosstalk noise between on-chip coupled interconnects. In *2009 11th Electronics Packaging Technology Conference* (pp. 697-701). IEEE.

[136] Vasilev, B., Bott, S., Rzehak, R., Kücher, P. and Bartha, J.W., 2011, May. Pad roughness effects on the planarization and material removal rate in CMP processes. In *2011 IEEE International Interconnect Technology Conference* (pp. 1-3). IEEE.

[137] Bhattacharya, S., Das, D. and Rahaman, H., 2017. Stability analysis in top-contact and side-contact graphene nanoribbon interconnects. *IETE Journal of Research*, *63*(4), pp.588-596.

[138] K. Ogata,.2009, Modern Control Engineering, Upper Saddle River, NJ: Pearson Education, 5th Ed.

[139] Nasiri, S.H., Moravvej-Farshi, M.K. and Faez, R., 2010. Stability analysis in graphene nanoribbon interconnects. *IEEE Electron Device Letters*, *31*(12), pp.1458-1460.

[140] Nishad, A.K. and Sharma, R., 2013. Analytical time-domain models for performance optimization of multilayer GNR interconnects. *IEEE journal of selected topics in Quantum electronics*, *20*(1), pp.17-24.

LIST OF PUBLICATIONS

Published SCI papers:

1. **Sharma, M.,** Rai, M.K. & Khanna, R. Temperature-dependent crosstalk and frequency spectrum analyses in adjacent interconnects of a mixed CNT bundle. ***J Comput Electron*** **19,** 177–190 (2020). **(IF-1.53)**
2. **Sharma, M.**, Rai, M.K. & Khanna, R. Performance analysis of irradiation induced defected mixed CNT bundle based coupled VLSI interconnects. ***J Mater Sci: Mater Electron*** (2020). **(IF-2.22)**
3. **Sharma, M**., Rai, M.K. & Khanna, R. Performance analysis of MCB-based VLSI interconnects depending on scattering induced by substrate surface roughness. ***J Comput Electron*** (2020). **(IF-1.53)**
4. **Sharma, M**., Rai, M.K. & Khanna, R Dielectric Surface Roughness Scattering Induced Crosstalk Performance of Coupled MCB Interconnects. ***Microelectronics Journal*** *(2021).https://doi.org/10.1016/j.mejo.2021.105084 (***IF-1.40)**

Patents

Sharma, M., Rai, M.K. 2021. Rough Surface scattering induced capacitively coupled mixed CNT bundle (MCB) interconnects. **Indian Patent**, 202111038795, published on 10th Sept' 2021.

International Conference /Scopus Papers:

5. **Sharma, M.**, Rai, M.K. and Khanna, R., 2019, October. Temperature-dependent analysis of Crosstalk noise in Capacitively Coupled Interconnects for Mixed Carbon Nanotubes Bundle. In *TENCON 2019- 2019 IEEE Region 10 Conference (TENCON)* (pp. 2544-2548). IEEE.
6. **Manvi Sharma**, Mayank Kumar Rai, Rajesh Khanna,"Performance Analysis of Mixed Carbon Nano Tubes as VLSI Interconnects" in "International Conference on Science, Engineering , Law and Management" held in Malaysia on 6th January' 2017.
   Extended paper accepted in *Indian Journal of Science and Technology, 10, p.16.*